

UNIVERSITAT POLITÈCNICA DE VALÈNCIA

ESCUELA TÉCNICA SUPERIOR DE INGENIERÍA DEL DISEÑO

PROYECTO FIN DE CARRERA

“DYNAMIC DESIGN OF A CUBE-SHAPED
SATELLITE EXCITED BY LAUNCH VIBRATIONS”



UNIVERSITAT
POLITÈCNICA
DE VALÈNCIA



Escuela Técnica Superior de Ingeniería del Diseño

ALUMNOS:

FRAILE IZQUIERDO, SERGIO

PILA VIGALONDO, ALEJANDRO

DIRECTOR:

DR. D. ANDRÉS ROVIRA CARDETE

INGENIERÍA AERONÁUTICA

DICIEMBRE DE 2014

“Picture, if you will, a multi-million euro altar to the triumph of function over form, precisely oriented and silently gliding on its orbit around Earth in a smooth, graceful state of free fall. Satellites appear serene and fragile in their often ungainly forms, designed for a life in orbit, untroubled by the Earth-bound stresses of gravity and vibration. But they are not.”

— Julian Simpson

Foremost, we would like to express our sincere gratitude to our advisor, director and friend, Dr. D Andrés Rovira Cardete for the continuous and valuable support of this Final Project. He did an excellent guidance job and provided us with an excellent work atmosphere. Without his help this could not have been possible.

We would also like to thank our family and friends, teachers and people that have helped us out one way or another to fulfil this Final Project. Thank you all.

FINAL PROJECT

Table of Contents

1	Introduction.....	13
2	Objective and Scope	15
3	Motivation	17
3.1	Technical Motivation	17
3.2	Academic Motivation	17
4	Project Overview.....	19
5	Background on Satellite Missions.....	21
5.1	UPMSAT.....	21
5.2	ANUSAT.....	22
5.3	SUNSAT.....	22
5.4	SSTL MicroSat Family.....	23
5.5	TATYANA 1	24
5.6	Oculus-ASR.....	25
5.7	HiakaSat	26
5.8	DANDE	26
5.9	Rising 2.....	27
6	Regulations	29
6.1	Ariane-5 Regulations	29
6.1.1	Center of Gravity Position	29
6.1.2	Inertia	29
6.1.3	Dimensions.....	29
6.1.4	Natural Frequency Requirements.....	29
6.1.5	Quasi-static Loads.....	30
6.1.6	Sine-equivalent dynamics.....	30
6.1.7	Random vibration.....	31
6.1.8	Shocks.....	31
6.2	Soyuz Regulations.....	31
6.2.1	Center of Gravity Position	32
6.2.2	Inertia	32
6.2.3	Dimensions.....	32
6.2.4	Natural Frequency Requirements.....	32
6.2.5	Quasi-static Loads.....	32
6.2.6	Sine-equivalent dynamics.....	33
6.3	VEGA Regulations.....	33
6.3.1	Center of Gravity Position	34
6.3.2	Inertia	34
6.3.3	Sine-equivalent dynamics.....	34
6.3.4	Random vibration.....	34
6.3.5	Acoustic vibration.....	35
6.3.6	Shocks.....	35
6.4	DNEPR Regulations	36
6.4.1	Natural Frequency Requirements.....	36

6.4.2	Quasi-static Loads.....	36
6.4.3	Sine-equivalent dynamics.....	37
6.4.4	Random vibration.....	38
6.4.5	Acoustic vibration.....	38
6.4.6	Shock.....	39
6.5	Selection of the launcher.....	39
7	Microsatellites	41
7.1	Definition.....	42
7.2	Applications.....	42
7.3	Subsystems	43
7.3.1	Structure Subsystem	44
7.3.2	Command and Data Handling Subsystem.....	45
7.3.3	Attitude Determination and Control Subsystem	45
7.3.4	Telemetry, Tracking and Command Subsystem	46
7.3.5	Electric Power Subsystem.....	46
7.3.6	Propulsion Subsystem	46
8	Geometric Modelling	49
8.1	Introduction	49
8.1.1	CATIA.....	49
8.1.2	CAD Nexus.....	50
8.2	CAD Modelling of the Structure.....	50
8.2.1	Shelf Structure.....	50
8.2.2	Column Structure.....	53
8.2.3	Tray A Modification	56
8.3	Mass Distribution.....	57
8.4	CoG Location	59
8.5	Inertia Check-up	59
9	FEM Model	61
9.1	Material Selection	61
9.2	Meshing.....	63
9.2.1	Tray A.....	67
9.2.2	Trays B and C.....	68
9.2.3	Tray D	69
9.2.4	Plates.....	71
9.2.5	Subsystems and payload.....	72
9.3	Connections	73
9.4	Loads and Boundary Conditions.....	73
9.4.1	Static Analysis.	73
9.4.2	Modal Analysis.....	74
9.4.3	Harmonic Analysis.....	74
10	Results.....	75
10.1	Static Structural	75
10.2	Modal properties	80
10.2.1	Mode shapes	82
10.3	Harmonic Analysis.....	87

10.3.1 Longitudinal.....	88
10.3.2 Lateral.....	93
10.3.3 Equivalent Loads.....	101
10.4 Compendium of Results.....	104
11 Conclusions	105
12 Future Work	107
13 Glossary	109
14 References.....	111

List of Figures

Figure 5.1 – UPM–Sat 1 [3].....	21
Figure 5.2 – ANUSAT [4].....	22
Figure 5.3 – SUNSAT [5].....	23
Figure 5.4 – SSTL MicroSat [6].....	24
Figure 5.5 – TATYANA 1 [7].....	25
Figure 5.6 – Oculus ASR [9].....	25
Figure 5.7 – HiakaSat [8].....	26
Figure 5.8 – Rising 2 [11].....	27
Figure 6.1 – Ariane 5 Acceleration vs Frequency of the Shock [12].....	31
Figure 6.2 – Soyuz Dimensional Envelope Soyuz [mm] [13].....	32
Figure 6.3 – VEGA Envelope acceleration Shock Response Spectrum (SRS) at the spacecraft base [15].....	36
Figure 7.1 – Number of Launches vs Time (from [19] and [20]).....	41
Figure 7.2 – Satellite Subsystems.....	43
Figure 7.3 – Typical Configuration of the Structure Subsystem in cube-shaped satellites.....	44
Figure 8.1. – Methodology followed during design.....	49
Figure 8.2 – Satellite primary structure without lateral plates.....	51
Figure 8.3– Parameters used – CATIA (left) ANSYS (right).....	51
Figure 8.4 – Satellite Structure with modelled Subsystems.....	52
Figure 8.5 – External view of satellite structure.....	52
Figure 8.6 – Column Structure.....	53
Figure 8.7 – Detail of contact between tray and column.....	54
Figure 8.8 – Zero Iteration of Contact Design.....	54
Figure 8.9 – First Iteration of Contact Design.....	54
Figure 8.10 - Second Iteration of Contact Design.....	55
Figure 8.11 – Circular Central Column Design.....	55
Figure 8.12 – Columns Structure with Subsystems onboard.....	56
Figure 8.13 – Tray A Modification.....	56
Figure 8.14 – Final appearance of the satellite with the subsystems onboard and the lateral plates hidden.....	57
Figure 8.14 – Detail of the subsystems distribution.....	59
Figure 9.1 – Meshing geometric figures [30].....	63
Figure 9.2 – Warping factor exhibition [30].....	63
Figure 9.3 – Final mesh view 1.....	65
Figure 9.4 – Final mesh view 2.....	65
Figure 9.5 – Final mesh view 3.....	66
Figure 9.6 – Final mesh view 4.....	66
Figure 9.7 – Skewness vs type vs number of elements.....	67
Figure 9.8 – Tray A meshing view 1.....	68
Figure 9.9 – Tray A meshing view 2.....	68
Figure 9.10 – Tray A meshing view 3.....	68
Figure 9.11 – Trays B and C meshing view 1.....	69
Figure 9.12 – Trays B and C meshing view 2.....	69
Figure 9.13 – Trays B and C meshing view 3.....	69

Figure 9.14 – Tray D meshing view 1	70
Figure 9.15 – Tray D meshing view 2	70
Figure 9.16 – Tray D meshing view 3Spars.....	70
Figure 9.17 – Spars meshing view	71
Figure 9.18 – Plates meshing view	72
Figure 9.20 – Subsystems meshing view 2.....	72
Figure 9.21 – Subsystems meshing view 3.....	72
Figure 9.19 – Subsystems meshing view 1.....	73
Figure 10.1 – ANSYS Workbench Project Schematic.....	75
Figure 10.2 – Acceleration Settings.....	76
Figure 10.3 – Static Analysis– Total Deformation.....	77
Figure 10.4 – Static Structural Total Deformation – 3D View	77
Figure 10.5 – Static Structural VM Stress Detail View 1	78
Figure 10.6 – Static Structural VM Stress Detail View 2	78
Figure 10.7 – Static Structural VM Stress Bottom to top View	79
Figure 10.8 – Static Structural VM Stress Detail View 3	79
Figure 10.9 – Static Structural Safety Factor	80
Figure 10.10 – Mode 1	82
Figure 10.11 – Mode 2	82
Figure 10.12 – Mode 3	82
Figure 10.13 – Mode 4	82
Figure 10.14 – Mode 5	82
Figure 10.15 – Mode 6	82
Figure 10.16 – Mode 1 ZX View.....	83
Figure 10.17 – Mode 1 3D View.....	83
Figure 10.18 – Mode 2 ZX View.....	83
Figure 10.19 – Mode 2 3D View.....	83
Figure 10.20 – Mode 3 ZX View.....	84
Figure 10.21 – Mode 3 3D View.....	84
Figure 10.22 – Mode 4 ZX View.....	84
Figure 10.23 – Mode 4 3D View.....	84
Figure 10.24 – Mode 4 Plates View Auto Scale.....	85
Figure 10.27 – Mode 5 Plates View	85
Figure 10.25 – Mode 5 ZX View.....	86
Figure 10.26 – Mode 5 3D View	86
Figure 10.28 – Mode 6 ZX View.....	86
Figure 10.29 – Mode 6 3D View	86
Figure 10.30 – Mode 6 Plates View	87
Figure 10.31 – Z Axis directional deformation / 4 – 6 Hz longitudinal	89
Figure 10.32 – Directional Deformation 6 Hz	89
Figure 10.33 – Z Axis normal stress / 4–6 Hz longitudinal.....	90
Figure 10.34 – Z Normal Stress 6 Hz longitudinal	90
Figure 10.35 – Z Axis directional deformation / 6 – 100 Hz longitudinal.....	91
Figure 10.36 – Maximum Z Axis Directional Deformation 94.75 Hz 3D View.....	91
Figure 10.37 – Maximum Directional Deformation 94.75 Hz Auto Scale.....	92
Figure 10.38 – Maximum Directional Deformation 94.75 Hz True Scale.....	92
Figure 10.39 –Z Axis normal stress / 6 – 100 Hz longitudinal.....	92

Figure 10.40 – Maximum Normal Stress Z Axis 93

Figure 10.41 – X Axis directional deformation / 2 – 6 Hz lateral..... 93

Figure 10.42 - Maximum Z Axis Directional Deformation 6 Hz 3D View 94

Figure 10.43 – Y Axis directional deformation / 2-6 Hz lateral..... 94

Figure 10.44 - Maximum Y Axis Directional Deformation 6 Hz 3D View 95

Figure 10.45 – Max Z Axis Normal Stress 6 Hz Detail 1 95

Figure 10.46 – Max X Axis Normal Stress 6 Hz Detail 1 95

Figure 10.47– Max Y Axis Normal Stress 6 Hz Detail 1 95

Figure 10.48 – Max Y Axis Normal Stress 6 Hz Detail 2..... 95

Figure 10.49 – X Axis normal stress / 2 – 6 Hz lateral 96

Figure 10.50 – Y Axis normal stress / 2 – 6 Hz lateral 96

Figure 10.51 – X Axis directional deformation / 6 – 100 Hz lateral 97

Figure 10.53 – Maximum Directional Deformation X Axis 94.5 Hz Auto Scale 97

Figure 10.54 – Maximum Directional Deformation X Axis 94.5 Hz True Scale 97

Figure 10.52 – Maximum Directional Deformation X Axis 94.75 Hz 3D View 98

Figure 10.55 – Y Axis directional deformation / 6 – 100 Hz lateral 98

Figure 10.56 – Maximum Directional Deformation Y Axis 100 Hz 3D View 99

Figure 10.57 – Maximum Directional Deformation Y Axis 100 Hz Auto Scale 99

Figure 10.58 – Maximum Directional Deformation Y Axis 100 Hz True Scale 99

Figure 10.59 – X Axis normal stress / 6 – 100 Hz lateral 100

Figure 10.60 – Maximum Normal Stress X Axis 94.75 Hz Detail View 100

Figure 10.61 – Y normal stress / 6 – 100 Hz lateral 101

Figure 10.62 – Maximum Normal Stress Y Axis 94 Hz Detail View..... 101

Figure 10.63 – VM Stresses distribution resonance point 3D view 102

Figure 10.64 – VM Stresses distribution down-top view 103

Figure 10.65 – VM Stresses distribution detail view 103

Figure 10.66 – Total Deformation in resonance point 103

List of Tables

Table 1 – Ariane 5 Quasi static loads	30
Table 2 – Ariane 5 Sine Equivalent Dynamics Ariane 5	30
Table 3 – Soyuz Quasi-Static Loads Soyuz	33
Table 4 – Soyuz Sine-equivalent dynamics Soyuz	33
Table 5 – VEGA Sine Equivalent dynamics VEGA	34
Table 6 – VEGA Acoustic Noise Spectrum under the Fairing Note: OASPL – Overall Acoustic Sound Pressure Level These values do not take into account any fill factor correction	35
Table 7 – DNEPR Accelerations at SC/LV interface during transportation	37
Table 8 – DNEPR Maximum Quasi-static and Dynamic Accelerations at SC/LV interface ..	37
Table 9 – DNEPR Amplitude of Harmonic Oscillations at SV/LV Interface. Longitudinal Axis	37
Table 10 – DNEPR Amplitude of Harmonic Oscillations at SC/LV Interface. Lateral Axes (Y, Z)	38
Table 11 – DNEPR Spectral Density of Vibro-accelerations at SC/LV Interface	38
Table 12 – DNEPR Acoustic Loads	39
Table 13 – DNEPR Shock Spectrum at Spacecraft Attachment Points / Number of shock impacts is contingent on a number of spacecraft installed in the SHM	39
Table 14 – Types of Satellites classified by mass	42
Table 15 – Mass Distribution	44
Table 16 – Satellite parts masses	50
Table 17 – Payload masses and percentages	57
Table 18 – Subsystems volumes, masses, densities and percentages	58
Table 19 – Center of Gravity location	59
Table 20 – Skewness Criteria [30]	64
Table 21 – Final mesh parameters	64
Table 22 – Tray A meshing parameters	67
Table 23 – Trays B and C meshing parameters	68
Table 24 – Tray D meshing parameters	69
Table 25– Spars meshing parameters	70
Table 26 – Plates meshing parameters	71
Table 27 – Subsystems and payload meshing parameters	72
Table 28 –Static Loads Setup	73
Table 29 – Harmonic Setup	74
Table 30 – Participation Factor Calculation – X Direction	81
Table 31 – Participation Factor Calculation – Y Direction	81
Table 32 – Participation Factor Calculation – Z Direction	81
Table 33 – Set up Conditions	88

1 Introduction

Artificial Satellites are manmade objects put into orbit. They are used for a large number of purposes. Its objectives range from earth observation to telecommunications or space exploration.

Without satellites we would be lost. Without satellites we would not know how the world looked like, we would not know even how to travel. Satellites are a very important part of our lives. Nowadays we depend on them. We live connected, and satellites are the links. They help us out in almost every task in our lives, making everything easier, faster and more reliable. With them, we are no longer at the mercy of hurricanes, storms and droughts. Patterns in weather are no longer unpredictable and we can establish communications with almost everyone in the planet, whether in a modern city or in the middle of a desert.

2 Objective and Scope

The objective of this Final Project is the structural design of a small cube-shaped satellite. Its primary structure should endure all launching vibrations. To fulfil that objective, a 3D Model of the satellite and a dynamic analysis must be done.

The satellite has been designed as a multipurpose platform, so it can satisfy all possible client requirements in order to put different payloads into orbit. To begin with, a general satellite with an arbitrary payload has been designed with the future intention to adapt the current design to each client if necessary.

To address the problem the following procedure has been used. First, and with a multi-platform CAD/CAM/CAE commercial software suite called CATIA (Computer Aided Three-Dimensional Interactive Application) a Computer Aided Design Model must be designed. Later, once the parameterized model is created, the engineering simulation software (CAE) ANSYS will be used to study the structural behaviour of the satellite during launch.

The scope of this project is to design a multipurpose satellite bus that satisfies the conditions of the ASAP Document (see Section 6.1). That is, a satellite which can withstand all inertial forces and loads during launch in the 0–100 Hz spectrum, with a correctly aligned center of gravity, small enough moments of inertia, and with its natural frequencies above a certain value for each axis.

The bus must fulfil the specifications given by the corresponding launch vehicle¹ manufacturer, so to choose the launch vehicle, a comparative study has been made between the different options evaluating reliability, availability of the information offered and payload requirements. Once this study has been carried out, the most restrictive launcher has been selected. This has been done in order to be able to use a wider range of LV.

¹ A launch vehicle is rocket is a rocket used to carry a payload from Earth's surface to outer space.

3 Motivation

In this section the main reasons why this project has been carried out are explained. The motivations behind this Final Project could be divided in two types, technical and academic.

3.1 Technical Motivation

A rigid structure is essential for any spacecraft to complete its mission. It is designed to act as a containment for all subsystems and maintain structural integrity against axial loading, strain, torsion and buckling.

Anything that has mass must carry structural loads due to inertia forces when accelerated, and launching vibrations shake the whole satellite violently in a wide range of frequencies. The satellite must survive the noise and subsequent vibration of the rocket engines and launch-pad environment, the agitation and bouncing of the transonic phase of the trajectory, pyroshock as stages separate, turbulent boundary layer... All of them trying to prevent its correct functioning and insertion into orbit. Due to all the above, a correct structural design is essential for the mission success.

The resonance problem is one of the main issues in satellite structural design. The Structural Subsystem must be designed so the amplitude peak during frequencies near resonance is avoided or, at least, dampened.

3.2 Academic Motivation

The Final Project is the culmination of the learning studies taken where the skills acquired are reflected, as well as their application and development. This is a research or application paper where students, according to their professional interests and motivations, delve into some aspect of the chosen specialization.

This Final Project is done to fulfil the requirements of the Aeronautical Engineering Degree imparted by the Universitat Politècnica de València.

4 Project Overview

Section 2 is a description of the scope of this project and includes a brief summary of the different goals as well as the method followed in the design process. In section 4 there is a technical and an academic motivational explanation about this project.

In section 4 there is a review of the already existing microsatellites similar to the one to be designed in this project. It is important to mention the “boom” of these kinds of satellites in the last years. This spontaneous growth is mainly due to the advantages that these types of satellites present. They are cheap, simple and reliable. That is why the university world and “small companies” have focused on these types of solutions for their space needs.

Section 6 will present the launch vehicles which are capable of putting the microsatellite into orbit and their manufacturer regulations which give the specifications that the payload of the rocket (in this case the satellite) has to fulfil to be certified for its launching.

Section 7 will explain briefly what a microsatellite is: the criteria for classifying them, what are they used for nowadays and the different subsystems that guarantee the proper operation of satellites in the space environment.

In section 8 there is a description of the geometric modelling performed to obtain the frame structure. Also, the different embedded subsystems and the payload are modelled to integrate them into the assembly and their mass is estimated from the mass distribution of similar satellites.

The next section, number 9, is a compendium and a report of the Finite Element Method (FEM). It describes the type of mesh used in the model and describes the materials used. Also, an analysis of the mesh quality of every part of the structure (separately and together) has been carried out.

Number 10 is the presentation of the results. First, the graphs and figures of the static analysis, then, the modal properties of the structure, and finally the harmonic response of the satellite as well as a compendium of the solutions adopted. In section 11 the conclusions of the Final Project are exposed.

Lastly, recommendations for Further Work are shown (number 12). Possible future analyses starting from the point where this project ends are explained. In the last pages of the document the references, bibliography and planes documentation are denominated and numerated.

5 Background on Satellite Missions

In the last two decades many universities around the world as well as many companies have gone on the adventure of designing, manufacturing and launching their own microsatellites.

The goal of the universities is mainly academic because of the knowledge that the mission itself gives, but also encourages research, with the inclusion of some experiments for microgravity environment, and for technology demonstration, employing some subsystems specifically designed for the mission.

On the other hand, companies have a more commercial objective offering a wide range of products and services such as space photography, earth observation...

In the following subsections some examples of microsatellites that have similar characteristics as the spacecraft of this project will be shown.

5.1 UPMSAT

On 7th July 1995 a small Spanish university satellite called UPM-Sat 1 was launched from French Guiana, which travelled into space as secondary payload in the V75 Flight onboard an Ariane IV-40 Launcher. [1] and [2].

Since then, the UPM-Sat 1 (shown in Figure 5.1), whose operative orbit life was of 213 days, follows a heliosynchronous polar orbit circling Earth every 98 minutes.

UPM-Sat 1 is a scientific and technological demonstration satellite, and also has educational purposes. Given these educational purposes, the first objective of the mission was the satellite itself. This was, to check the ability of the Polytechnic University of Madrid to design, develop, build, test, integrate and operate a humble spacecraft with all the complexity of a complete space system. UPM-Sat weighted 50 kg.

In addition to this, there were other objectives related to using liquid bridges as space accelerometers and making the satellite a technological space demonstration platform.

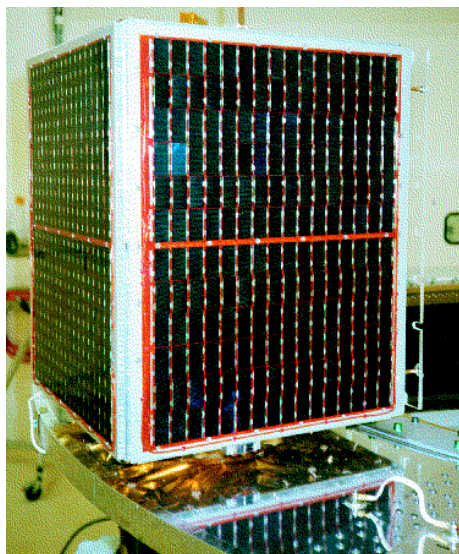


Figure 5.1 – UPM-Sat 1 [3]

5.2 ANUSAT

The Anna University Satellite (ANUSAT) is an Indian student research microsatellite designed, developed and integrated at Madras Institute of Technology belonging to Anna University. It carries an amateur radio and technology demonstration experiments. It was successfully launched aboard an Indian PSLV-CA (Polar Satellite Launch Vehicle) designated PSLV-C12, along with RISAT-2, from the Second Launch Pad at the Satish Dhawan Space Centre on 20 April 2009.

The satellite's development was sponsored by the Indian Space Research Organisation (ISRO), who were also responsible for launch services.

ANUSAT (displayed in Figure 5.2) is a 38 kg cube shaped satellite with sides of 600 mm long. It operated at 40W power with body mounted GaAs cells. All communications to and from ANUSAT were carried out in the VHF/UHF band amateur radio store and forward communications system. It is orbiting at a height of 547 km with a 41 degree inclination and a period of 120 minutes. This satellite is spin stabilised and its spin axis is pointed perpendicularly towards the sun.

The main objective of the ANUSAT project was to enable students of Anna University to gain experience in the design, building, testing and operation in orbit of a complete microsatellite.

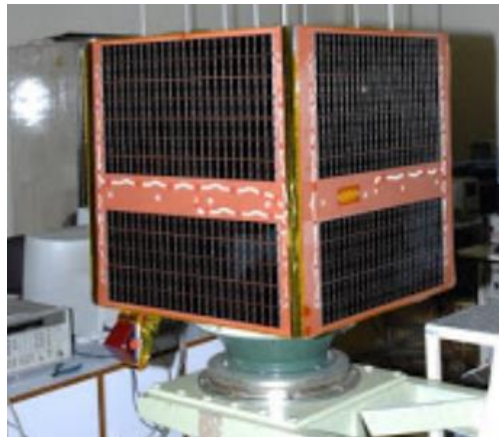


Figure 5.2 – ANUSAT [4]

5.3 SUNSAT

The Stellenbosch UNiversity SATellite (SUNSAT) is the first miniaturized satellite designed and manufactured in South Africa. It was launched aboard a Delta II rocket from the Vandenberg Air Force Base on 23 February 1999. SUNSAT was built by post-graduate engineering students at the University of Stellenbosch.

SUNSAT (shown in Figure 5.3) is a cube shaped satellite with sides of 45x45x60 cm long and with a mass of 64 kg [5]. Its payload includes NASA experiments, amateur radio communications, a high resolution imager, accurate attitude control and school experiments.

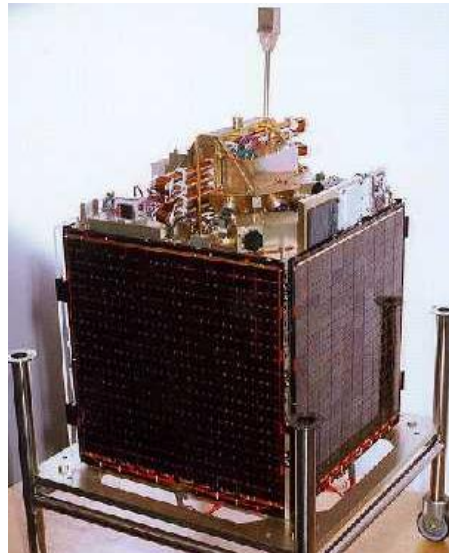


Figure 5.3 - SUNSAT [5]

5.4 SSTL MicroSat Family

SSTL (Surrey Satellite Technology LTD) is an independent British company within the Airbus Defence and Space group. The company is leading the low cost access to space providing complete in-house design, manufacture, launch and operation of small satellites.

Specifically the MicroSat-70 and MicroSat-100 models are the most similar to the satellite of this project. Those platforms are a flexible modular design capable of supporting a wide range of mission in LEO, from earth observation to communications and technology demonstration missions for civil and military use.

Mechanically, the MicroSat Family consists of a stack of modular trays, containing all avionics and some of the payload electronics. These trays form the mechanical structure of the spacecraft, providing a very efficient use of the internal volume. Above the main module stack is a payload bay dedicated to the mission payloads.

SSTL use the MicroSat-70 platform for missions ranging from 50 to 70 kg total mass with payloads of up to 25 kg. On the other hand, the MicroSat-100 expanded the range of SSTL's modular microsatellite to missions of 70 to 130 kg total mass, with a typical payload mass up to 40 kg [6].

They are compatible with an extremely wide range of launch vehicles, and have been successfully launched on Ariane 4, Zenit, Kosmos, Tsyklon, Athena and Dnepr.

Within this type of satellites family, Demos 1 satellite must be highlighted. The external configuration of Deimos 1 can be seen in Figure 5.4.

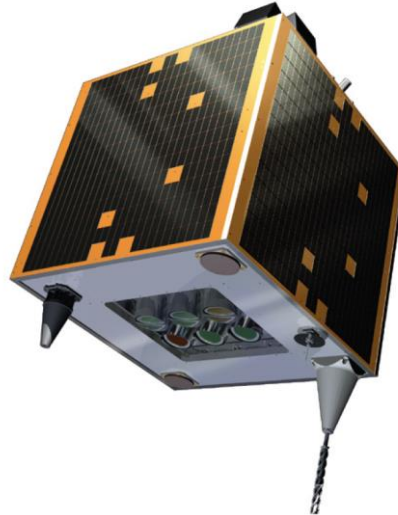


Figure 5.4 – SSSL MicroSat [6]

Deimos 1 is a small Earth observation satellite, which was built by SSSL to be launched in 2009. It is part of the Disaster Monitoring Constellation (DMC). The satellite provides imagery for commercial applications, for government use and for rapid-response following disasters.

The satellite has an expected lifetime of five years [6]. It carries a multi-spectral imager with a resolution of 22 metres and 600 kilometres of swath, operating in green, red and near infrared spectra. The contract covered the provision of the ground system to allow operation of the satellite from Valladolid, Spain and it established SSSL as the launch agent for procurement of launch services.

The launch was conducted by ISC Kosmotras, who used a Dnepr-1 carrier rocket, with DubaiSat-1 as the primary payload. The rocket was launched on 29 July 2009, from the Baikonur Cosmodrome in Kazakhstan.

This contract is Deimos' first step into satellite ownership. Since it was formed in 2001, Deimos has grown rapidly to become one of Europe's leading space consultancies with over 200 staff.

5.5 TATYANA 1

Tatyana is a 31 kg microsatellite manufactured by Production Corporation "Polyot" (Omsk, Russia) in the interests of Lomonosov Moscow State University. Tatiana-1 was launched by a Kosmos-3M on 22 January 2004 on the eve of the University's 250th anniversary [7].

The scientific equipment of Tatyana was developed for the detection and registration of abnormal physical phenomena resulting from seismic activity, for their operative analysis and selection of strong earthquake precursors, and also for global monitoring of abnormal seismogenic phenomena and their consequences.

The Tatyana (see Figure 5.5) satellite was tracked by two ground stations, in Kaluga and in Moscow State University. On 6 March 2007, the satellite stopped transmitting data.



Figure 5.5 - TATYANA 1 [7]

5.6 Oculus-ASR

Aerospace Enterprise, a student organization at Michigan Technological University, designed and build the Oculus-ASR microsatellite to improve to exercise and validate techniques for determining an orbiting object's pose using unresolved ground imagery.

Oculus-ASR is a 70 kg satellite with a volume envelope of 50 cm by 50 cm by 80 cm [8]. It consists of two modules that are permanently attached. An octagonal module, referred to as the Oculus module, sits atop a square module, known as the ASR module.

The Oculus-ASR will perform coordinated manoeuvres during overflights of the Air Force Maui Optical Site (AMOS), which is an array of mountain-top telescopes used to inspect orbiting objects. AMOS investigators will attempt to determine the orientation and shape of the vehicle and will compare these measurements with the actual "truth" data that is downloaded from the satellite. The vehicle has the capability to change its shape by deploying panels to exercise the AMOS algorithms and see if ground observers can detect the shape changes. The Oculus-ASR also carries two sensitive imaging cameras that were donated by SAIC and Raytheon Missile Systems. These cameras will be used to gather space-to-space images of other orbiting objects that can then be compared with the ground-to-space images obtained by AMOS.

Oculus-ASR was selected as the winner of the sixth University Nanosat mission for launch in 2013 as piggy-back payload on a Falcon 9 but the launch was probably delayed until 2016 [9]. Its preliminary design is described in Figure 5.6.

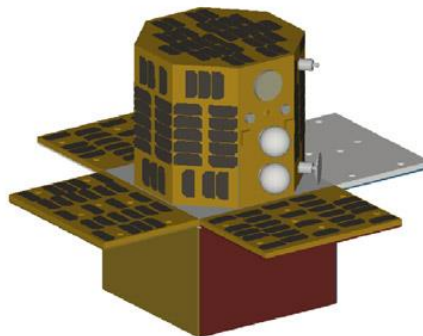


Figure 5.6 - Oculus ASR [8]

5.7 HiakaSat

HiakaSat (Hyperspectral Imaging, Aeronautical Kinematic Analysis Satellite), also known as HawaiiSat 1, is a 55 kg microsatellite mission developed by students of the University of Hawaii, Honolulu (Ma-noa) [9].

The mission has the following goals: establish a cost effective on-orbit platform for performing technology demonstrations, perform remote sensing with the newly designed Space Ultra-Compact Hyper-spectral Imager (SUCHI), perform imaging with two HSFL (Hawaii Space Flight Laboratory) colour cameras which are co-aligned with SUCHI and provide workforce development opportunities for students and recent graduates.

Originally the HawaiiSat 1 mission was to be built on a larger bus and was to feature the THI (Thermal Hyperspectral Imager) payload so it was to weigh 80 kg. Later during development, the available mass was cut to 40 kg, and finally raised to 55 kg. Therefore the HawaiiSat 1 structure was cut almost in half and the THI payload was replaced by the light weighted SUCHI. This redesigned satellite was renamed HiakaSat.

HiakaSat (shown in Figure 5.7) will be launched as the prime payload of the new low-cost Super-Strypi launch vehicle from Kauai in 2015.

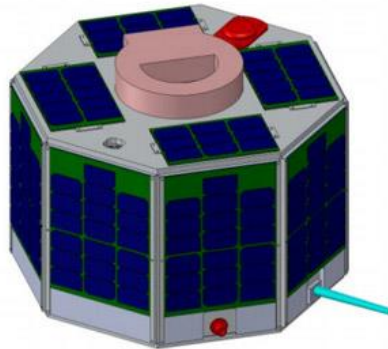


Figure 5.7 – HiakaSat [9]

5.8 DANDE

DANDE (Drag and Atmospheric Neutral Density Explorer) is a low-cost 50 kg satellite which makes in-situ measurements at altitudes of 200 – 350 km of the neutral atmosphere. It was developed at the University of Colorado at Boulder (CU) as a part of the Air Force sponsored University Nanosat Programme [10].

DANDE is the first spacecraft to be specifically designed to measure winds, drag, and number densities simultaneously. These measurements will reduce the uncertainty in drag-deduced density values especially during storms when in-track winds can contribute significantly to spacecraft drag. To accomplish this, DANDE will carry a novel drag measuring system as well as a Wind and Temperature Spectrometer which will characterize the horizontal wind vector. The project is a joint venture between Colorado Space Grant Consortium and the Aerospace Engineering Sciences department wherein students design and build the hardware under the mentorship of faculty, government and industry advisors.

It was launched as a “piggyback” payload on the maiden flight of the Falcon 9 v1.1 launch vehicle on 29th September 2013. The spacecraft is expected to be operational for about 1.5 years before solar radiation disables DANDE's communication abilities. According to STK analyses, DANDE will be in orbit for about 18 more years before it burns up in the atmosphere as it re-enters.

5.9 Rising 2

Rising-2 is a cooperative microsatellite project of Tohoku University (Sendai) and Hokkaido University, Sapporo, Japan. The primary objective of the mission is Earth observation with a resolution of 5 m, the highest in the world among 50 kg-class satellites.

The spacecraft structure is cube-shaped with a side length of 50 cm and a launch mass of 42 kg [11]. The central pillar configuration shown in Figure 5.8 is inherited from SpriteSat, using an aluminum alloy material for the central pillar and the side panels.

The Rising-2 microsatellite (displayed in Figure 5.8) was launched as a secondary payload on May 24, 2014 on a H-IIA vehicle from the Tanegashima Space Center, Japan. The launch provider was Mitsubishi Heavy Industries and the primary payload on this flight was the ALOS-2 spacecraft of JAXA.



Figure 5.8 – Rising 2 [11]

6 Regulations

There are not any national regulations in structural criteria for satellite loading during launch. Every LV has its own vibrations, loads and dimensional requirements. They are very similar between them giving information as that the natural frequencies of the satellite must be bigger than certain value and that low spectrum vibrations could be analysed as harmonic loads. Other parameters regulated by this type of documents are the position of the centre of gravity of its payload, the maximum moments of inertia or the shocks inducted by the stages separation. In the following sections step by step analyses of the different requirements of the launchers will be done.

6.1 Ariane-5 Regulations

Ariane 5 is a European rocket that is a part of the Ariane rocket family, an expendable launch system used to deliver payloads into geostationary transfer orbit (GTO) or low Earth orbit (LEO). Ariane 5 rockets are manufactured under the authority of the European Space Agency (ESA) and the Centre National d'Etudes Spatiales (CNES) [12].

In its document called Ariane 5 User's Manual [12], it presents the loads and vibrations that the satellite will suffer in its launch. On the other hand the ASAP-5 (Ariane Structure for Auxiliary Payload) User's Manual [13] describe, among other things, the dimensioning and qualification of micro auxiliary payloads (≤ 120 kg).

6.1.1 Center of Gravity Position

The center of gravity position requirements for the Soyuz launcher are the following:

- In the longitudinal axis: ≤ 450 mm from mounting plane of the spacecraft
- In the lateral axes: $\leq \pm 5$ mm

6.1.2 Inertia

The inertia requirements for the Soyuz launcher are that in all axes the moments of inertia must be less or equal than 20 kg m^2 (wrt CoG)

6.1.3 Dimensions

The maximum cross-section dimensions for the Micro Auxiliary Payload are $600 \text{ mm} \times 600 \text{ mm}$ (600 mm in both the tangential and radial directions).

The typical allowable height is 710 mm . This dimension can be adjusted on a case by case basis depending on the main passenger for the configuration with 8 microsats.

6.1.4 Natural Frequency Requirements

To avoid dynamic coupling between the low frequency vehicle and spacecraft modes, the spacecraft should be designed with a structural stiffness which ensures that the fundamental frequencies of the spacecraft fulfil the following criteria for micro auxiliary payloads.

- In the longitudinal axis: ≥ 90 Hz.
- In the lateral axes: ≥ 45 Hz.

As a curiosity, In the case of mini auxiliary payloads (≤ 300 kg), the structural stiffness must ensures the following fundamental frequencies:

- In the longitudinal axis: ≥ 60 Hz.
- In the lateral axes: ≥ 30 Hz.

6.1.5 Quasi-static Loads

During flight, various static and dynamic loads are superimposed. The design and dimensioning of the satellite primary structure must therefore allow for the most severe load combination that can be encountered at a given instant of flight.

The flight limit loads for micro auxiliary payloads are given in the following list:

	Longitudinal (Static + Dynamic)	Lateral (Static + Dynamic)
Acceleration [G]	-7.5/+5.5	-6/+6

Table 1 – Ariane 5 Quasi static loads

Notes:

- Lateral loads may act in any direction simultaneously with longitudinal loads.
- Loads applied on payload’s center of gravity.
- The gravity load is included.
- Dimensioning must take into account safety factors, which are defined by the spacecraft authority, with a minimum requested value of 1.25 at ultimate stress and 1.1 at yield stress.
- Should the adequacy of the structure be demonstrated by a dimensioning file analysis, a minimum requested safety factor of 2.0 shall apply.

6.1.6 Sine-equivalent dynamics

Sinusoidal excitations affect the LV during its powered flight, mainly the atmospheric flight, as well as during some of the transient phases.

The qualification levels, applied at the interface plane, are given in the following table.

	Frequency range (Hz)	Qualification levels (0 - peak)	Acceptance level (0 - peak)
Longitudinal	4 - 6	25 mm	20 mm
	6 - 100	3.75 G	3 G
Lateral	2 - 6	20 mm	16 mm
	6 - 100	2.5 G	2 G

Table 2 – Ariane 5 Sine Equivalent Dynamics Ariane 5

The sweep rate required for this test in Qualification is 2 octaves per minute and 4 in Acceptance.

6.1.7 Random vibration

The random vibration tests must be performed along the 3 satellite axes and its durations are two minutes per axis for qualification. The random vibration test levels for the qualification are $0.0727 G^2/\text{Hz}$ flat power spectral density between 20 Hz and 2000 Hz.

6.1.8 Shocks

The micro Auxiliary payload is subjected to shocks during interstages separations, fairing and carrying structures jettisoning and on actual payload separation. The microsat and in particular its equipment, must therefore demonstrate its ability to withstand the shock specified in the Figure 6.1.

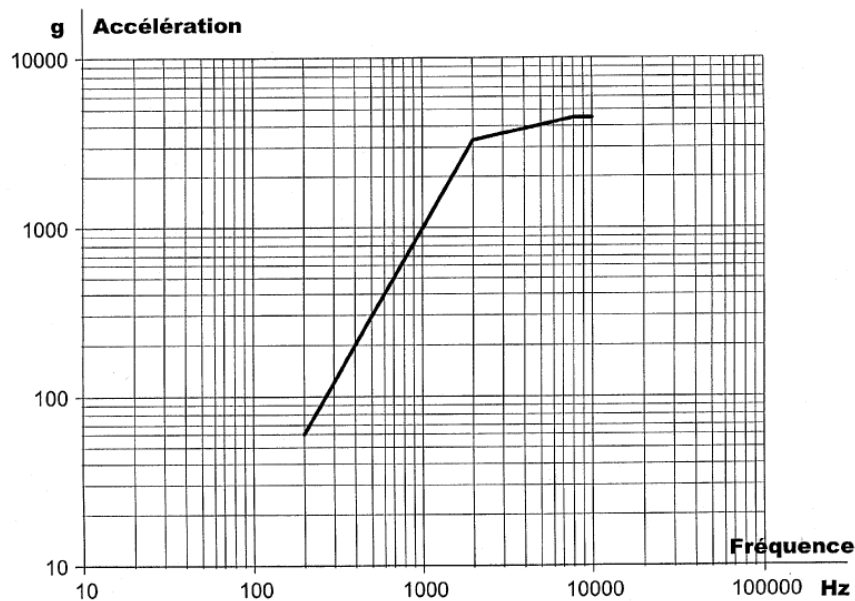


Figure 6.1 – Ariane 5 Acceleration vs Frequency of the Shock [12]

6.2 Soyuz Regulations

Soyuz is a family of expendable launch systems developed by OKB-1, and manufactured by TsSKB-Progress in Samara, Russia. According to the European Space Agency, the Soyuz launch vehicle is the most frequently used launch vehicle in the world.

The Soyuz vehicles are used as the launcher for the manned Soyuz spacecraft as part of the Soyuz programme, as well as to launch unmanned Progress supply spacecraft to the International Space Station and for commercial launches marketed and operated by Starsem and Arianespace. For micro satellites, the document used for the regulations is the ASAP-S

In its document called Soyuz User's Manual [13], it presents the loads and vibrations that the satellite will suffer in its launch. On the other hand the ASAP-S (Ariane Structure for Auxiliary Payload – Soyuz) User's Manual describe, among other things, the dimensioning and qualification of micro auxiliary payloads (≤ 200 kg).

6.2.1 Center of Gravity Position

The center of gravity position requirements for the Soyuz launcher are the following:

- In the longitudinal axis: <700 mm from mounting plane of the spacecraft
- In the lateral axes: <±5 mm

6.2.2 Inertia

The inertia requirements for the Soyuz launcher are:

- In the longitudinal axis: <60 m² kg (wrt CoG)
- In the lateral axes: <120 m² kg (wrt CoG)

6.2.3 Dimensions

The dimensional envelope necessary to meet the secondary payload rocket requirements is the following:

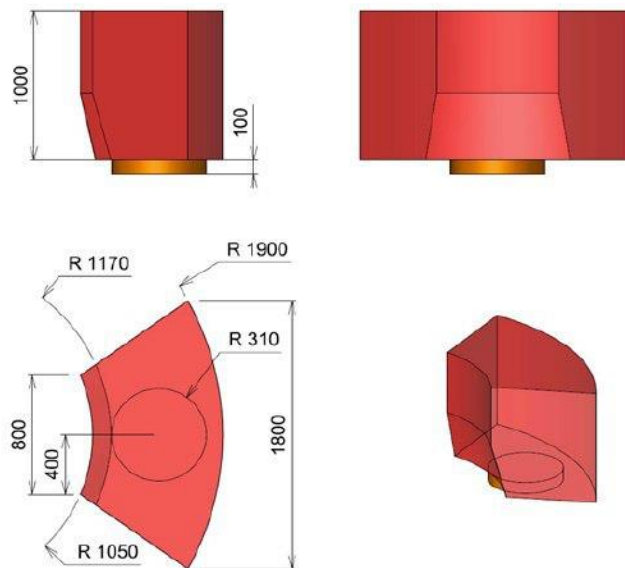


Figure 6.2 – Soyuz Dimensional Envelope Soyuz [mm] [13]

6.2.4 Natural Frequency Requirements

To prevent dynamic coupling with fundamental modes of the LV, the spacecraft should be designed with a structural stiffness which ensures that the following requirements are fulfilled [14].

- In the longitudinal axis: ≥ 90 Hz.
- In the lateral axes: ≥ 35 Hz.

6.2.5 Quasi-static Loads

During ground operations and flight, the spacecraft is subjected to static and dynamic loads. Such excitations may be of operational origin (e.g. transportation or mating), aerodynamic origin (e.g. wind and gusts or buffeting during transonic phase) or propulsion origin (e.g.

longitudinal acceleration, thrust buildup or tail-off transients, or structure-propulsion coupling, etc.).

The design and dimensioning of the satellite primary structure must therefore allow for the most severe load combination that can be encountered at a given instant.

The flight limit loads for micro auxiliary payloads are given in the following list:

	Longitudinal (Static + Dynamic)	Lateral (Static + Dynamic)
Acceleration [G]	-5.75/+3.6	±3.4

Table 3 – Soyuz Quasi-Static Loads Soyuz

Notes:

- Lateral loads may act in any direction simultaneously with longitudinal loads.
- Loads applied on payload’s center of gravity.
- The gravity load is included.
- Dimensioning must take into account safety factors, which are defined by the spacecraft authority, with a minimum requested value of 1.3 at ultimate stress and 1.1 at yield stress.

6.2.6 Sine-equivalent dynamics

Sinusoidal excitations derived from motors pressure oscillations and controlled POGO effect may affect the LV during its flight (mainly the atmospheric flight), as well as during some of the transient phases of the flight.

The qualification levels, applied at the interface plane, are given in the following table.

	Frequency range (Hz)	Qualification levels (0 - peak)
Longitudinal	4 – 6	25 mm
	6 – 100	3.75 G
Lateral	2 – 6	20 mm
	6 – 100	2.5 G

Table 4 – Soyuz Sine-equivalent dynamics Soyuz

The sweep rate required for this test is 2 octaves per minute. The qualification test is one sweep through the specified frequency range along each axis.

6.3 VEGA Regulations

Vega is an expendable launch system in use by Arianespace jointly developed by the Italian Space Agency and the European Space Agency. Development began in 1998 and the first launch took place from the Guiana Space Centre on 13 February 2012.

It is designed to launch small payloads from 300 to 2,500 kg for scientific and Earth observation missions to polar and low Earth orbits. The reference Vega mission is a polar orbit bringing a spacecraft of 1,500 kilograms to an altitude of 700 kilometres [16].

6.3.1 Center of Gravity Position

The pointing at separation can be specified by the Customer in any direction fixed in the inertial coordinate system for the entire launch window. The AVUM on-board control system may adjust the separation attitude with regard to the actual lift-off time if required. The spacecraft separation can be performed in various modes:

- 3-axis stabilization;
- Spin stabilization.

The typical attitude accuracy after separation for both three-axis stabilized and spin mode are given assuming that the spacecraft balancing characteristics are in accordance with Section 4 and the standard separation system is used. Possible perturbations induced by spacecraft sloshing masses are not considered.

The LV axis system O, X, Y, Z, the spacecraft CoG must be located within a distance:

- Less than 15 mm from the longitudinal axis OX for the spin-up stabilisation and
- Less than 30 mm for 3-axis stabilization.

If the Spacecraft is outside this domain, Arianespace should be contacted.

6.3.2 Inertia

There is no predefined requirement for spacecraft dynamic balancing with respect to ensuring proper operation of the LV. However, these data have a direct effect on spacecraft separation. To ensure the separation conditions in spin-up mode described in the Chapter 2, the maximum spacecraft dynamic unbalance ε corresponding to the angle between the spacecraft longitudinal geometrical axis and the principal roll inertia axis shall be: $\varepsilon \leq 1$ degree [16].

6.3.3 Sine-equivalent dynamics

Sinusoidal excitations derived from motors pressure oscillations and controlled POGO effect may affect the LV during its flight (mainly the atmospheric flight), as well as during some of the transient phases of the flight.

The envelope of the sinusoidal (or sine-equivalent) vibration levels at the spacecraft base does not exceed the values given in Table 4:

	Frequency Range (Hz)	Sine Amplitude [G]
Longitudinal	5 - 45	0.8
	45 - 100	1.0
Lateral	5 - 25	0.8
	25 - 100	0.5

Table 5 - VEGA Sine Equivalent dynamics VEGA

6.3.4 Random vibration

For payload above 300 kg, the broadband vibrations are covered by the acoustics.

6.3.5 Acoustic vibration

6.3.5.1 On ground

The noise level generated by the venting system does not exceed 94 dB.

6.3.5.2 In flight

Acoustic pressure fluctuations under the fairing are generated by engine operation (plume impingement on the pad during lift-off) and by unsteady aerodynamic phenomena during atmospheric flight (i.e., shock waves and turbulence inside the boundary layer), which are transmitted through the upper composite structures. Apart from lift-off and transonic/Q max flight, acoustic levels are substantially lower than the values indicated hereafter.

The envelope spectrum of the noise induced inside the fairing during flight is shown in Table 6. It corresponds to a space-averaged level within the volume allocated to the spacecraft stack, as defined in Chapter 5 of [15].

This maximum environment is applied during a period of approximately 30 seconds.

It is assessed that the sound field under the fairing is diffuse and spacecraft have a minimum acoustic absorption characteristics.

Frequency range (Hz)	Sine Amplitude [G]
31.5	124
63	129
125	135
250	132
500	1131
1000	120
2000	100
OASPL (20-2828 Hz)	

Table 6 – VEGA Acoustic Noise Spectrum under the Fairing
 Note: OASPL – Overall Acoustic Sound Pressure Level
 These values do not take into account any fill factor correction

6.3.6 Shocks

The spacecraft is subject to shock primarily during stage separations, fairing jettisoning, and actual spacecraft separation. The envelope acceleration shock response spectrum (SRS) at the spacecraft base (computed with a Q-factor of 10) is showed in Figure 6.3.

These levels are applied simultaneously in axial and radial directions.

The dimensioning shock event is the payload separation.

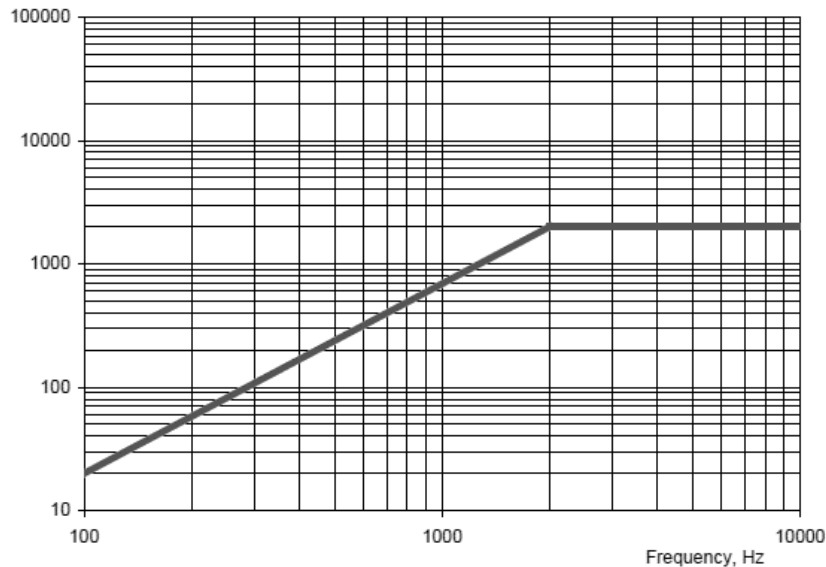


Figure 6.3 – VEGA Envelope acceleration Shock Response Spectrum (SRS) at the spacecraft base [15]

6.4 DNEPR Regulations

The Dnepr rocket is a space launch vehicle named after the Dnieper River. It is a converted R-36M ICBM used for launching artificial satellites into orbit, operated by launch service provider ISC Kosmotras. The first launch, on April 21, 1999, successfully placed UoSAT-12, a 350 kg demonstration mini-satellite, into a 650 km circular Low Earth orbit.

The Dnepr launch vehicle has only a small number of modifications compared to the R-36M ICBM in service. The main difference is the payload adapter located in the space head module and modified flight-control unit. This baseline version can lift 3,600 kg into a 300 km low earth orbit at an inclination of 50.6° , or 2,300 kg to a 300 km sun-synchronous orbit at an inclination of 98.0° [17]. On a typical mission the Dnepr deploys a larger main payload and a secondary payload of miniaturized satellites.

6.4.1 Natural Frequency Requirements

The spacecraft should be designed with a structural stiffness, which ensures that the values of fundamental frequency of the spacecraft, hard mounted at the separation plane, are safe for the operation [17].

- In the longitudinal axis: ≥ 20 Hz.
- In the lateral axes: ≥ 10 Hz.

6.4.2 Quasi-static Loads

Spacecraft sizing and testing must take into account safety factors, which are defined by the spacecraft authority, but should be no less than the values given that follow:

- 2.0 for ground handling.
- 1.5 during launch while LV is moving inside the TLC.
- 1.3 during launch after the LV exits from the TLC.
- 1.3 during the LV flight.

Accelerations at SC/LV Interface during transportation are shown in Table 7:

Load Source	Acceleration [G]		
	Longitudinal (X)	Lateral (Y)	Lateral (Z)
SHM Transportation	±0.4	-1.0±0.7	±0.5

Table 7 – DNEPR Accelerations at SC/LV interface during transportation

Note that Russian use another system of reference criteria, using X as the longitudinal axis and z as one of the lateral axes. The Table 8 hoards all the rest load sources for the maximum quasi static and dynamic accelerations.

Load Source	Acceleration [G]	
	Longitudinal (X)	Lateral (Y, Z)
LV Movement inside TLC	±0.4	-1.0±0.7
After LV exit from TLC	±1.0	±0.8
1 st Stage burn:		
Maximum dynamic head	3.0±0.5	0.5±0.5
Maximum longitudinal acceleration	7.5±0.5	0.1±0.5
2 nd stage burn – maximum longitudinal acceleration	7.8±0.5	0.2
3 rd stage burn	-0.3...-0.5	0.25

Table 8 – DNEPR Maximum Quasi-static and Dynamic Accelerations at SC/LV interface

Some aspects to consider are that the lateral accelerations may act in any direction, simultaneously with longitudinal ones; the above values are inclusive of gravity force component; dynamic accelerations are preceded by "±" symbol and that the above values are correct for the spacecraft complying with the fundamental frequency requirements.

6.4.3 Sine-equivalent dynamics

The harmonic oscillations are characterized by the amplitude of vibro-accelerations and frequency. The parameters of harmonic oscillations are given by Table 9 in the longitudinal axis:

Frequency sub-band [Hz]	5-10	10-15	15-20
Amplitude [G]	0.5	0.6	0.5
Duration [s]	10	30	60

Table 9 – DNEPR Amplitude of Harmonic Oscillations at SV/LV Interface. Longitudinal Axis

And in the lateral axes (see Table 10):

Frequency sub-band [Hz]	2-5	5-10	10-15
Amplitude [G]	0.2-0.5	0.5	0.5-1.0
Duration [s]	100	100	100

Table 10 – DNEPR Amplitude of Harmonic Oscillations at SC/LV Interface. Lateral Axes (Y, Z)

6.4.4 Random vibration

The random vibrations are characterized by spectral density of vibro-accelerations and the duration of influence. The random vibration parameters are given in Table 11.

The random vibrations are spatial with approximately equal intensity of vibroaccelerations in each of the three randomly selected mutually perpendicular directions.

The values of amplitude and spectral densities are given in the extreme octave points. The change of these values within the limits of each octave is linear in the logarithm frequency scale.

Frequency sub-band [Hz]	Load Source	
	Liftoff, LV flight segment where $M=1, q_{max}$	1 st stage burn (except for LV flight segment where $M=1, q_{max}$), 2 nd stage burn, 3 rd stage burn
	Spectral Density [g^2/Hz]	
20-40	0.007	0.007
40-80	0.007	0.007
80-160	0.007-0.022	0.007
160-320	0.022-0.035	0.007-0.009
320-640	0.035	0.009
640-1280	0.035-0.017	0.009-0.0045
1280-2000	0.017-0.005	0.0045
Root Mean Square Value, σ [G]	6.5	3.6
Duration [s]	35	831

Table 11 – DNEPR Spectral Density of Vibro-accelerations at SC/LV Interface

6.4.5 Acoustic vibration

The sources of acoustic loads are:

- 1st stage motor burn;
- Frame surface pressure fluctuations in the turbulent boundary layer.

The acoustic loads are characterized by the duration of action, integral level of the sound pressure within the frequency band of 20–8,000 Hz, and the levels of sound pressure within the octave frequency band with the mean geometric frequencies of 31.5; 63; 125; ...; 2,000; 4,000; 8,000 Hz.

Mean Geometric Frequency of Octave Frequency Band [Hz]	Level of Sound Pressure [dB]
31.5	125
63	132
125	135
250	134
500	132
1000	129
2000	126
4000	121
8000	115
Integral Level of Sound Pressure [dB]	140
Duration [s]	35

Table 12 – DNEPR Acoustic Loads

6.4.6 Shock

Shock loads are wide-band, fading processes and are characterized by the shock spectrum and the duration of action.

The activation of the separation pyrodevices is a source of the vibro-pulse loads at the spacecraft attachment points (the duration of shock process is up to 0.1 sec). The shock spectrum values are given in Table 13. They are accurate for the $Q=10$ and for each of the three randomly selected mutually perpendicular directions. The change of the shock spectrum values versus frequency within each sub-band is linear (in the logarithm frequency scale and shock spectrum values).

Load Source	Frequency Subband [Hz]							Number of Shock impacts
	30-50	50-100	100-200	200-500	500-1000	1000-2000	2000-5000	
Shock Spectrum Values [G]								
Separation of fairing, 3 rd stage and neighbouring spacecraft	5-10	10-25	25-100	100-350	350-1000	1000	1000	*
Separation of SC	5-10	10-25	25-100	100-350	350-1000	1000	1000-3000	1

Table 13 – DNEPR Shock Spectrum at Spacecraft Attachment Points
/ Number of shock impacts is contingent on a number of spacecraft installed in the SHM

6.5 Selection of the launcher

It has been impossible to obtain the complete documentation for the DNEPR and VEGA relative to auxiliary payload requirements. Hence, the information proportioned for both is only valid for the main satellites launched with this vehicles. With the complete documentation of the Ariane 5 in hand, it is easy to see that the requirements vary widely

between primary and secondary payloads. However, it has been observed reports that use the primary payload criteria for auxiliary payloads too.

Reliability of the four launchers analysed is high (about 97% [16]), so this has not been a determinant factor during selection.

Within the remaining two regulations, the Ariane 5 ones are the most restrictive. So it has been chosen this as the design setup of the FEM analysis.

7 Microsatellites

According to [17] the box configuration is the most common shape for small satellites. Also, starting from the point that Universities are not big private companies that could afford expensive missions, it is self-evident that this configuration is the cheapest (see [18] and [19]). Another reason is simplicity. The simpler the satellite is, the less the possibility of failure is. And box structures are the simplest geometry possible in 3D. Because of all the reasons previously explained, it has been decided the cube-shaped structural design is the optimal for this microsatellite project.

As it has been said, this project is not the first in using the box configuration, and without any doubt, it will not be the last. Microsatellites segment of satellite launch industry have been growing rapidly in recent years. Development activity in the 1–50 kg range has been significantly exceeding that in the 50–100 kg range [19].

In the 1–50 kg range alone, there were fewer than 15 satellites launched annually from 2000 to 2005, 34 in 2006, then fewer than 30 launches annually from 2007 to 2011. This rose to 34 launched in 2012, and 92 launched in 2013 [19]. So needless to say it is a growing and promising market. This trend can be observed in the graph below (Figure 7.1).

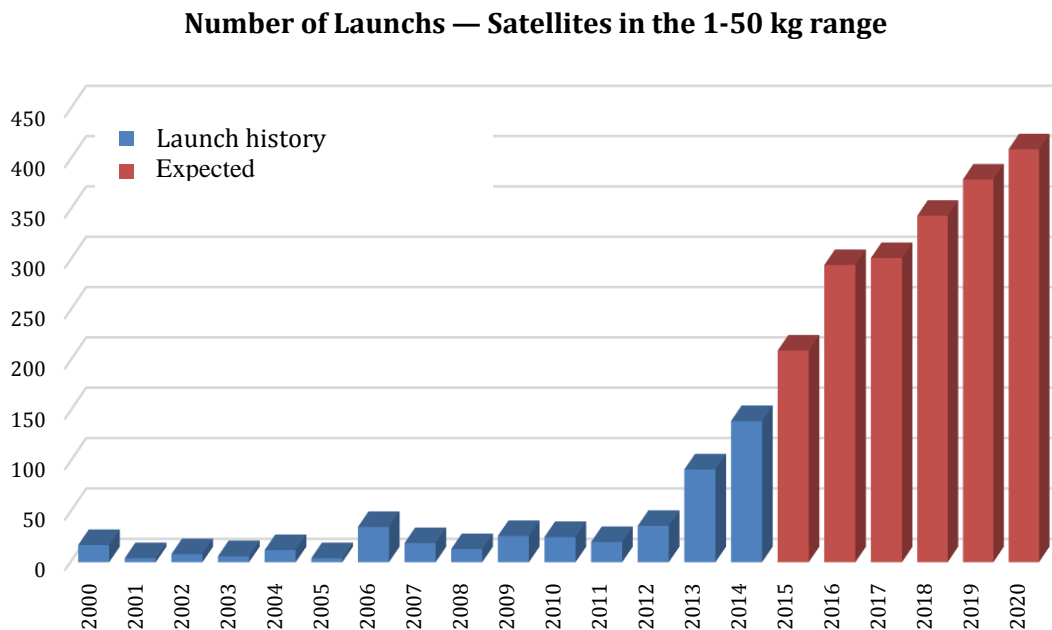


Figure 7.1 – Number of Launchs vs Time (from [19] and [20])

Although it has been said that the satellite proposed is one of "micro" type, in order to provide further information Table 14 has been created. It describes the different types of satellites classified by their masses. Also it informs of the typical altitudes for every type and gives an estimation of the average live in years of the spacecraft. One must note that the average life is closely related to the altitude of the orbit.

	Mass [kg]	Altitude [km]	Average Life [years]
Mini	100 – 500	1000 – 5000	4 – 7
Micro	10 – 100	500 – 2000	2 – 5
Nano	1 – 10	300 – 800	2 – 3
Pico	0.1 – 1	200 – 400	1 – 2
Femto	< 0.1	200 – 400	~ 1

Table 14 – Types of Satellites classified by mass

7.1 Definition

It has been pointed the main advantages this configuration has, but it has not been defined what a microsatellite is.

Microsatellites have a wet mass between 10 and 120 kg [21]: roughly between the size of a small refrigerator and a microwave. Microsatellites, also known as microsats, are popular among universities and companies who want to perform experiments in space but lack the funding to launch a conventionally sized satellite. The current cost to launch something into space is about \$5000 per kg, so launching a microsats still costs between \$50,000 and \$500,000.

Heavier satellites require larger rockets with greater thrust which also have greater costs to finance. In contrast, smaller and lighter satellites require smaller and cheaper launch vehicles and can sometimes be launched in multiples. They can also be launched as 'piggyback', using leftover capacity on larger launch vehicles. Miniaturized satellites allow for cheaper designs as well as ease of mass production, although few satellites of any size other than 'communications constellations' where dozens of satellites are used to cover the globe, have been mass-produced in practice.

7.2 Applications

There are many reasons to put something into space. Usually it is done because of the advantages that provide the orbit conditions. Such as height, velocity, absence of atmosphere...

Some applications of the satellites are the following:

- Earth observation (meteorology, environmental, geology)
- Space observation (Hubble Telescope, Webb Telescope)
- Store and forward communications
- GNSS tracking (NAVSTAR-GPS, GLONASS, Galileo)
- Science and technology (testing onboard subsystems, experiments)
- Military (espionage)

In case of microsatellites, the main applications are more limited. They are usually deployed for earth observation, telecommunications and science and technology purposes.

7.3 Subsystems

There are different classifications of the systems and subsystems onboard a satellite. Generally speaking, a satellite has two main systems. Platform and Payload. The Payload, as it will be further said, is the main purpose of the satellite. It is why it has been put into orbit. The Platform is everything else. It is formed by all the subsystems that make possible the payload to work correctly (structure, solar panels, batteries, onboard computer, attitude determination and control...) [22].

The second and more common classification is the subsystems arrangement. All basic functional groups of a satellite can be divided into different clusters by its mission in the spacecraft. Not all types of spacecraft have the same subsystems, however. For example, an atmospheric probe spacecraft may lack propulsion or controls subsystems entirely.

There are eight main subsystems that usually are onboard orbiter-class spacecraft.

- Structure Subsystem (SS)
- Command and Data Handling Subsystem (C&DHS)
- Attitude Determination and Control Subsystem (AD&CS)
- Telemetry, Tracking and Command Subsystem (TT&C)
- Electrical Power Subsystem (EPS)
- Propulsion Subsystem (PS)

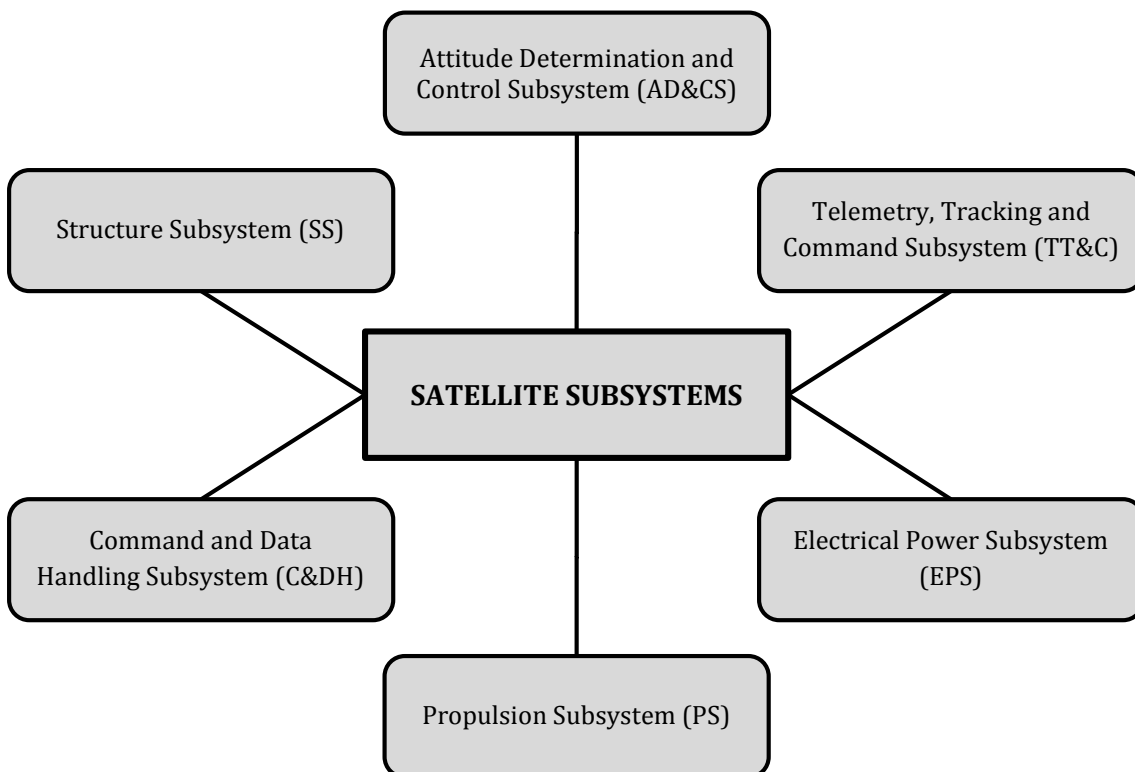


Figure 7.2 – Satellite Subsystems

7.3.1 Structure Subsystem

The Structure Subsystem provides overall mechanical integrity of the spacecraft. It must ensure that all satellite components are supported, and that they can withstand handling and launch loads as well as flight in freefall and during operation of propulsive components.

The Structure Subsystem is the backbone of the satellite. It will provide a lightweight, extremely strong chassis to house the physical satellite components.

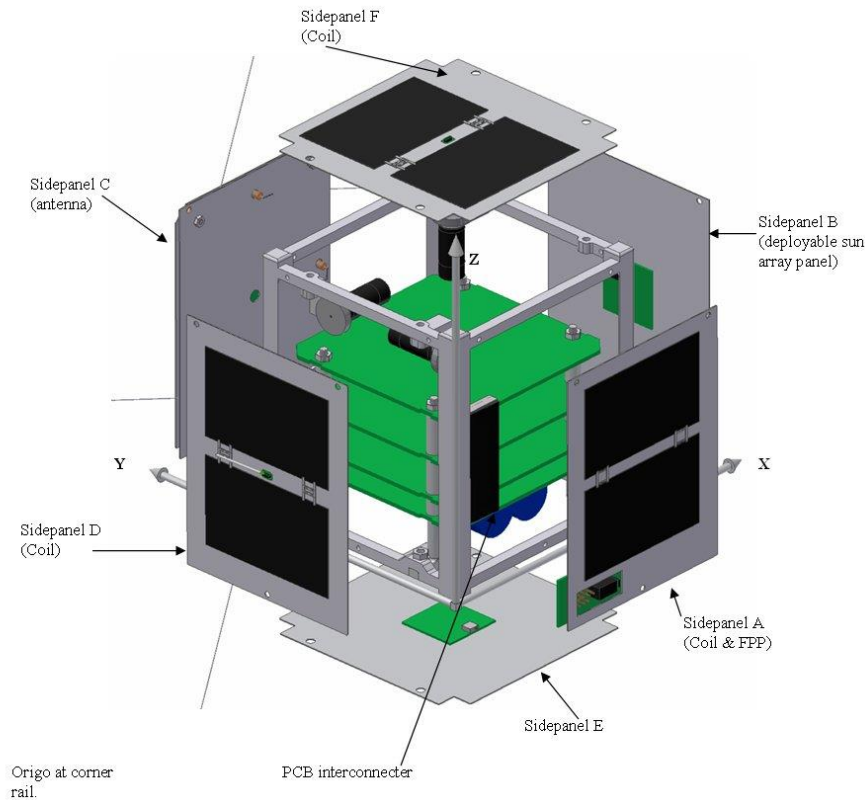


Figure 7.3 – Typical Configuration of the Structure Subsystem in cube-shaped satellites

Another detail noteworthy is the table of masses of the different subsystems. It's a crucial information to start dimensioning the satellite and to make a first estimation of the masses distribution (see Table 15).

Subsystem	Mass [kg]	Percentage [%]
ADCS ₁	2.5	5
ADCS ₂	1.5	3
ADCS ₃	1.0	2
EPS	10	20
OBDH + TC	2.5	5
PL ₁	8.1	17
PL ₂	6.3	13
PL ₃	3.6	10
TTC	2.5	5
STR	12.1	20

Table 15 – Mass Distribution

In Table 15 there are only shown the masses of the different subsystems but later, in the Section 6.5 they will be explained. Thermal Control has been contemplated within the OBDH because its influence speaking of weight is negligible. Table 15 was obtained with calculations that were based on [23] and [24]. All results were truncated to one decimal.

7.3.2 Command and Data Handling Subsystem

The Command and Data Handling Subsystem is essentially the brain of the spacecraft. It controls all satellite functions. This subsystem carries and stores data from various electronic units and the Ground Segment via the telemetry, tracking and command (TTC) Subsystem.

The modules that compose this subsystem are important for the overall design because are dense and therefore heavy, so the best location for mounting them is near the aft end. C&DHS equipment will be electrically connected to virtually all of the satellite's non-structural components therefore by grouping electronics, wiring losses and mass can be minimized [25].

Functions commonly performed by the OBDH are:

- Manages all forms of data on the spacecraft.
- Carries out commands sent from Earth.
- Prepares data for transmission to Earth.
- Manages collection of solar power and charging of the batteries.
- Collects and processes information about all subsystems and payloads.
- Keeps and distributes the spacecraft time.
- Calculates the spacecraft's position in orbit.
- Carries out commanded manoeuvres; and, autonomously monitors and responds to a wide range of onboard problems that might occur.

Depending on the type of satellite and its complexity, these functions may not all be required.

7.3.3 Attitude Determination and Control Subsystem

The Attitude Determination and Control Subsystem has two basic functions. On one hand, it is responsible for determining the real time attitude from the information given by the sensors onboard the spacecraft and previous attitude reports. On the other hand, ADCS also is tasked to actuate using the propulsion elements the satellite has and to correct possible deviations in its spatial planned orientation. Also it is in charge of doing attitude manoeuvres, that is, changing the attitude of the spacecraft from the initial state to a desired one. To do so, different propulsion and momentum elements should be used, such as torque rods, small thrusters or accelerometers and gyroscopes.

The microsatellite is preferred to be symmetric, this will reduce aerodynamic drag and solar radiation pressure, hence the net torque. To minimize this, the spacecraft's centre of mass should be as close as possible to its centre of pressure, which is the centroid of the satellite's projected area.

7.3.4 Telemetry, Tracking and Command Subsystem

Telemetry, Tracking and Command (TTC) deals with:

- Receiving control signals from the ground to initiate manoeuvres and to change the state or mode of operation of equipment.
- Transmitting results of measurements, information concerning satellite operation, the operation of equipment and verification of the execution of commands to the ground.
- Enabling measurement of the ground–satellite distance, and possibly the radial velocity, in order to permit location of the satellite and determination of orbit parameters.

On–Board Data Handling (OBDH) is often associated with the TTC subsystem. OBDH includes all housekeeping, data processing and formatting, together with data traffic and time management on board the satellite.

One of the major characteristics required of TTC links is availability. Ensuring availability of the TTC links is fundamental for diagnostics in case of breakdown and for performing corrective actions. The necessary reliability is obtained by means of suitably replicated transmitting and receiving equipment (transponders). This equipment is associated with one or more antennas which have a radiation pattern such that the gain is as constant as possible or at least, greater than a minimum value, throughout most of the space around the satellite. This permits links to be established whatever the attitude of the satellite.

7.3.5 Electric Power Subsystem

Microsatellite configuration is strongly influenced by the electric power subsystem components, especially the solar arrays. The design of solar arrays is based on the satellite's power requirements, the orbit altitude, sun–angle conditions, the method of attitude control, and mission and payload requirements. For this case, fixed solar panels mounted on the satellite body surfaces are chosen because the available surface area is enough to generate the required power [26].

The electric power to be provided is directly related to the radiofrequency power of the amplifiers in the payload as a function of their efficiency. The electric power supply subsystem consists of:

- A primary source of energy which converts energy available in another form into electrical energy (for civil applications it consists of a solar generator).
- A secondary source of energy (such as a battery of electrochemical accumulators) which is substituted for the primary energy source when this cannot fulfil its function, for example in an eclipse period.
- Conditioning (regulation and distribution) and protection circuits.

7.3.6 Propulsion Subsystem

The role of the propulsion subsystem is mainly to generate forces which act on the centre of mass of the satellite. These forces modify the satellite orbit, either to ensure injection into

a predetermined orbit or to control drift of the nominal orbit. The propulsion system also serves to produce torques to assist the attitude control system. The forces generated by the propulsion units are reaction forces resulting from the expulsion of material.

There are two classes of thruster to be considered:

- Ion power thrusters, from a few millinewtons to a few newtons, which are used for attitude and orbit control (Reaction Control System or RCS).
- Medium and high power thrusters, from several hundreds of newtons to several tens of thousands of newtons, which are used for orbit changes during the launch phase.

The specific characteristics of attitude and orbit control thrusters (RCS) are:

- Low thrust levels (several tens of millinewtons to about ten millinewtons).
- A large number of operating cycles of limited duration (a few hundred milliseconds to a few hours).
- A cumulative operating time of several hundred or thousand hours.
- A lifetime greater than 15 years.

8 Geometric Modelling

Performing a Finite Element Analysis using available tools and software is usually a 4 stem process. Firstly, the geometry has to be created. To do so, a CAD software is used. Secondly, the geometry is imported into the FEM software and the assignment of analysis parameters is usually done in a pre/post process tool (ANSYS Workbench). Thirdly, the solver analysis is made. Finally, the post-process stage begins reviewing the analysis results.

8.1 Introduction

The first step in performing a structural analysis of a cube-shaped microsatellite is to get a simplified enough computer aided design model composed of the frame and the different subsystems. This simplification is needed to be able to simulate the different loads using finite element methods (FEM) within a relatively short period of time since the computing resources are limited.

Because of the optimization objective of the project, a wide range of parameters have been considered for the characterization of the frame. This parameter dependent design made posteriors frame modifications easier to obtain the optimal microsatellite structure.

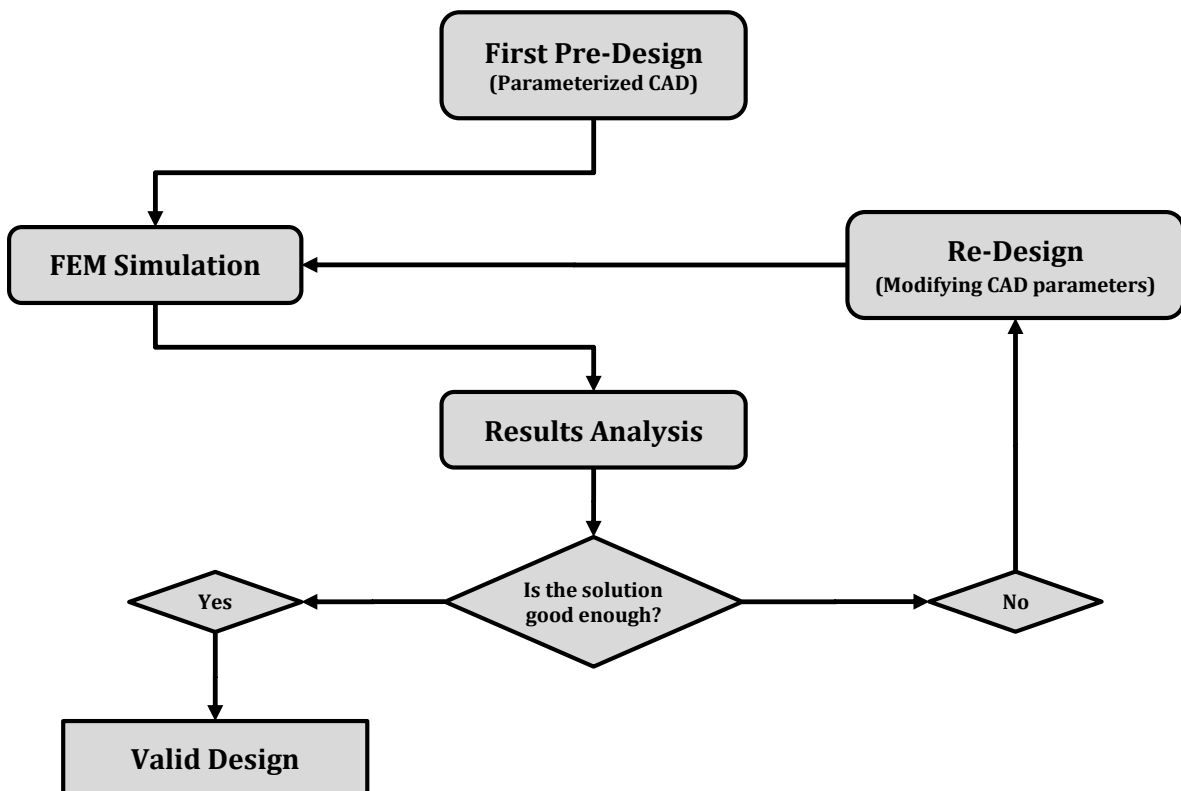


Figure 8.1. – Methodology followed during design

8.1.1 CATIA

CATIA (Computer Aided Three-dimensional Interactive Application) is a multi-platform CAD/CAM/CAE commercial software suite developed by the French company Dassault Systèmes.

Nowadays the v6 is the latest version of this software suite, but the v5 is still the most popular version in the aerospace industry so that is what has been used for this project. Also, both students working on this project had a good background of experience with this specific version of the software.

8.1.2 CAD Nexus

CAD Nexus is a simple and running in the background programme that helps with parameterization of the structure and links together CATIA V5 R20 parameters with ANSYS 14.5's.

8.2 CAD Modelling of the Structure

As it has been said before, the CAD Modelling of the structure is an iterative and parameterized design, so numerous drafts have been done to get a final model of the frame. First it began with a simple “shelf” structure.

8.2.1 Shelf Structure

The primary structure of the satellite consists of three trays (one of them will act as ceiling), twelve spars, four plates and the LV/SC adapter (called also as Tray A) which will remain with the satellite after injection into orbit. The three trays are reinforced with a rectangular isogrid. The trays’ basic dimensions as well as the isogrids are parameterized with its main dimensions. The adapter diameter ring is normalized with the Launch Vehicle User’s Manual.

The geometric envelope of the satellite is a 0.5 x 0.5 x 0.5m cube. A conservative distance of 10.4 cm between the first and the second tray has been decided to provide proper volume to accommodate the different subsystems. The distance between the second and third tray has been determined to be 17.35 cm for the same reasons and the third one with the ceiling is separated by 20 cm to provide sufficient space to the payload.

Launch Vehicle Adaptor mass, as well as the masses of trays, plates and spars are calculated knowing their volume and the density of their materials. The estimated masses of the primary structure elements are shown in the Table 16:

	Tray	Spar 1	Spar 2	Spar 3	Adaptor	Plate
Mass [Kg]	1.906	0.025	0.042	0.049	6.805	0.986

Table 16 – Satellite parts masses

The next figure (Figure 8.2) illustrates how the primary structure looks without any plates. As can be seen, it is a very simple configuration. That is because a simple configuration would cheapen costs and would make fabrication and assembly tasks easier.

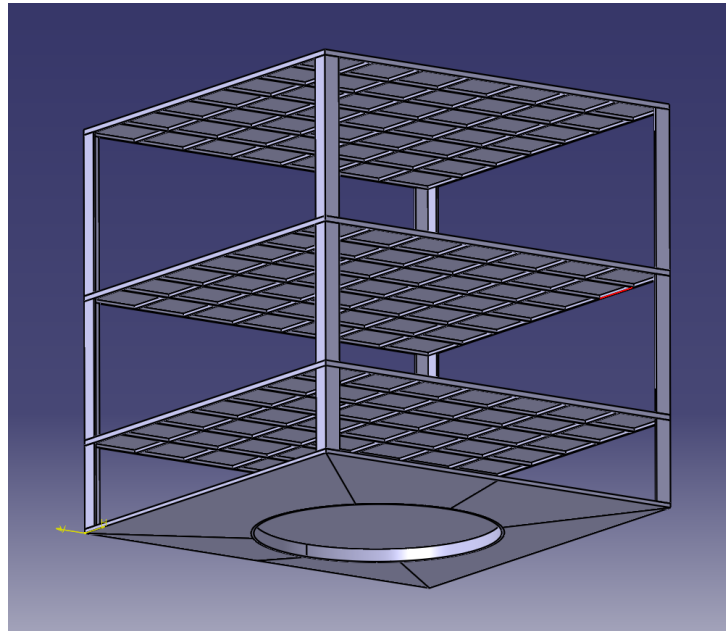


Figure 8.2 – Satellite primary structure without lateral plates

Once the pictured above structure is assembled, the subsystem design and location begins. Starting with masses distribution percentages shown in [24] and [23], knowing which tray every subsystem will be in (some of them are in more than one) and that the satellite total mass is of 50 kg, the allocation process begins.

Considering this project is about studying the vibration behaviour of the satellite and not the exact distribution of the systems and neither is it a complete satellite design project, all subsystems have been simplified to single elements such as boxes. Moreover, this way will save modelling, meshing and calculation time. Realizing that, and aware of the volume every subsystem takes up in the CAD design, new materials have been designed with an equivalent density to simplify de subsystem mechanical behaviour during the dynamic analysis.

Figure 8.3 shows all parameters involved in the design of the frame.

Parameter	Value	Formula	Details View
Tray\DS_Length_Tray	500mm		DS_Thickness_Tray
Tray\DS_Thickness_Tray	1,5mm		DS_Heigh_Rib_Tray
Tray\DS_Heigh_Rib_Tray	6mm		DS_Thickness_Tray_Top
Tray\DS_Thickness_Rib_Tray	4mm		DS_Heigh_Rib_Tray_Top
Tray\DS_Num_Ribs_Tray	10		DS_Length_Tray
Tray\Length_Cell	51,111mm	= (Tray\DS_Length_Tray - Tr...	Tray\DS_Length_Tray
Tray\DS_Thickness_Central_Cell	2,5mm		Tray\DS_Thickness_Tray
L_Spar_2\DS_Thickness_L_Spar	2,5mm		Tray\DS_Heigh_Rib_Tray
L_Spar_2\DS_Width_L_Spar	20mm		Tray\DS_Thickness_Rib_Tray
L_Spar_2\DS_Heigh_L_Spar_2	167mm		Tray\DS_Num_Ribs_Tray
L_Spar_2\DS_Ratio	1,3		Tray\DS_Thickness_Central_Cell
L_Spar_2\DS_Thickness_Interface	2,5mm		L_Spar_2\DS_Thickness_L_Spar
L_Spar_3\Thickness_L_Spar_3	2,5mm	= 'L_Spar_3\External Parame...	L_Spar_2\DS_Width_L_Spar
L_Spar_3\Width_L_Spar_3	20mm	= 'L_Spar_3\External Parame...	L_Spar_2\DS_Heigh_L_Spar_2
L_Spar_3\DS_Heigh_L_Spar_3	180mm		L_Spar_2\DS_Ratio
Tray_Top\Length_Tray_Top	500mm	= 'Tray_Top\External Param...	L_Spar_2\DS_Thickness_Interface
Tray_Top\DS_Thickness_Tray_Top	1mm		L_Spar_3\DS_Heigh_L_Spar_3
Tray_Top\DS_Heigh_Rib_Tray_Top	6mm		Tray_Top\DS_Thickness_Tray_Top
Tray_Top\DS_Thickness_Rib_Tray_Top	4mm		Tray_Top\DS_Heigh_Rib_Tray_Top
Tray_Top\DS_Num_Ribs_Tray_Top	6		Tray_Top\DS_Thickness_Rib_Tray_Top
Tray_Top\Length_Cell_Top	95,2mm	= ('Tray_Top\External Param...	Tray_Top\DS_Num_Ribs_Tray_Top
L_Spar_1\Thickness_L_Spar_1	2,5mm	= 'L_Spar_1\External Parame...	L_Spar_1\DS_Heigh_L_Spar_1
L_Spar_1\Width_L_Spar_1	20mm	= 'L_Spar_1\External Parame...	Tray_ASAP\DS_Length_Tray_ASAP
L_Spar_1\DS_Heigh_L_Spar_1	80mm		Tray_ASAP\DS_Thickness_Tray_ASAP
Tray_ASAP\DS_Length_Tray_ASAP	500mm		Tray_ASAP\DS_Heigh_Rib_Tray_ASAP
Tray_ASAP\DS_Thickness_Tray_ASAP	2,5mm		Tray_ASAP\DS_Thickness_Rib_Tray_ASAP
Tray_ASAP\DS_Heigh_Rib_Tray_ASAP	6mm		Tray_ASAP\DS_Num_Ribs_Tray_ASAP
Tray_ASAP\DS_Thickness_Rib_Tray_ASAP	6mm		Tray_ASAP\DS_Thickness_Interface
Tray_ASAP\DS_Num_Ribs_Tray_ASAP	2		Plate1\DS_Thickness_Plate
Tray_ASAP\DS_Thickness_Interface	6,5mm		Plate1\Plate_Height
Plate1\DS_Thickness_Plate	1mm		Central_Spar\DS_Thickness_Central_Spar
Plate1\Plate_Height	457,5mm	= 'Plate1\External Parameter...	Central_Spar\DS_Width_Central_Spar
Central_Spar\DS_Thickness_Central_Spar	2,5mm		Central_Spar_2\Thickness_Central_Spar_2
Central_Spar\DS_Width_Central_Spar	20mm		Central_Spar_2\Width_Central_Spar_2
Central_Spar_2\Thickness_Central_Spar_2	2,5mm	= 'Central_Spar_2\External P...	Central_Spar_2\DS_Thickness_Interface_Spar
Central_Spar_2\Width_Central_Spar_2	20mm	= 'Central_Spar_2\External P...	Central_Spar_3\Thickness_Central_Spar_3
Central_Spar_2\DS_Thickness_Interface_Spar	2,5mm		Central_Spar_3\Width_Central_Spar_3
Central_Spar_3\Thickness_Central_Spar_3	2,5mm	= 'Central_Spar_3\External P...	
Central_Spar_3\Width_Central_Spar_3	20mm	= 'Central_Spar_3\External P...	

Figure 8.3– Parameters used – CATIA (left) ANSYS (right)

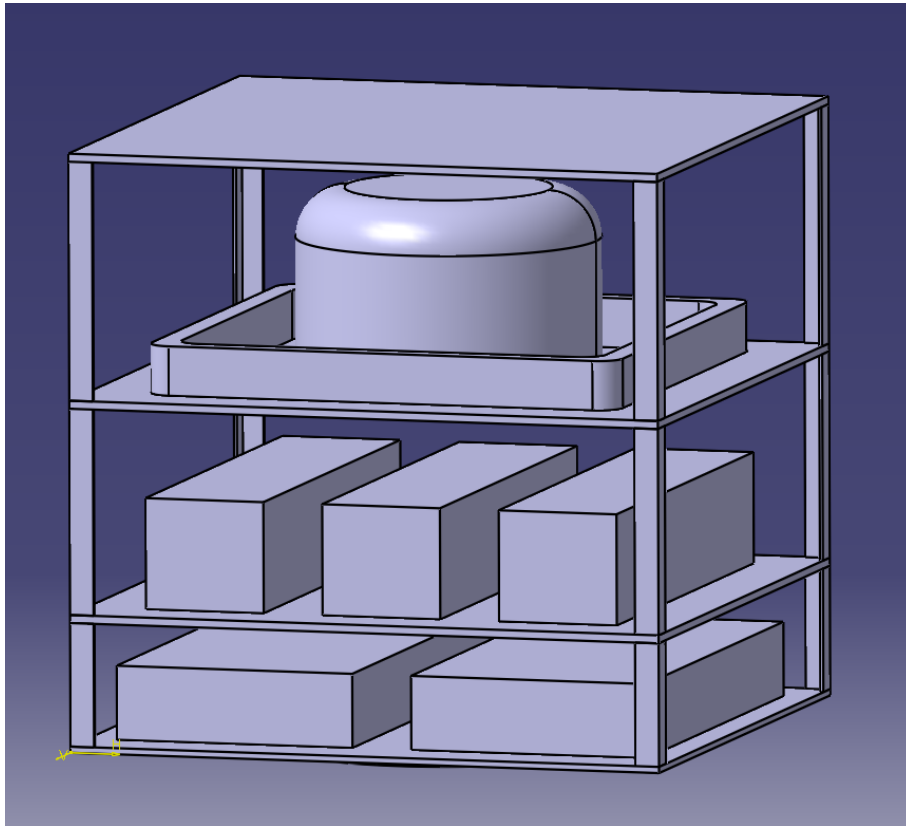


Figure 8.4 – Satellite Structure with modelled Subsystems

And this is the final appearance of the satellite primary structure first design with the plates on.

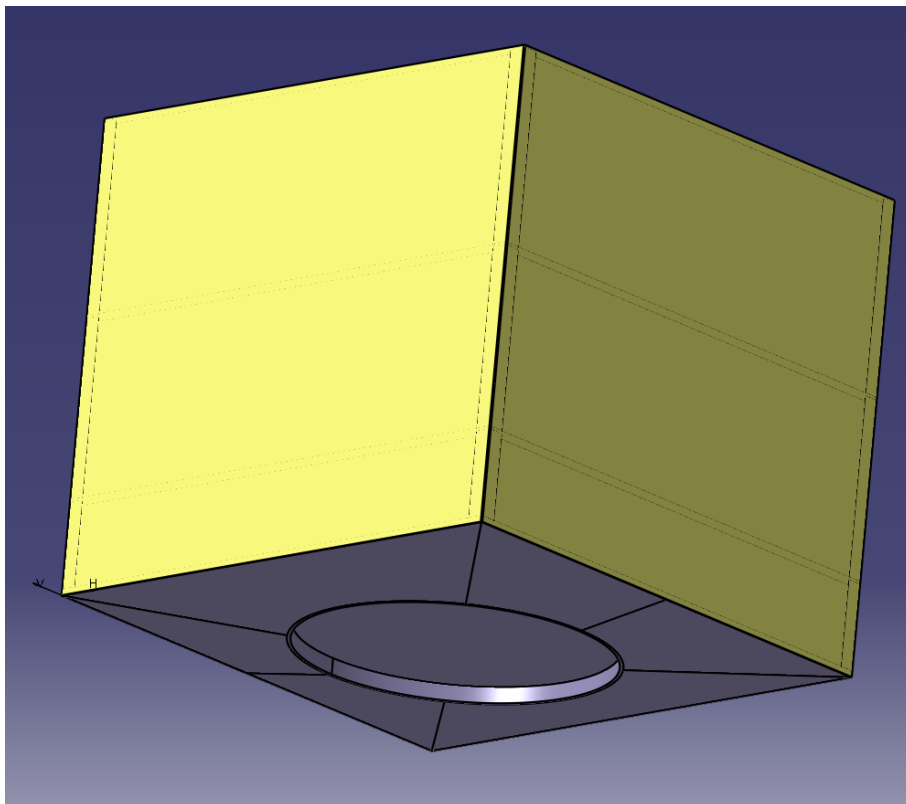


Figure 8.5 – External view of satellite structure

Once Geometric Modelling Stage was finished, the structure was simulated, obtaining natural frequencies that were not allowed by Regulations. So the structure needed to be stiffened. To do so, the “Column Structure” modification was designed and implemented.

As it has previously been said, the software employed has been CATIA V5R20 for CAD modelling and CAD Nexus for linking the CATIA’s CAD model parameters with the FEM software.

8.2.2 Column Structure

Sadly, the first design did not work because it did not satisfy natural frequency requirements indicated by Rocket User Manuals [21].

Once it has been shown that the so-called “Shelf Structure” didn’t work, a new design should be done. Rather than a new design, this one is a modification, and actualization of the previous one. In order to stiffen the structure, a central hollow column was allocated. This column has two basic functions. Firstly, it moves natural frequencies to bigger values. And secondly, it provides a way to link the subsystems of different trays with wires in an orderly manner. The new frame is shown in Figure 8.6. As can be seen, the number of ribs in the third tray has been reduced to two per direction, since it wasn’t a problem in the structural analysis and a reduction in the number of ribs also means a decrease in the overall weight of the structure and in its price.

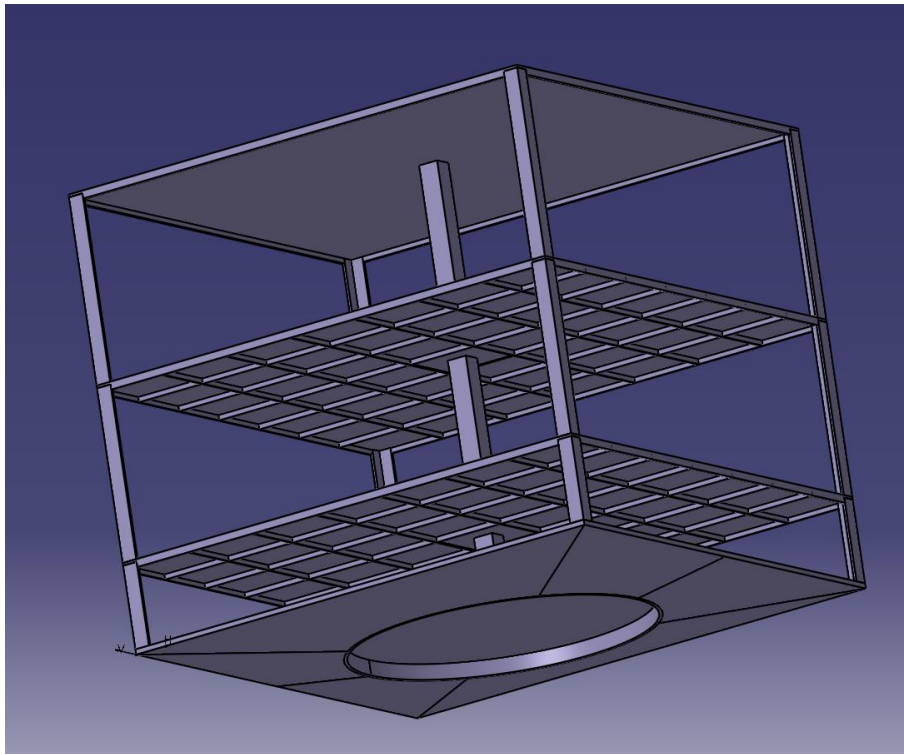


Figure 8.6 – Column Structure

Another modification done is the central square that is crossed by the column. It has been made thicker so the vibrations and loads could transmit more easily and smoothly. In Figure 8.7 the thickening can be seen closer.

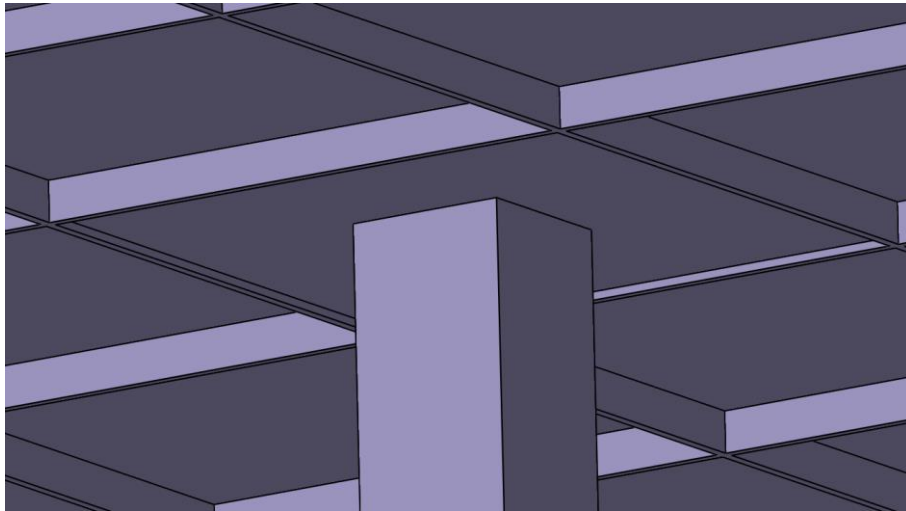


Figure 8.7 – Detail of contact between tray and column

Finally, the contact between the tray and the lateral columns has been redesigned to make sure that a smooth contact is made. To do so, the columns touch the plate zone of the tray instead of the ribs as they did before (Figure 8.8). This way, if the thickness of the ribs is less than the thickness of the lateral columns, all should stand correctly.

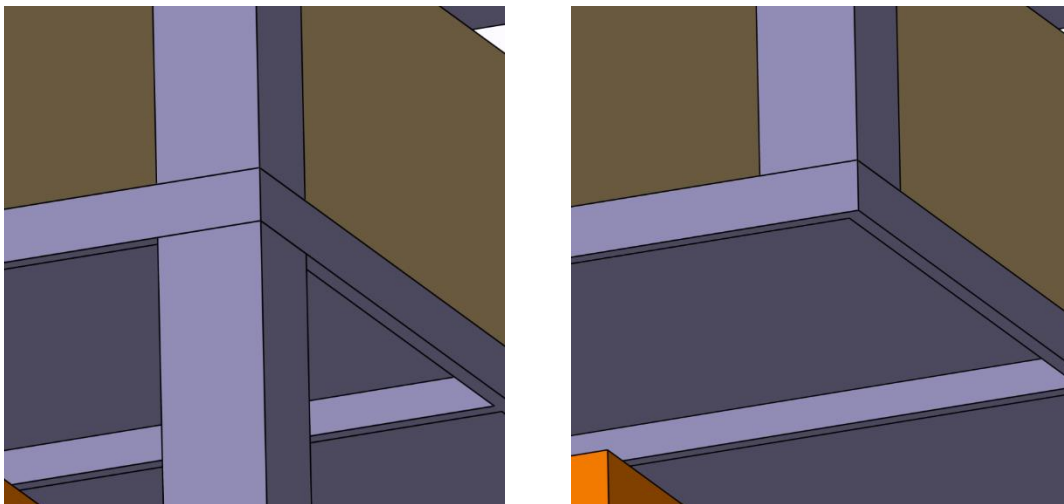


Figure 8.8 – Zero Iteration of Contact Design

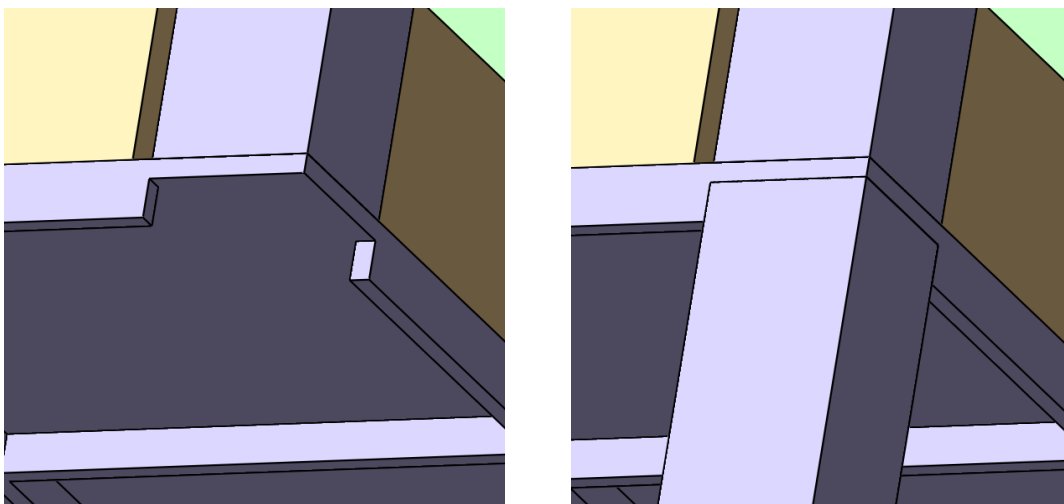


Figure 8.9 – First Iteration of Contact Design

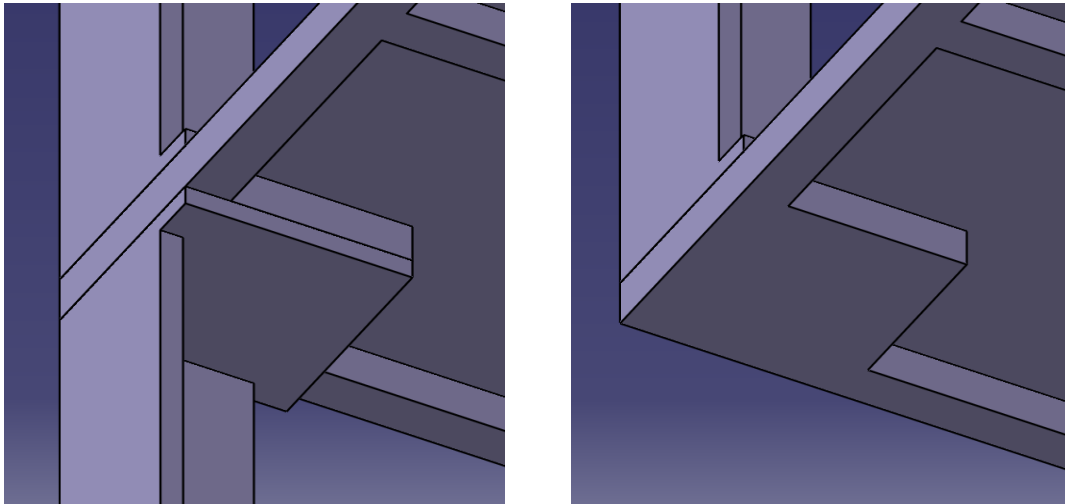


Figure 8.10 - Second Iteration of Contact Design

But this design (Figure 8.9) is harder to manufacture than the previous one, so a new way to support the lateral columns into the trays was needed. The second iteration of the sketch is shown in Figure 8.10.

Two designs have been tried for the central column. One with a squared cross section and another with a circle section area. Both types of columns have been simulated in ANSYS obtaining similar results, so the squared cross sectional column has been chosen. That is because it is easier to mesh and more or less just as easy to manufacture.

In Figure 8.11 the circular central column design is shown.

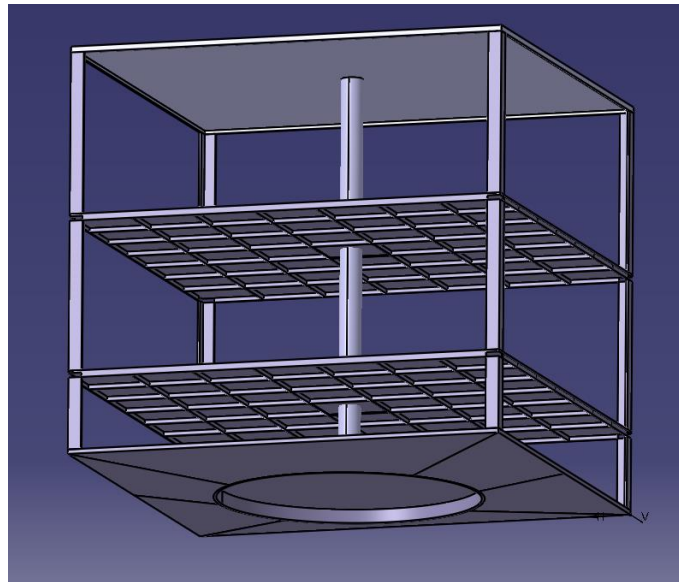


Figure 8.11 - Circular Central Column Design

Finally, the appearance of the structure is displayed in Figure 8.12. Every different subsystem is represented with a different colour in order to distinguish them (see section 8.3).

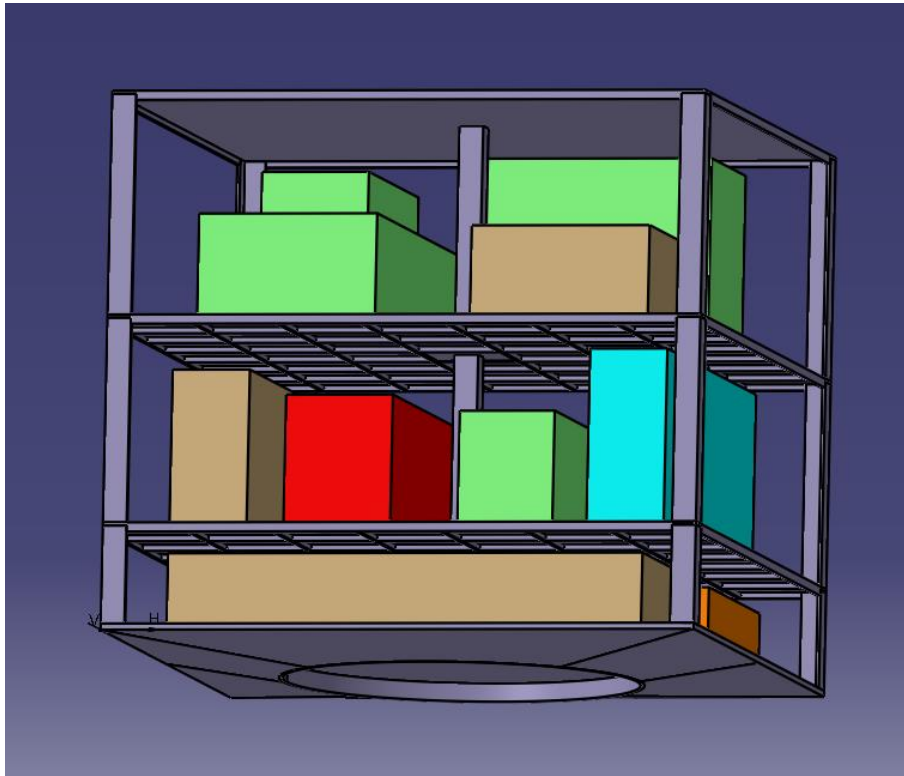


Figure 8.12 – Columns Structure with Subsystems onboard

8.2.3 Tray A Modification

With the previous design of the lower tray (named as Tray A), the structure would weigh too much, so a redesign was needed. A lighter structure was required that could endure all the previous cyclic and static loads. To do so, a structural framework of radial ribs was designed and parameterized. In Figure 8.13 the final design of the Adapter ASAP Module can be seen.

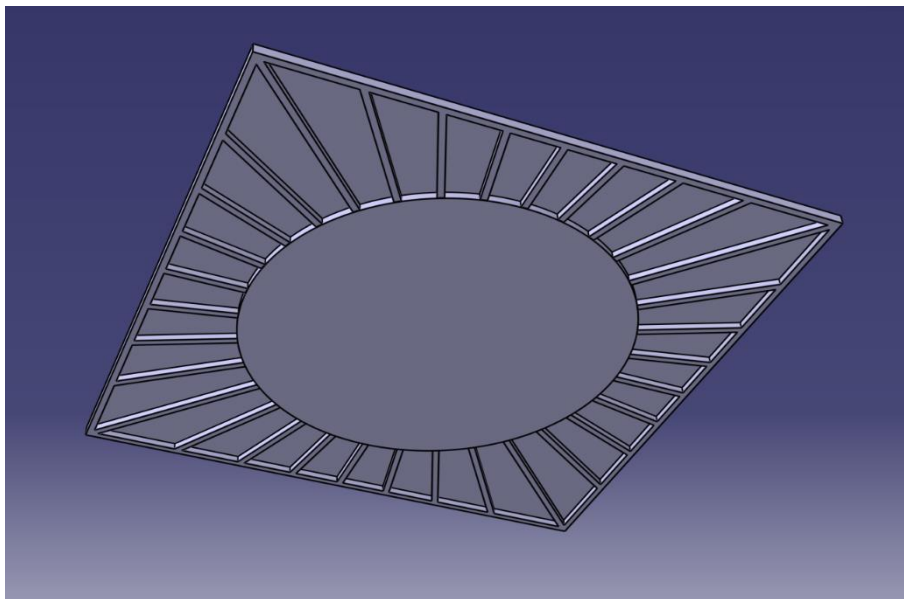


Figure 8.13 – Tray A Modification

The mass of this part of the satellite was diminished from 6 Kg to 4 Kg (approx.), making the structure lighter and more in line with the bibliography consulted [27]. So, the final appearance of the satellite is shown in Figure 8.14.

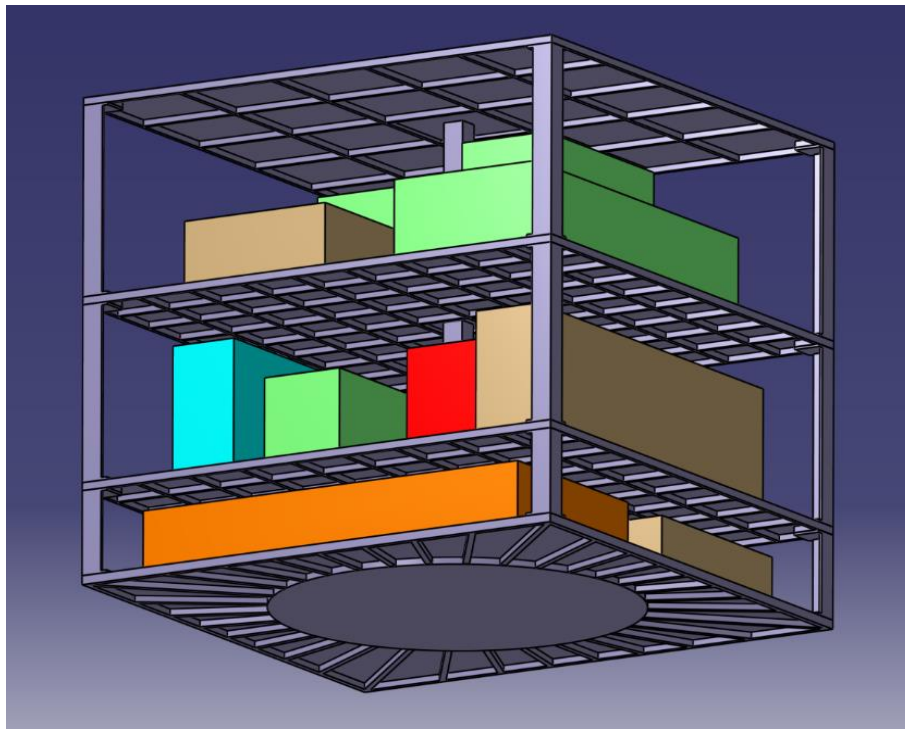


Figure 8.14 – Final appearance of the satellite with the subsystems onboard and the lateral plates hidden

8.3 Mass Distribution

Mass distribution has been done with information of other similar satellites. From the estimation made in [24] the percentages of the satellite could be approximated.

To do so, a total mass of 50 kg was supposed. Also, knowing that the bus of the satellite would be formed by an Al 7075 T-73 alloy (this will be explained in section 9.1), and once the model of the structure was designed, the mass of this subsystem was calculated (12.088 kg). Talking in percentages, that is 24% approx. of the total structure mass. This value was compared with the percentages of [23], [24], [25] and [27] that say that the frame of the satellite should range roughly about 20 or 25 %. So it was given as a valid result.

Total Mass [kg]	50
Payload Mass [kg]	17.91
Payload Percentage [%]	35.82

Table 17 – Payload masses and percentages

Once this has been checked up, the estimation of the masses and densities of the other subsystems begins. Firstly, a dimensional envelope of every subsystem was defined. They were all approximated as boxes because most of them have a very similar shape and also because it would lighten computational costs. Then, realizing the mass percentages of the different subsystems, the density of every box could be estimated. In the case of the payload the approximation was slightly different. The mass of the payload was calculated as a subtraction between the rest of the subsystems and the total satellite mass. Once estimated,

the Payload mass and its percentage associated to the satellite total were calculated (Table 18). Lastly, the payload mass was distributed among the three trays (45%² for Tray A, 35% for Tray B and 20% for Tray C).

Finally, these data were introduced as a density input into ANSYS. Different materials were defined for every subsystem, materials with the same name as the subsystems themselves and with the same mechanical properties as the 7075 aluminium alloy but with previously determined densities.

Subsystem	Volume [m ³]	Mass [kg]	Density [kg/m ³]	Percentage [%]
ADCS _A	0.00468	2.5	534.19	5
ADCS _B	0.00325	1.5	461.54	3
ADCS _C	0.00204	1	490.20	2
EPS	0.00468	10	2136.75	20
OBDH + TC	0.00309	2.5	808.02	5
PL ₁	0.00563	8.0604	1431.81	16.12
PL ₂	0.00371	6.2692	1692.09	12.54
PL ₃	0.00264	3.5824	1356.97	7.16
TTC	0.00311	2.5	805.15	5
STR	0.00430	12.088	2810.00	24.18

Table 18 – Subsystems volumes, masses, densities and percentages

The Thermal Control Subsystem has been fused with the Onboard Data Handling Subsystem because its influence on weight was negligible (a passive TCS has been supposed, that is one that consumes no power).

The final distribution of the subsystems attending to the masses above calculated and the distribution of similar sized satellites is shown in the Figure 8.15.

² All percentages were referred to the payload total mass.

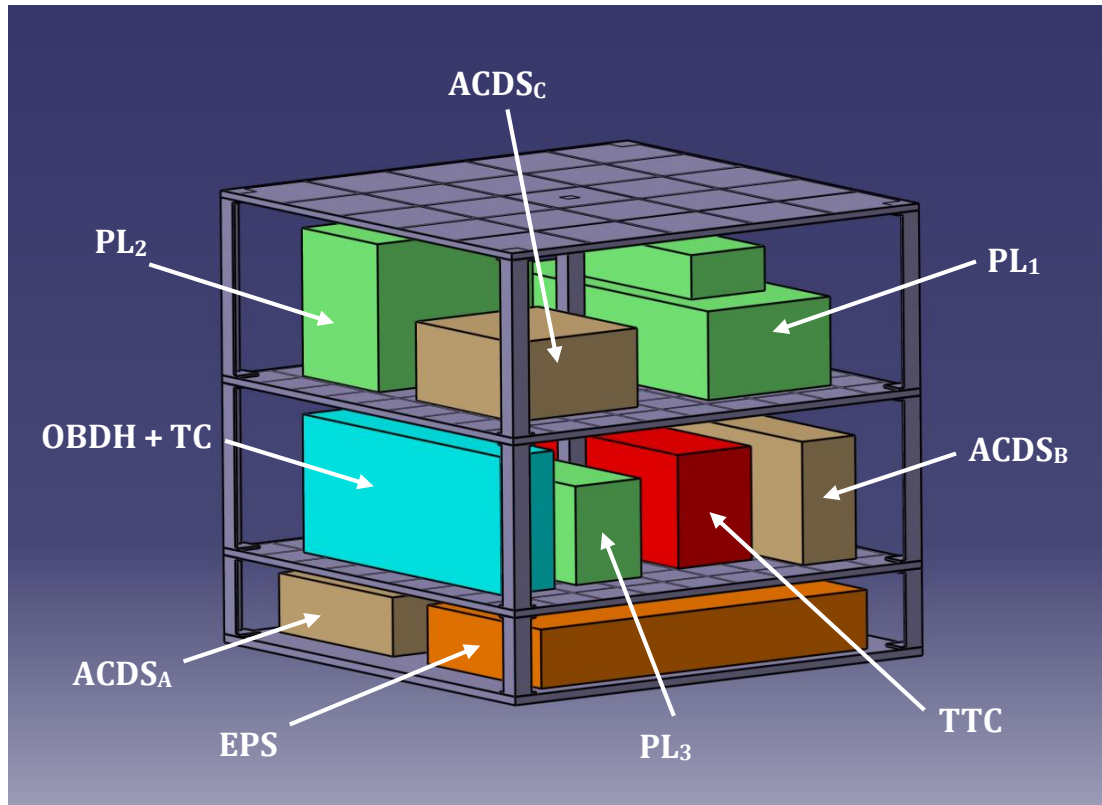


Figure 8.15 – Detail of the subsystems distribution

8.4 CoG Location

All the subsystems onboard as well as the structure of the satellite have been designed in such a way that the Center of Gravity of the whole spacecraft could satisfy the CoG position requirements provided by the launcher document that is shown in section 6.1. To do so, the material properties have been added not only in ANSYS (see section 9.1), but in the CATIA model.

Axis	Distance [mm]
X	0.388
Y	3.747
Z	182.437

Table 19 – Center of Gravity location

Note that X and Y axes distance is measured from the geometric center of the squared tray, while X distance is measured from the mounting plane part (Ariane 5 Adapter).

From these data, it is concluded that the satellite satisfies the centre of gravity requirements (X and Y are $\leq \pm 5\text{mm}$ and Z $< 450\text{mm}$)

8.5 Inertia Check-up

Also, various measurements have been done in order to see if the satellite fulfils the inertia requirements. The next equation represents the inertia matrix referring to the principal axes of the satellite.

$$\bar{I} = \begin{pmatrix} I_{xx} & I_{xy} & I_{xz} \\ I_{yx} & I_{yy} & I_{yz} \\ I_{zx} & I_{zy} & I_{zz} \end{pmatrix} = \begin{pmatrix} 1.81 & 0.071 & 0.025 \\ 0.071 & 1.802 & 0.255 \\ 0.025 & 0.255 & 1.694 \end{pmatrix} \text{ kg m}^2 \quad \text{Equation 7.1}$$

In section 6.1.2 it is written that the maximum inertial moments (I_{xx} , I_{yy} , I_{zz}) allowed are 20 kg m². Consequently, it can be appreciated that the inertia requirements of the launcher are correctly satisfied.

Values of the inertia matrix were automatically calculated by CATIA once the satellite structure material as well as the materials of the subsystems were added. This inertia matrix CATIA showed is obtained with reference to the center of gravity, so it was not needed to be changed.

9 FEM Model

In this chapter the Finite Element Method Model, the boundary conditions in order to simulate the correct behaviour of the frame, and the materials chosen to build the structure will be explained.

9.1 Material Selection

Space has very aggressive physical conditions. Materials used in the construction of the structure must survive ground, launch, and on-orbit environments (time-varying applied forces, pressure, humidity, radiation, contamination, thermal cycling, and atomic particles) without rupturing, collapsing, buckling, excessively distorting, or contaminating critical components. Depending on the mission, some of these characteristics will be given more importance than others.

The next step in the design process is to choose the optimum material for the frame. A large number of materials with space heritage are available for satellite structural design and are presented in the literature review. However, in the last few years, there has been a growth in the use of “new” solid materials such as fibre composite and honeycomb sandwich. These two adding in alloys, are the three kinds of materials suitable for primary structure design. To select the best kind of material, each of these materials is evaluated in more detail based on several design criteria. An evaluation clearly demonstrates that metallic materials are the most effective in structural design for Small Sat [28]. There are several reasons for this decision. Fibre composite structures are very expensive to manufacture and require costly structural testing. Honeycomb sandwich materials require potted inserts to attach fasteners, which create safety concerns and parasitic mass. The metallic materials are relatively simple to manufacture and minimize the safety and testing requirements. Finally, historically they had been the most used in construction, so there is a lot of background experience and information about the behaviour of these materials in space.

The next step in the design process is to develop an optimum metallic material for structural design. Several metals are used in satellite fabrication, such as aluminium, titanium, beryllium, and stainless steel.

The most commonly used material in spacecraft manufacturing are Aluminium alloys. They usually have high ductility and stiffness to weight ratio. Also they are relatively easy to machine. However, aluminium alloys have a high coefficient of thermal expansion and low hardness. Probably that is its main disadvantage in space use because of the huge thermal gradients on orbit. Also, it has a relatively low strength to volume ratio. That is why alloys are tempered to increase the material strengths. Of all possible alloys, Aluminium 7075 is probably one of the most used. It has zinc as the primary alloying element and its strength is comparable to many steels. Also it has good fatigue strength. Nevertheless, it has less resistance to corrosion than other alloys, and also has high cost limits. Aluminium alloy 6061 has magnesium and silicon as its alloying elements. It has good mechanical properties and exhibits good weldability. It is the most common aluminium alloy for general purpose use [29].

Steel is mainly used in aerospace applications where low-volume strength and stiffness are important. It has a broad range of strength, hardness, and ductility. Steel provides high wear resistance; is generally easy to machine, and weldable. However it is not efficient for structural stability because it provides low buckling strength vs. weight. Steels are combined with many trace elements to address a wide range of needs. Austenitic stainless steel is by far the most abundant steel alloy used in spacecraft. It contains 12 % chromium which results in a tough chromium-oxide coating that protects parts from corrosion. Stainless steels are generally used for fasteners and mechanisms whereas many heat-resistant alloys are used for heat shields, rocket nozzles, and other high-temperature applications. Steel will not be used in the construction of the main frame because of its cost [25] and [29].

Titanium and titanium alloys are used for applications requiring very high strength materials or high strength at high temperatures. The materials have high strength to weight ratios, low coefficients of thermal expansion, and excellent corrosion resistance. However, they are hard to machine, and some alloys have poor fracture toughness. Ti-6Al-4V, which contains 6 % aluminium and 4 % vanadium, is the most popular titanium alloy used in aerospace applications. The alloy has heritage in wings and missile bodies. Perhaps its most famous applications are the castings used to connect the external fuel tank to the space shuttle and its boosters. Nevertheless, it is a very expensive material, so it will not be chosen (from [25] and [29]).

Beryllium is used for very high-stiffness aerospace applications. Its specific stiffness, which is the ratio of Young's modulus to density, is about six times that of most metals. The material is nonisotropic due to its grain alignment, and therefore has low ductility and fracture toughness in its short-grain direction. It is commonly used in lightweight optics and mirrors because it performs well at cryogenic temperatures due to its low coefficient of thermal expansion and high thermal conductivity. However, beryllium is expensive, difficult to machine, toxic, and requires special machining equipment. Beryllium parts are machined in a controlled environment because its powder is a known carcinogen when inhaled. The parts may be safely handled once machined (from [25] and [28]).

Composites typically consist of a matrix and a resin. The matrix material (metal, epoxy) surrounds and supports the reinforcement materials (carbon, graphite) by maintaining their relative positions. The physical properties of composite materials are anisotropic such that properties are different depending on the direction of the loads. Delamination may occur during shock or impact, where it causes the laminates to separate between two layers. Continuous fibre composites are called laminate composites, which are produced in several layers aligned in different angles to create a more stable structure. Manufacturing for composite structures is costly and time consuming because of its mathematical intricacy. But it has been said before, they are almost "new" in the industry and harder to find and fabricate (see [28]).

It has been decided that the most suitable material to build the primary structure of the satellite is an aluminium alloy, because it fits all the design requirements. More particularly, a 7075-T73 temper aluminium alloy. That is because, although it is more complicated to machine and manufacture than 6061 and a little bit expensive all its benefits outweigh its

handicaps. Notice that the designation T73 refers to an aluminium heat treated and then artificially aged to make the material resistant to stress–corrosion.

9.2 Meshing

The aim is to discretize the structure and its different components in the most optimal way to obtain accurate results, the closest possible to real ones, without an excessive computational cost. To measure the mesh quality, the following parameters have been taken into account:

- **Element Quality:** provides a composite quality metric that ranges between 0 and 1. This metric is based on the ratio of the volume to the sum of the square of the edge lengths for 2D quad/tri elements, or the square root of the cube of the sum of the square of the edge lengths for 3D elements. A value of 1 indicates a perfect cube or square while a value of 0 indicates that the element has a zero or negative volume [30].
- **Aspect Ratio:** measures the length ratio between the different sides of the element. The best possible triangle aspect ratio is 1, this is the case of equilateral triangles and squares. Figure 9.1 shows different examples of aspect ratios from different geometric figures.



Figure 9.1 – Meshing geometric figures [30]

- **Warping Factor:** measures the twist or distortion in the shape or form of the elements. It is computed for each element face (for the 6 quadrilateral faces of a hexa, or 3 quadrilateral faces of a wedge, or 1 quadrilateral face of a pyramid) and then the bigger value is displayed. Any brick element having all flat faces has a warping factor of zero. For example, looking at Figure 9.2, twisting the top face of a unit cube by 22.5° and 45° relative to the base produces warping factors of about 0.2 and 0.4, respectively.



Figure 9.2 – Warping factor exhibition [30]

- **Skewness:** is one of the primary quality measures for a mesh. Skewness determines how close to ideal (i.e. equilateral or equiangular) a face or cell is. Highly skewed faces and cells are unacceptable because the equations being solved assume that the cells are relatively equilateral/equiangular [30].

Value of Skewness	Cell Quality
1	Degenerate
0.9 — <1	Bad (sliver)
0.75 — 0.9	Poor
0.5 — 0.75	Fair
0.25 — 0.5	Good
>0 — 0.25	Excellent
0	Equilateral

Table 20 – Skewness Criteria [30]

- **Orthogonal Quality:** the range for orthogonal quality is 0–1, where a value of 0 is the worst and a value of 1 is the best [30]. The orthogonal quality for faces is computed using the normal vector edge and the vector from the face centroid to the centroid of each edge.

The meshing methods and the typical element sizes used for the different components of which the satellite is composed are detailed in the subsections 9.2.X

Consequently, the final mesh consists of 135,572 elements and 450,776 nodes. The details of its quality and geometry can be found in Table 21.

	Average	Minimum	Maximum	Standard Deviation
Element Quality	0.7272	1.5180E-02	0.9998	0.2107
Aspect Ratio	2.5123	1.0046	970.37	4.7625
Warping Factor	7.7272E-03	0	0.4831	0.0296
Skewness	0.2252	1.3057E-10	0.9999	0.2157
Orthogonal Quality	0.8597	1.6397E-02	1	0.1583

Table 21 – Final mesh parameters

Figures 9.3, 9.4, 9.5 and 9.6 show different views of the final mesh, with and without lateral plates.

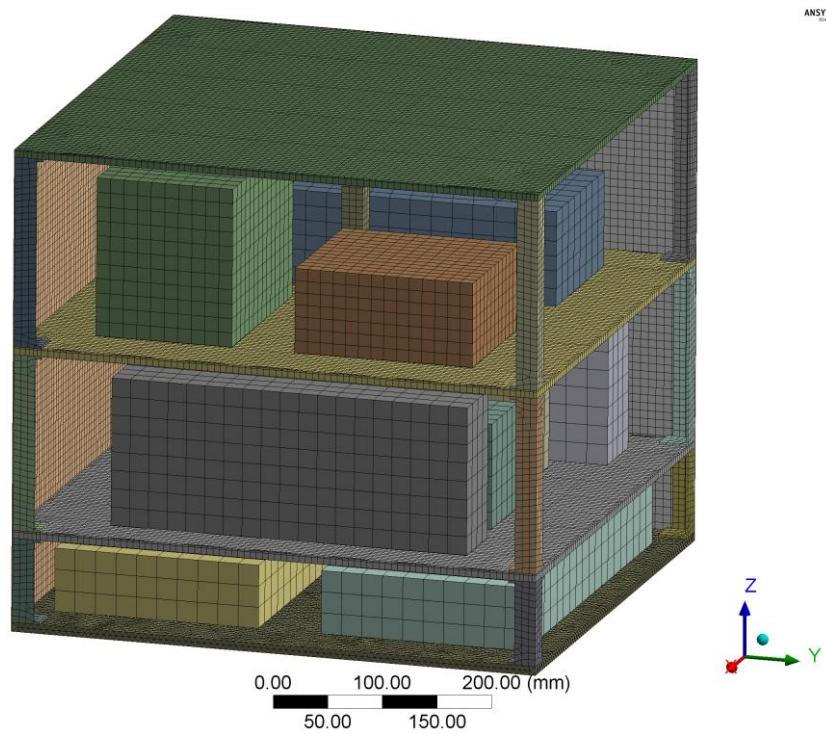


Figure 9.3 – Final mesh view 1

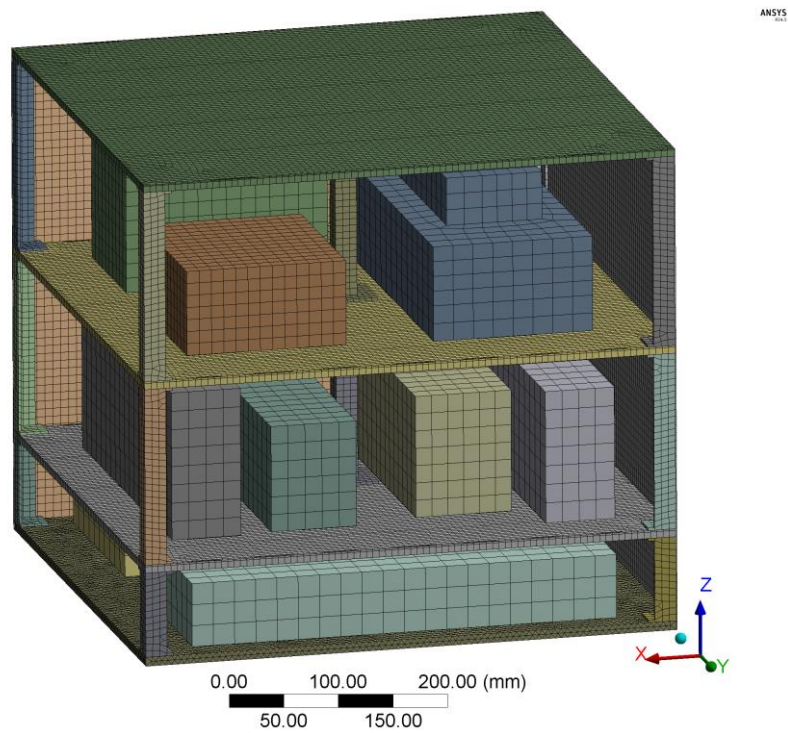


Figure 9.4 – Final mesh view 2

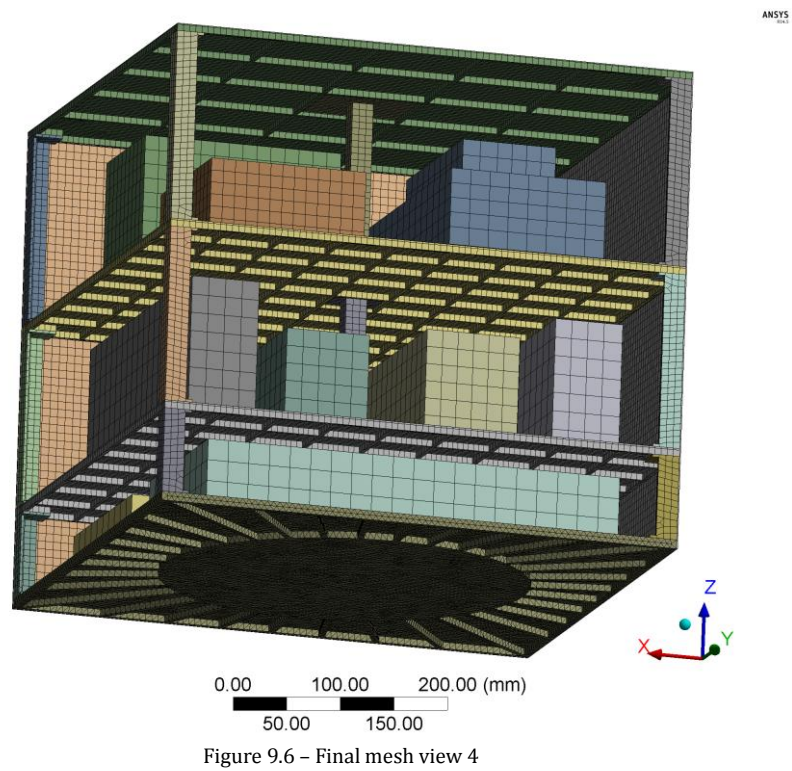
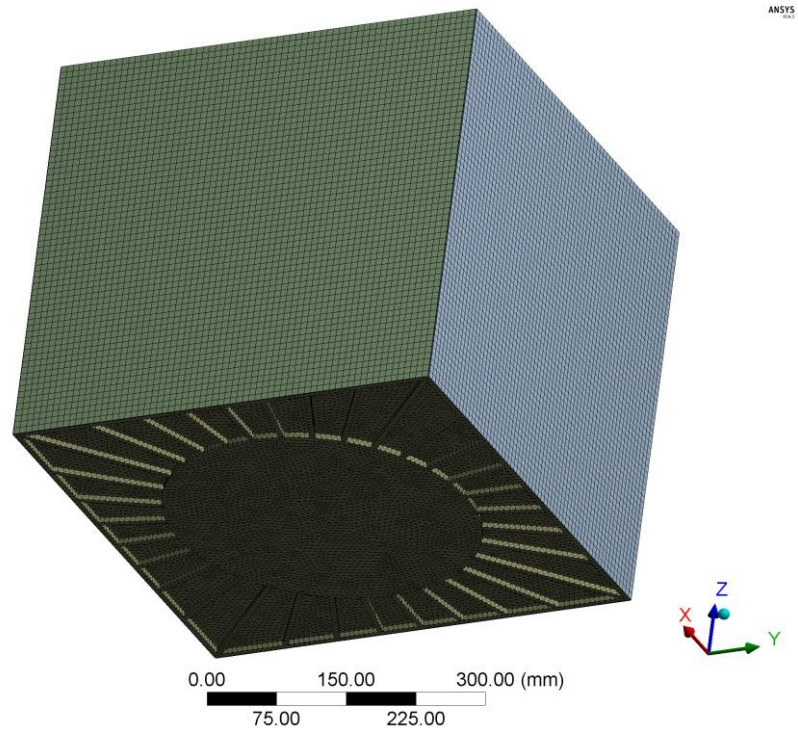


Figure 9.7 shows the number of elements of each type and their skewness.

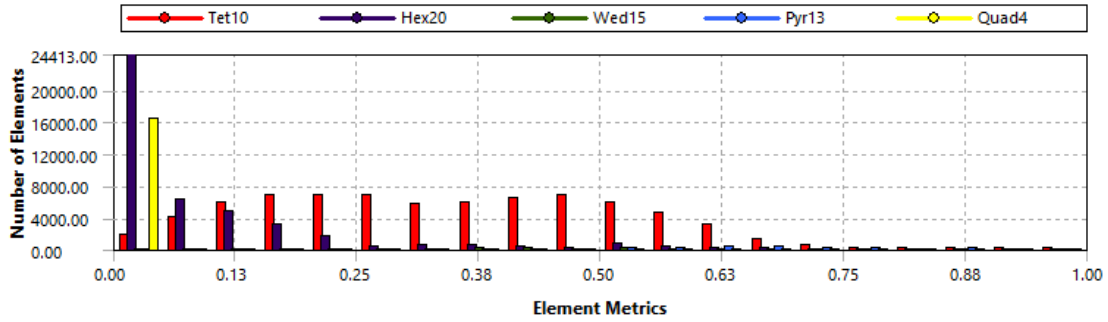


Figure 9.7 – Skewness vs type vs number of elements

All the elements are under 0.75 which is the border line of poor quality elements, in addition, most of the elements are under 0.25 which is considered excellent cell quality.

9.2.1 Tray A

Interface tray has been meshed with “Tetrahedrons” method following a “Path Conforming” algorithm and using 10-nodes tetrahedral-shaped elements (Tet10 – SOLID 187) with a size of 6 mm. As result, the tray is composed of 72,145 elements and 129,970 nodes with the following quality:

	Average	Minimum	Maximum	Standard Deviation
Element Quality	0.7039	0.1126	0.9998	0.1586
Aspect Ratio	2.4144	1.0806	18.19	0.7973
Warping Factor	5.4907E-03	0	0.1216	1.3718E-03
Skewness	0.2753	1.3057E-10	0.9836	0.1982
Orthogonal Quality	0.8305	0.1553	1	0.1380

Table 22 – Tray A meshing parameters

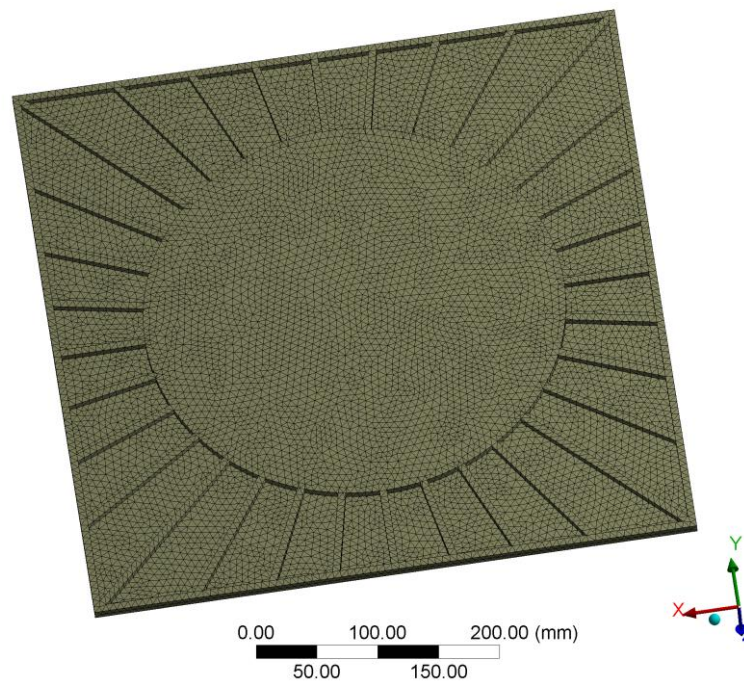


Figure 9.8 – Tray A meshing view 1

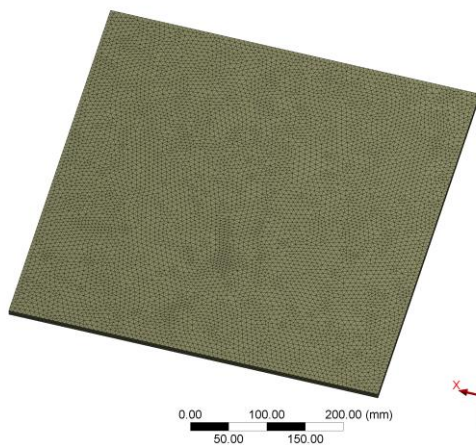


Figure 9.9 – Tray A meshing view 2

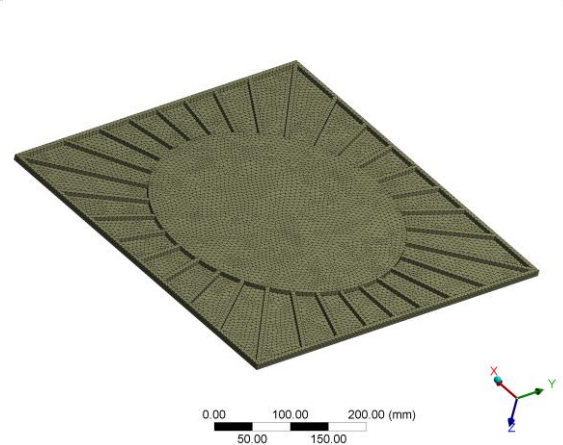


Figure 9.10 – Tray A meshing view 3

9.2.2 Trays B and C

The Trays B and C have been meshed using “MultiZone” method with 20-nodes hexahedral-shaped elements (Hex20 – SOLID 186) and a size of 6 mm. As result, the two trays are composed of 24,618 elements and 171,632 nodes with the following quality:

	Average	Minimum	Maximum	Standard Deviation
Element Quality	0.5667	0.3039	0.9956	0.1036
Aspect Ratio	3.1692	1.0806	5.2531	0.7219
Warping Factor	5.4907E-03	0	0.1216	1.3718E-02
Skewness	7.5759E-02	1.3058E-10	0.6845	0.1036
Orthogonal Quality	0.98	0.5003	1	5.5637E-02

Table 23 – Trays B and C meshing parameters

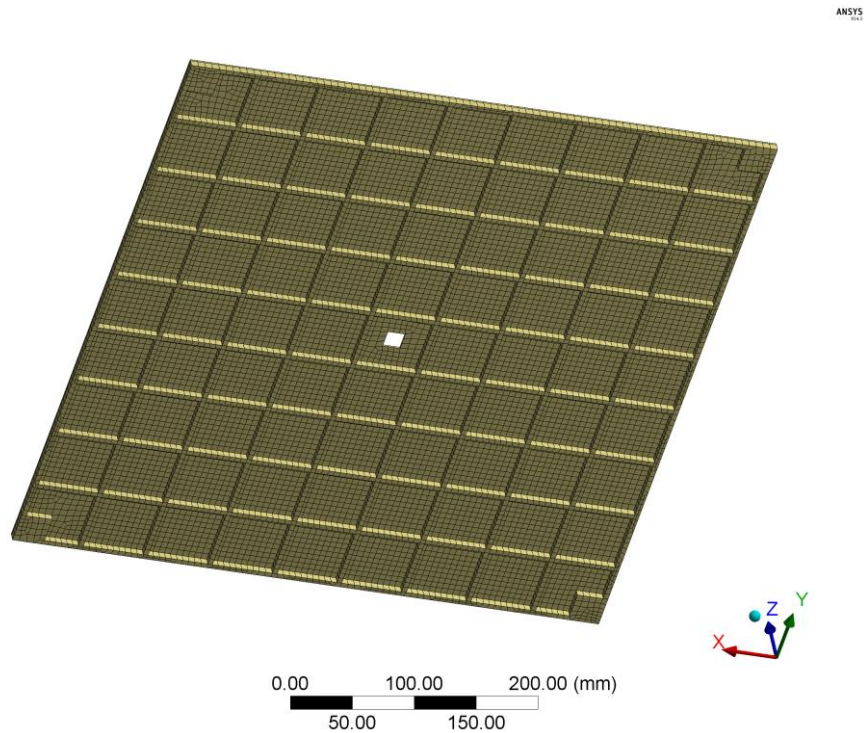


Figure 9.11 – Trays B and C meshing view 1

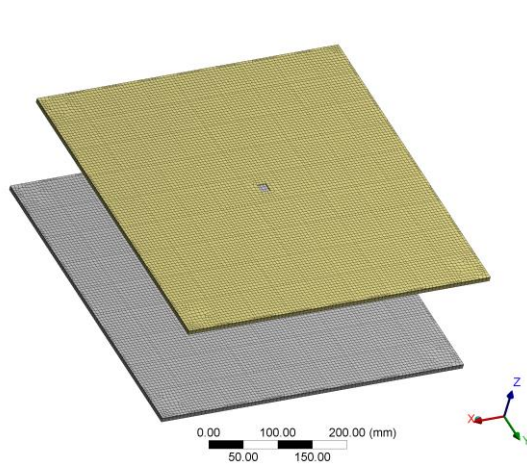


Figure 9.12 – Trays B and C meshing view 2

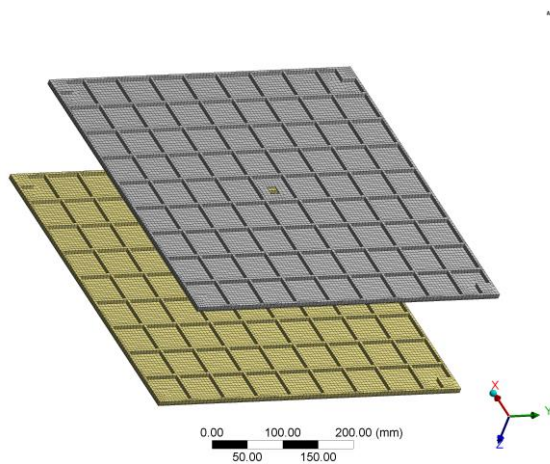


Figure 9.13 – Trays B and C meshing view 3

9.2.3 Tray D

The Tray D has been meshed using “MultiZone” method with 20-nodes hexahedral-shaped elements (Hex20 – SOLID 186) and a size of 6 mm. As result, the two trays are composed of 8,712 elements and 61,325 nodes with the following quality:

	Average	Minimum	Maximum	Standard Deviation
Element Quality	0.3804	0.2133	0.9939	0.1936
Aspect Ratio	5.3699	1.1294	7.9802	1.4702
Warping Factor	3.0389E-03	0	0.1006	1.0210
Skewness	6.8217E-02	1.3057E-10	0.6866	9.0359E-02
Orthogonal Quality	0.9848	0.5009	1	4.0830E-02

Table 24 – Tray D meshing parameters

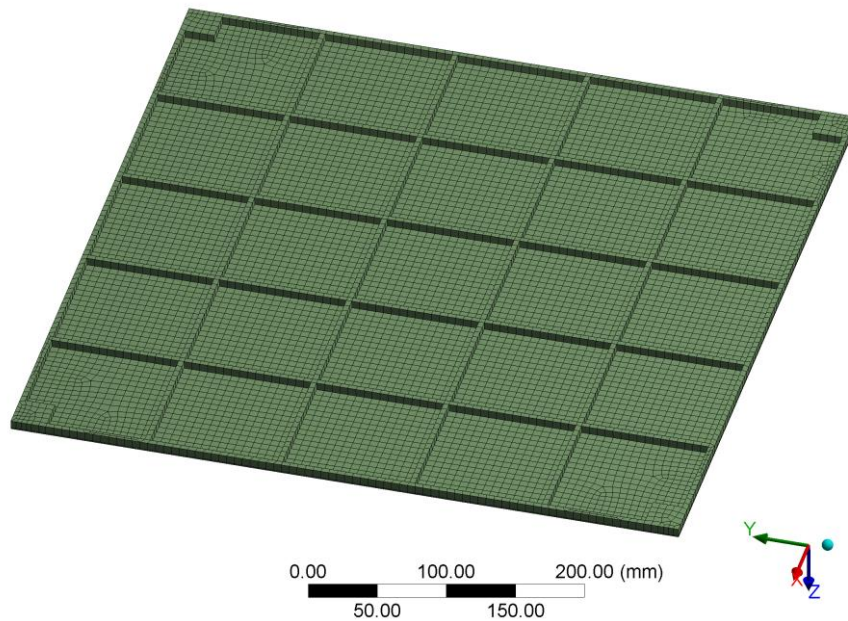


Figure 9.14 - Tray D meshing view 1

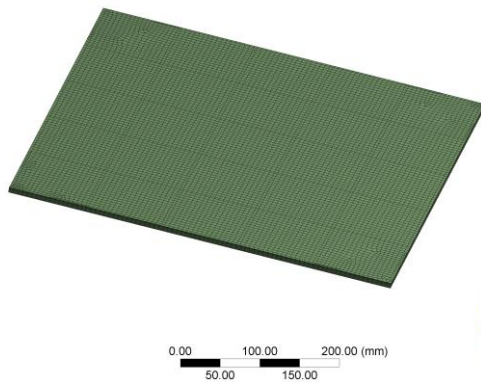


Figure 9.15 - Tray D meshing view 2

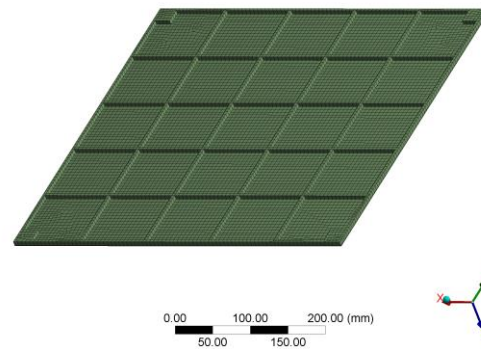


Figure 9.16 - Tray D meshing view 3Spars

Meshed using “Hex Dominant” method with a wide range of types of elements such as: 10-node tetrahedral-shaped (Tet10 – SOLID 187), 20-node hexahedral-shaped (Hex20 – SOLID 186) 15-node prism-shaped (Wed15 – SOLID 186) and 13-node pyramid-shaped (Pyr13 – SOLID 186), totalling 5,981 elements and 31,032 nodes. All of them with a typical size of 6mm.

	Average	Minimum	Maximum	Standard Deviation
Element Quality	0.5079	4.1359E-03	0.8834	0.1675
Aspect Ratio	7.5972	1.4769	2219.8	52.3518
Warping Factor	5.6625E-02	0	0.4914	7.8171E-02
Skewness	0.5520	3.8157E-03	0.9999	0.2082
Orthogonal Quality	0.5582	6.5697E-03	0.9999	0.2558

Table 25- Spars meshing parameters

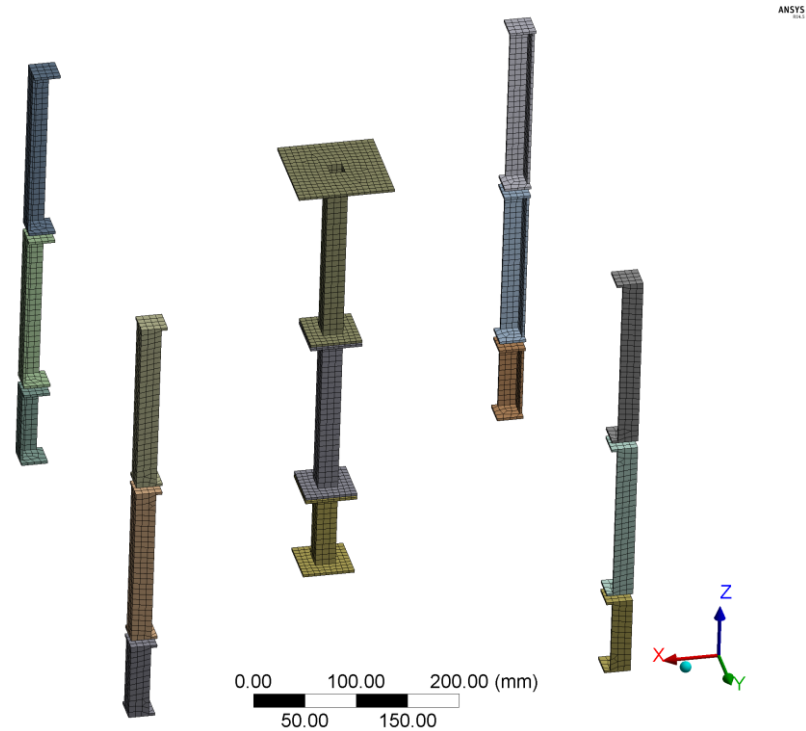


Figure 9.17 – Spars meshing view

9.2.4 Plates

The lateral plates of the satellite have been transformed to surfaces in order to use thick shell elements. As a result, the mesh quality is really good enabling “MultiZone Quad” method with quadrilateral elements (Quad4 – SHELL 181). The resulting mesh is composed of 16,348 elements and 16,864 nodes with the following quality:

	Average	Minimum	Maximum	Standard Deviation
Element Quality	0.9995	0.9995	0.9995	1.1589E-06
Aspect Ratio	1.0050	1.0046	1.0065	1.8885E-04
Warping Factor	3.2773E-16	0	9.9609E-13	0
Skewness	1.3059E-10	1.3057E-10	1.3075E-10	0
Orthogonal Quality	1	1	1	0

Table 26 – Plates meshing parameters

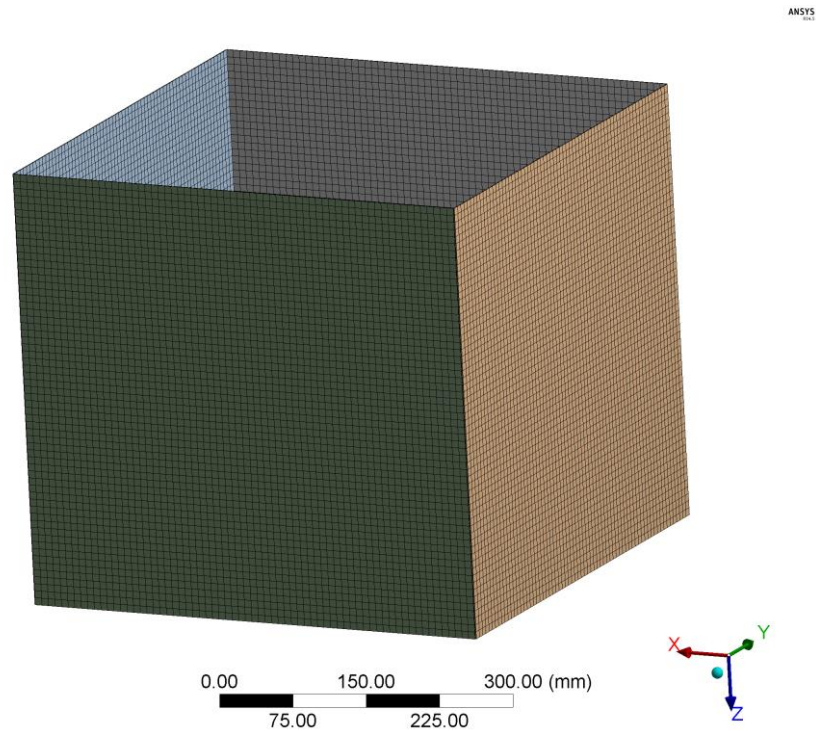


Figure 9.18 – Plates meshing view

9.2.5 Subsystems and payload

Meshed using “MultiZone” method with 20-nodes hexahedral elements (Hex20 – SOLID 186) and a size of 20 mm because of its non-structural behaviour. The total number of elements is 7,768 and the number of nodes rises to 39,953.

	Average	Minimum	Maximum	Standard Deviation
Element Quality	0.9880	0.7653	0.9997	2.2975E-02
Aspect Ratio	1.1193	1.0197	1.796	0.1157
Warping Factor	5.2074E-05	0	0.0006	1.2954E-04
Skewness	9.9012E-03	1.3057E-10	0.5198	4.6169E-02
Orthogonal Quality	0.9979	0.7951	1	1.4684E-02

Table 27 – Subsystems and payload meshing parameters

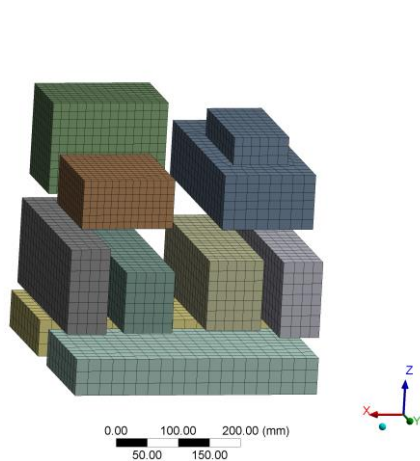


Figure 9.19 – Subsystems meshing view 2

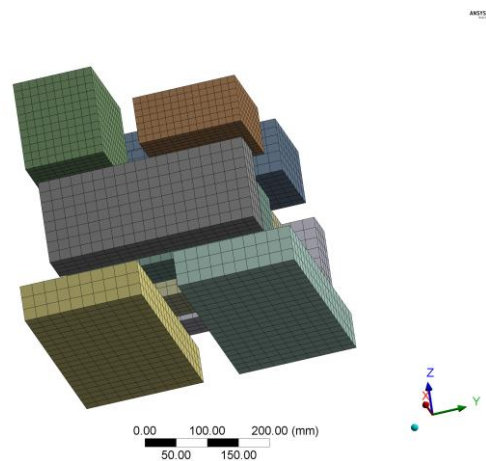


Figure 9.20 – Subsystems meshing view 3

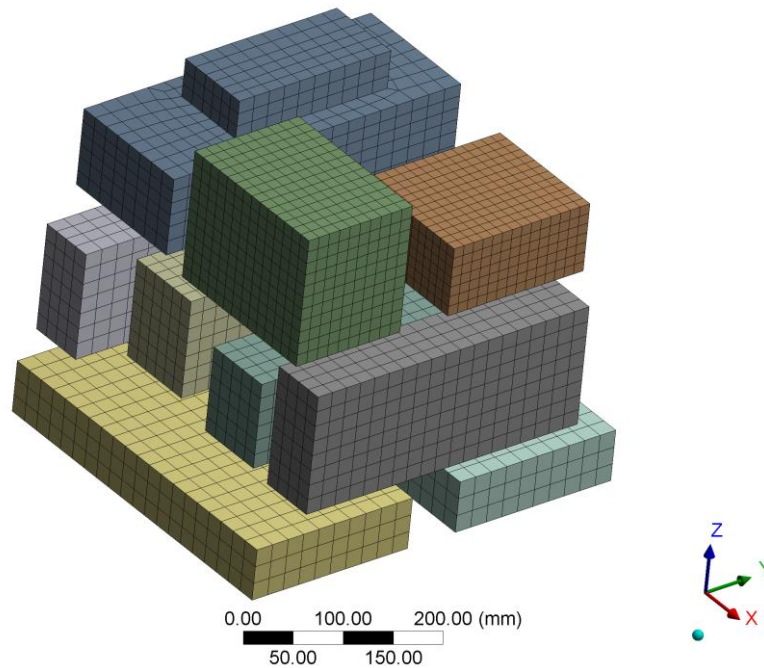


Figure 9.21 – Subsystems meshing view 1

9.3 Connections

The connections have been simplified to minimize errors during meshing and avoid the time and effort required to simulate the real connections between all the pieces through the contact surfaces.

This simplification has been modelled as a bonded contact where the parts are not allowed to separate nor slide. Surfaces will fit together irrespective of gap, penetration, loading and behaviour of other parts or contacts.

Also other types of connections were tested but the results given were not satisfactory.

9.4 Loads and Boundary Conditions

Section 6.1 contains all the information required by the LV manufacturer for the correct load setup of the analysis.

All the simulations conducted have been modelled using a constant damping ratio of 3% (0.03). This value has been obtained from [31]

9.4.1 Static Analysis.

For the static analysis, the loads defined in section 6.2.5 have been taken into account. These are shown in Table 28.

	Longitudinal (Static + Dynamic)	Lateral (Static + Dynamic)
Acceleration (<i>G</i>)	-7.5 <i>G</i> / +5.5 <i>G</i>	-6 <i>G</i> / +6 <i>G</i>

Table 28 –Static Loads Setup

To apply these loads, the following conditions have been considered

- Lateral loads act in all directions simultaneously.
- Loads are applied on the satellite’s center of gravity³
- The gravity load is included.

Also, the boundary condition used in this type of analysis is that the interface plane with the launch vehicle is completely fixed.

9.4.2 Modal Analysis.

The modal analysis has been performed by a frequency sweep from 0 to 300 Hz and a maximum number of modes to find 50.

As in the previous section the boundary condition used has been the fixed interface plane [12].

9.4.3 Harmonic Analysis

Section 6.1.6 contains all the information required by the LV manufacturer for the correct load setup of the analysis. The following accelerations have been used:

	Frequency range (Hz)	Qualification levels
Longitudinal	4 – 6	25 mm
(Z Axis)	6 – 100	3.75 <i>G</i>
Lateral	2 – 6	20 mm
(Z,Y Axes)	6 – 100	2.5 <i>G</i>

Table 29 - Harmonic Setup

In order to make a correct configuration of the pre-process, a solution was needed. This was achieved thanks to the ACT Enforced Motion ANSYS extension.

³ Needless to say that Ansys applies (in the Static Analysis Module) all inertial forces in the center of gravity of every finite element, so strictly speaking, it do not apply the inertial forces in the center of gravity of the satellite.

10 Results

In this section the results of the calculations are shown. They are classified as static, modal, and harmonic analysis. Results displayed in this section belong to the last design iteration. But before this results there have been others that did not satisfy the requirements and consequently have not been shown.

Figure 10.1 represents the Workbench Structure to simulate the model. As can be seen, it is divided into different blocks or modules. The first one consists of the material information of the model. The second one is a modal analysis of the structure. It tries to find the modes of vibration of the structure as well as the natural frequencies. Thirdly, the block called “Static Structural” is a structural analysis for the static forces. Finally, the last four modules of the Workbench are an analysis of the harmonic excitation of the satellite during launch. They are divided by frequency as the Rocket User’s Guide demanded.

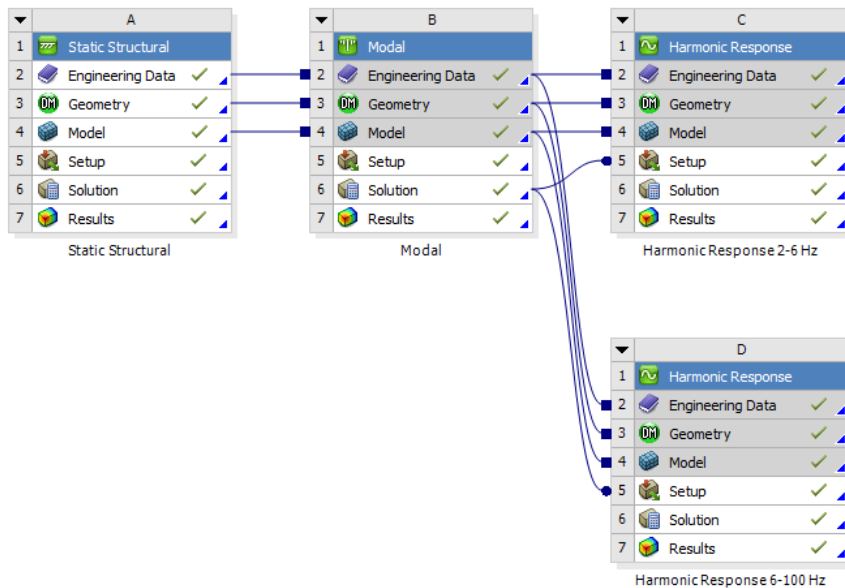


Figure 10.1 – ANSYS Workbench Project Schematic

Also, in the Harmonic Response modules an ANSYS extension called ACT has been used. It helped a lot in the simulation pre-process and in the model setup. It eased the calculations by helping a correct and simple input for the displacement requirements in the 4–6 and 2–6 Hz range.

10.1 Static Structural

There are several definitions of quasi-static loads. On the one hand, in the ECSS-E-ST-32 documents, they are defined as “Loads independent of time or which vary slowly, so that the dynamic response of the structure is not significant”. Note that this definition could be applied for almost every quasi static event.

On the other hand, NASA ([32] and [33]) says that a quasi-static load is a “Combination of static and low frequency loads into an equivalent static load specified for design purposes as CoG acceleration”. This is a more practical definition, as it is fully adequate for the design

of the spacecraft primary structure. So, from [34] it concludes that quasi static loading means under steady-state accelerations (unchanging applied force balanced by inertia loads). For design purposes (e.g. derivation of design limit loads, selection of the fasteners, etc.), the quasi-static loads are normally calculated by combining both static and dynamic load contributions. In this context the quasi static loads are equivalent to (or interpreted by the designer as) static loads, typically expressed as equivalent accelerations at the CoG.

Once defined what a quasi-static load is, the static analysis is started. The pre-process settings of this type of problem are shown below. First an acceleration has been added in order to simulate the inertial static loads during launch. The satellite has been put under a load of 58.8 m/s^2 ($6 G$) in the X and Y component, and 73.575 m/s^2 ($7.5 G$) in the Z Axis. Boundary conditions are the same in all the different types of analysis. That is, a fixed plane in the lower face of the satellite adaptor with the launcher. In Figure 10.2 the acceleration vector can be seen more clearly.

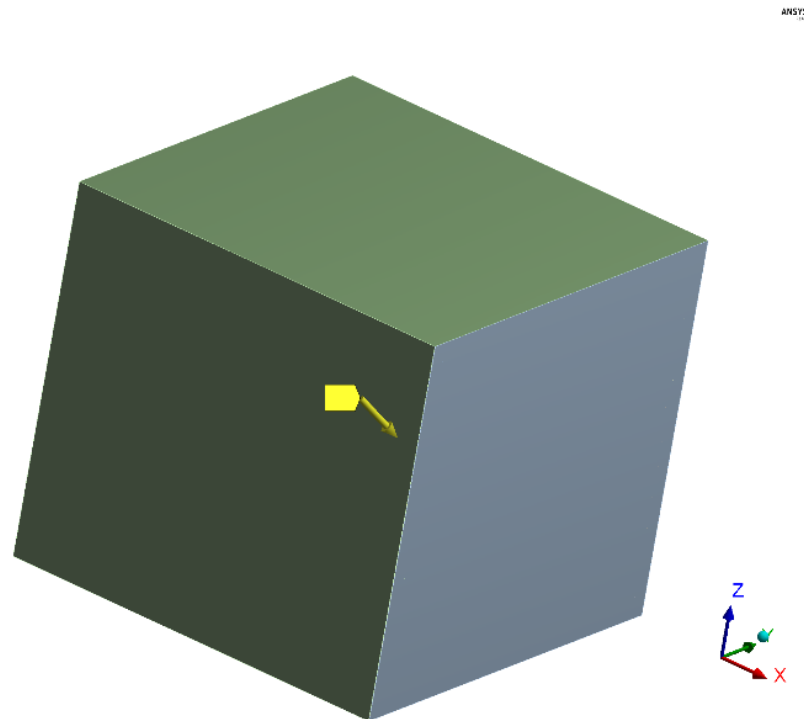


Figure 10.2 – Acceleration Settings

As soon as this has been explained, the mathematical model is run obtaining the following results shown below. It has been decided to show the total deformation of the structure and the von Mises Stress because they are good ways to study and analyse the behaviour of the structure.

Firstly, the total deformation of the satellite is displayed.

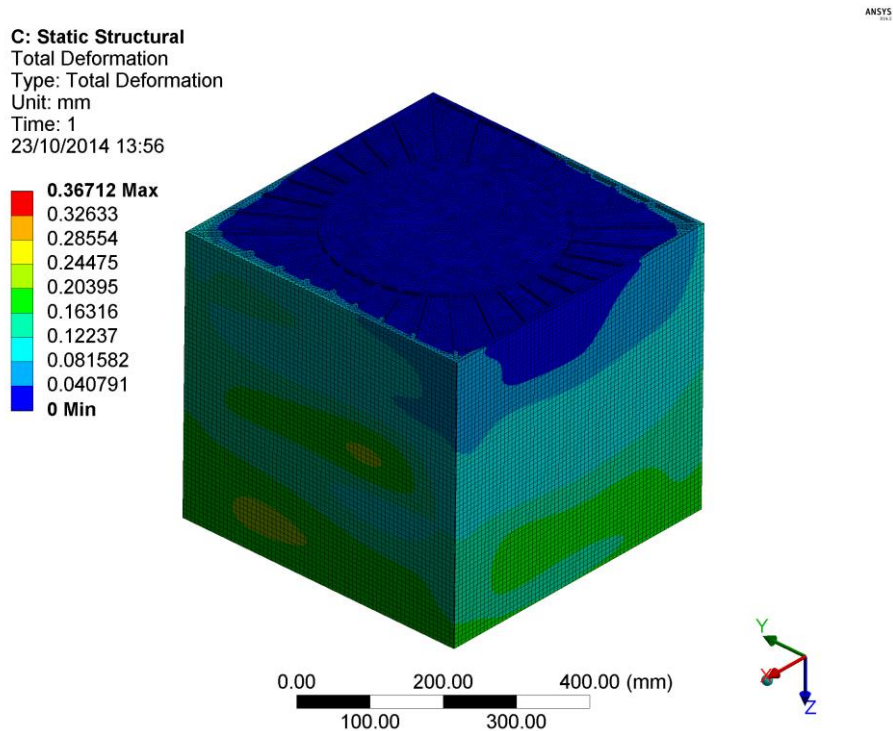


Figure 10.3 – Static Analysis- Total Deformation

The maximum deformation is of 0.36 mm approx. and occurs in the satellite subsystems, thus, this will not be a problem. Also it is a small value. This can be seen in the next view of the total deformation. Additionally, one must remember that the point where the maximum deformation occurs does not need to be precisely the most critical. That is why the von Mises stresses are shown in Figure 10.5.

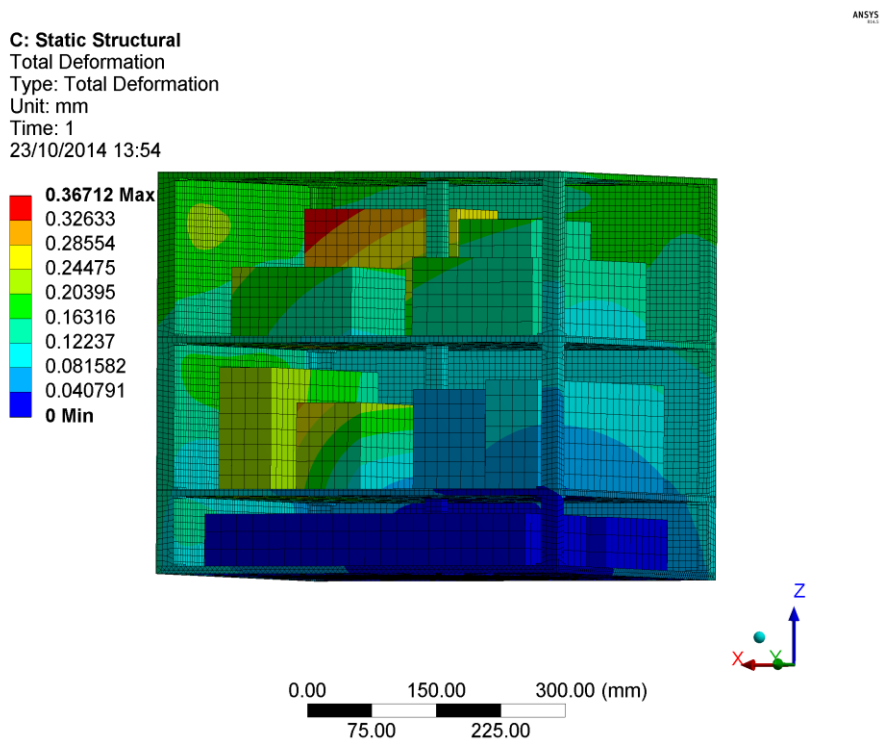


Figure 10.4 – Static Structural Total Deformation – 3D View

In terms of stresses, the results were low for most of the structure, obtaining its maximums in some of the trays' ribs. Therefore it was decided to show only the maximum VM stress areas. Also, in order to help the view of the trays, the subsystems have been hidden.

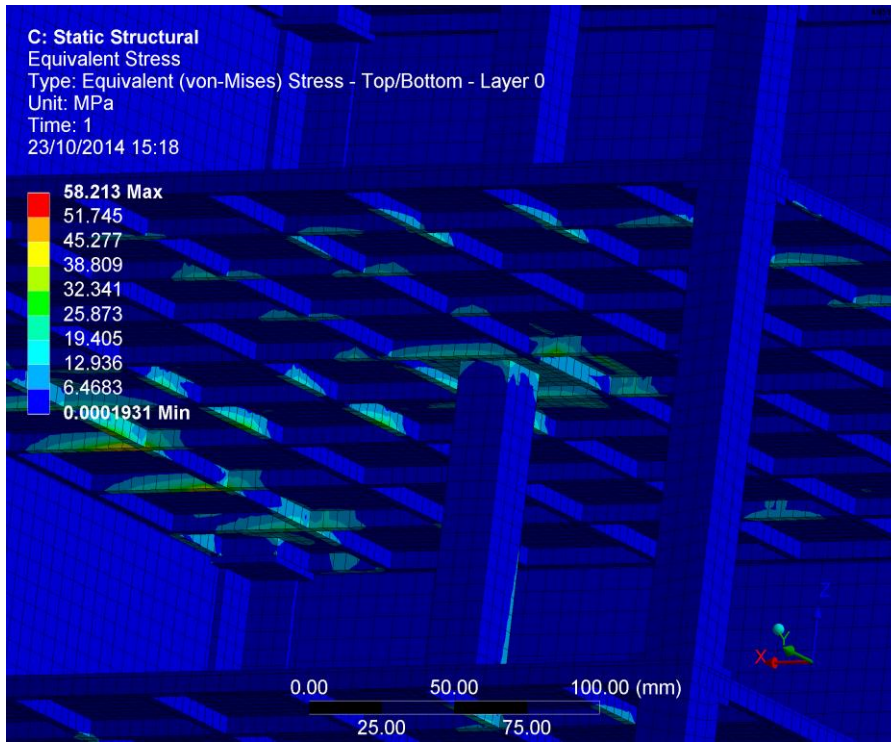


Figure 10.5 – Static Structural VM Stress Detail View 1

In the upper zone of the tray there are only little stresses as a by-product of the rib stresses.

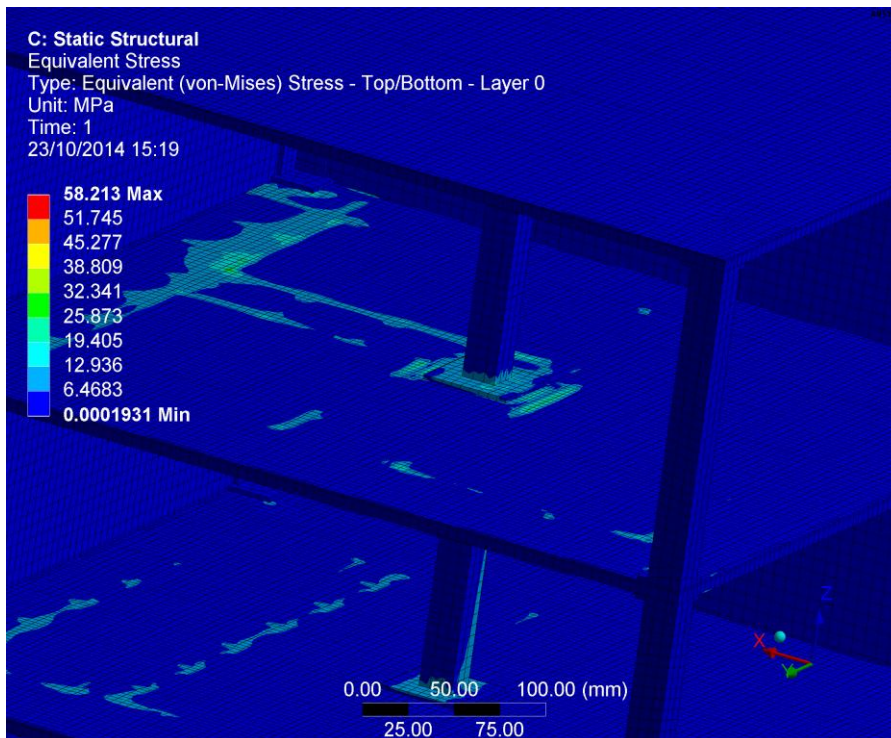


Figure 10.6 – Static Structural VM Stress Detail View 2

The maximum stresses are achieved, as it has been said, in the ribs of the satellite interface with the launcher. The next figure is a bottom-up view of this part.

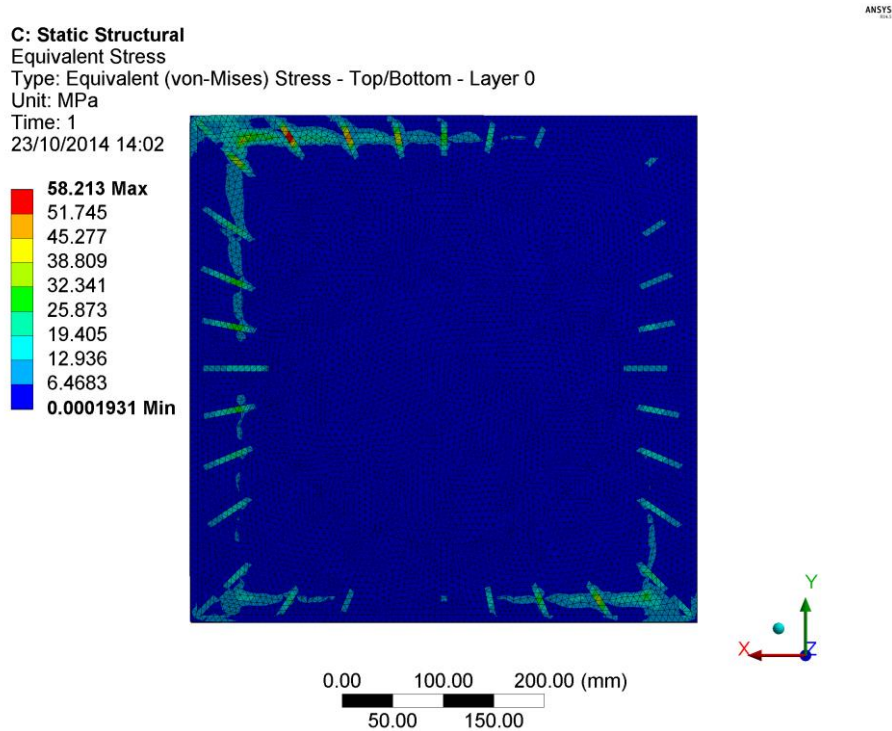


Figure 10.7 – Static Structural VM Stress Bottom to top View

The maximum of all the stresses supported is of 58.213 MPa, and take place in the ribs located in the left side of the upper zone of Figure 10.7. A detailed view is shown in Figure 10.8.

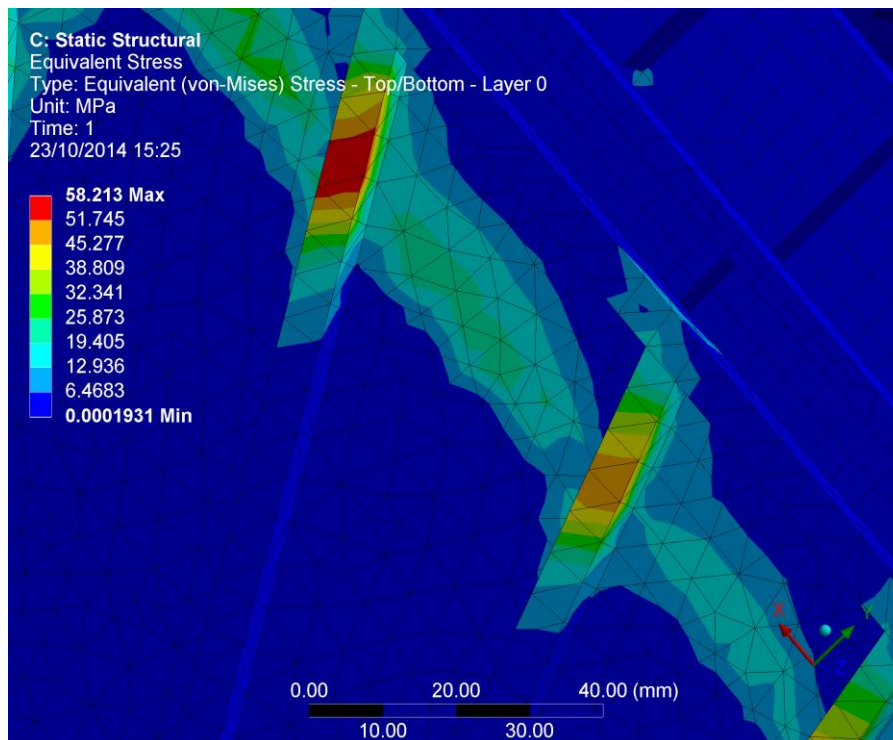


Figure 10.8 – Static Structural VM Stress Detail View 3

Considering that the Yield Strength of the Aluminium 7075 T-73 is 435 MPa, the minimum Safety Factor calculated with VM Equivalent Stress is of 7.4725. Here is a closer look at the Safety Factor distribution in the adapter:

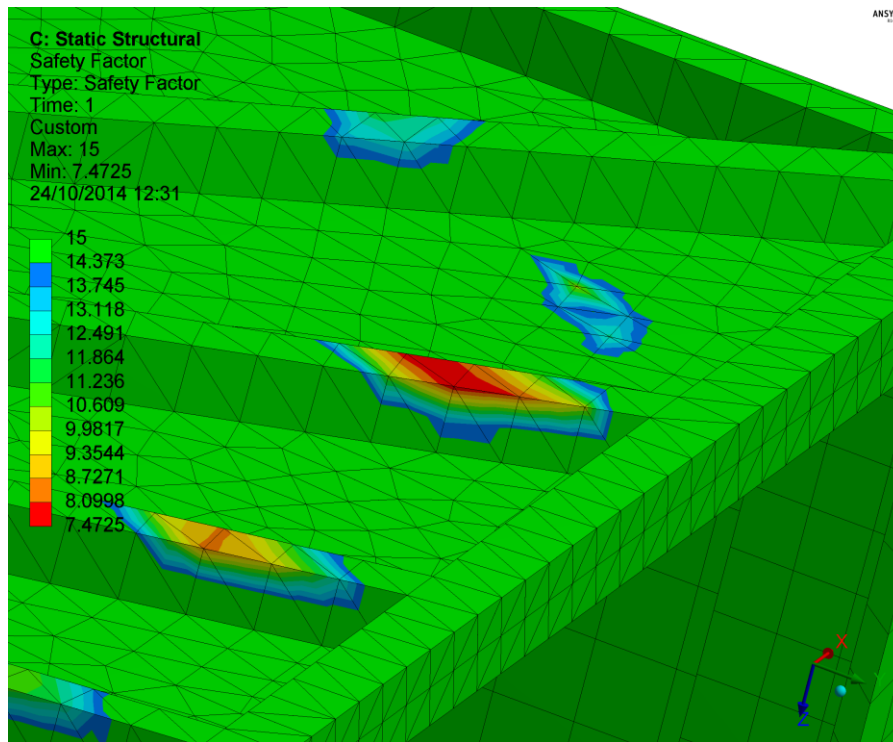


Figure 10.9 – Static Structural Safety Factor

It is a relatively high Safety Factor. That is because of the natural frequencies. The ribs and the satellite structure could be made thinner globally, but this would affect the frequencies of the natural modes, moving them to smaller values and preventing the satellite from fulfilling the launcher requirements. A minimum SF of 7.4725 widely satisfies the manufacturer's regulations (it must be remembered that in section 6.1.5 a SF of at least 2 is needed).

10.2 Modal properties

Once the Static analysis is done, the "Modal Analysis" block is computed. With the same boundary condition as always, it will find the natural frequencies of the structure as well as its vibration modes. All its modes up to 300 Hz have been calculated, but in Table 30 only the first six are shown.

Table 30, Table 31 and Table 32, are a very good way of knowing the type of every mode, that is, if it is a pure lateral, longitudinal or a mix of both. Strictly speaking, it is only the column "Ratio" which gives information about the purity of the vibration mode. If the Ratio is of one, the mode only exists in the axis of the table. From this it follows that the first lateral mode is contained in the X axis and has a frequency of 94.7989 Hz. Additionally, the first longitudinal mode has a frequency of 139 Hz.

Mode	Frequency (Hz)	Period	Partic. Factor	Ratio	Effective Mass
1	94.7989	1.05E-02	0.12811	1.000000	1.64E-02
2	108.733	9.20E-03	3.85E-02	0.300901	1.49E-03
3	111.69	8.95E-03	-2.29E-02	0.178886	5.25E-04
4	139.081	7.19E-03	2.56E-02	0.199526	6.53E-04
5	152.012	6.58E-03	-1.29E-02	0.10102	1.67E-04
6	158.426	6.31E-03	2.03E-02	0.158651	4.13E-04

Table 30 – Participation Factor Calculation – X Direction

So, given this information it can be concluded correctly that with the design shown in the previous chapter of the report, the structure fulfils the modal requirements of the launcher for small payloads.

Mode	Frequency (Hz)	Period	Partic. Factor	Ratio	Effective Mass
1	94.7989	0.10549E-01	0.6453E-02	0.059781	0.41642E-04
2	108.733	0.91968E-02	0.4565E-01	0.422904	0.20839E-02
3	111.690	0.89534E-02	0.10794	1.000000	0.11652E-01
4	139.081	0.71901E-02	-0.16175E-01	0.149848	0.26164E-03
5	152.012	0.65784E-02	0.18693E-01	0.173173	0.34943E-03
6	158.426	0.63121E-02	0.29508E-01	0.273367	0.87075E-03

Table 31 – Participation Factor Calculation – Y Direction

In the Y axis there is only one pure mode. It is the third one, with a frequency of 111.69 Hz.

The participation factor table lists participation factors, mode coefficients, and mass distribution percentages for each mode extracted. The participation factors and mode coefficients are calculated based on an assumed unit displacement spectrum in each of the global Cartesian directions. The reduced mass distribution is also listed. Also in the table is the effective mass. Ideally the sum of the effective masses in each direction should equal total mass of structure. Another detail worth noting is that the square root of the effective mass is the participation factor. [35]

Mode	Frequency (Hz)	Period	Partic. Factor	Ratio	Effective Mass
1	94.7989	0.10549E-01	-0.1403E-01	0.129366	0.19693E-03
2	108.733	0.91968E-02	0.63661E-01	0.586857	0.40527E-02
3	111.690	0.89534E-02	0.97748E-02	0.090109	0.95546E-04
4	139.081	0.71901E-02	0.10848	1.000000	0.11767E-01
5	152.012	0.65784E-02	0.68305E-02	0.062967	0.46655E-04
6	158.426	0.63121E-02	-0.67961E-02	0.062650	0.46187E-04

Table 32 – Participation Factor Calculation – Z Direction

It is important to note the various criteria to differentiate between an insignificant and significant mode frequency. The cumulated effective mass associated to the modes must exceed 60% or 70% of the total mass to be considered as primary modes. The percentages were obtained from [36] and [15]. In conclusion, all natural frequencies are above 45 and 90 Hz so the structure fulfils the frequencies requirements for lateral and longitudinal modes respectively (6.1.4).

10.2.1 Mode shapes

In the next chapter the first six mode shapes will be shown. To begin, a preview of the modes will be displayed (Figures 9.10-9.15), and following that, they will be explained.

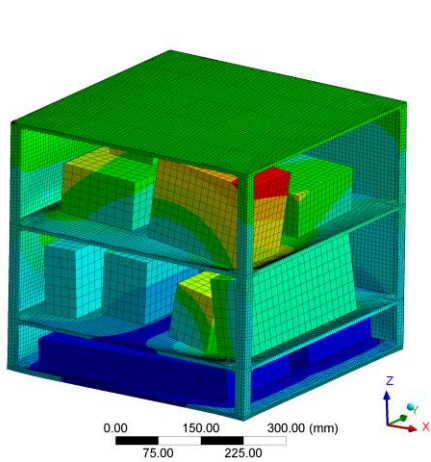


Figure 10.10 - Mode 1

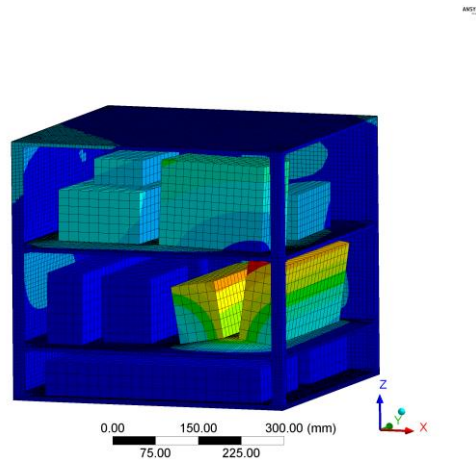


Figure 10.11 - Mode 2

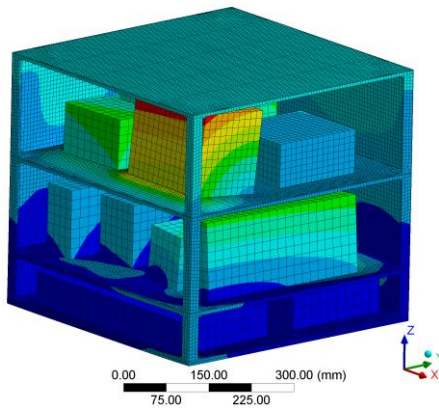


Figure 10.12 - Mode 3

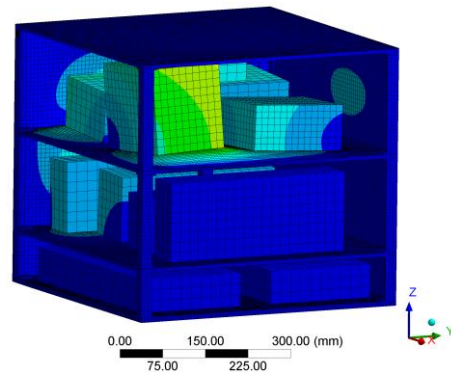


Figure 10.13 - Mode 4

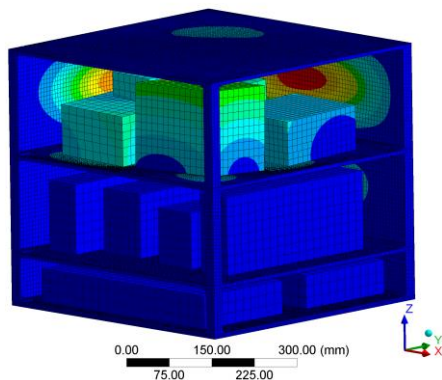


Figure 10.14 - Mode 5

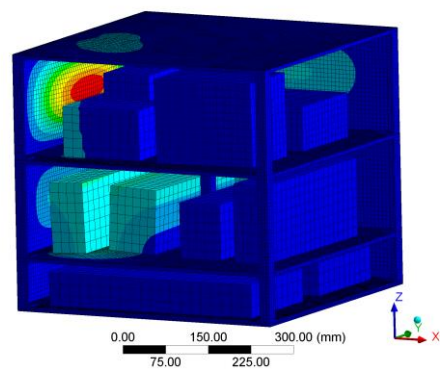


Figure 10.15 - Mode 6

10.2.1.1 Mode 1

The first mode is a pure lateral mode in the X axis. As can be seen, it affects almost all of the subsystems and the plates.

Figure 10.17 has its displacements augmented by a factor greater than one in such a way that the real behaviour of the satellite movements can be easily noticed. This will happen with all the 3D views in this chapter.

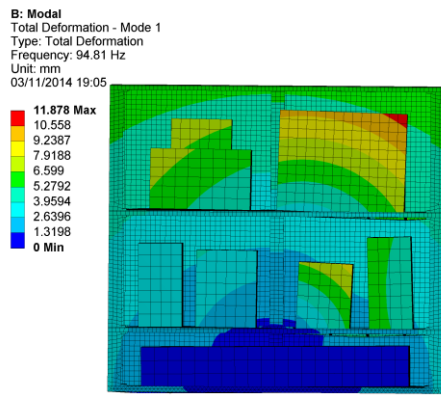


Figure 10.16 – Mode 1 ZX View

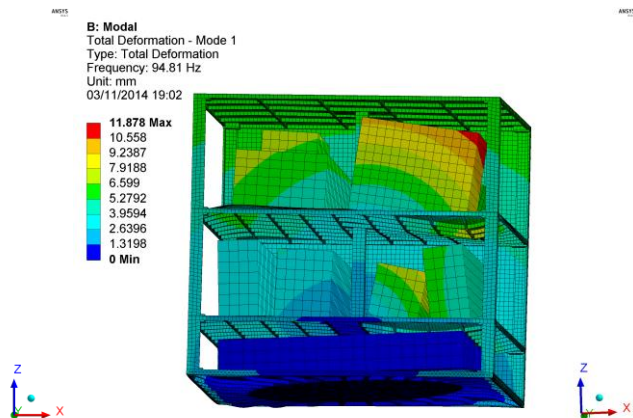


Figure 10.17 – Mode 1 3D View

10.2.1.2 Mode 2

The second mode is a mixed mode, with a participation of all three axes. As can be observed, it only affects half of the subsystems, particularly the OBDH and PL of the second tray leaving the subsystems of the first Tray static. That will happen in nearly every mode analysed.

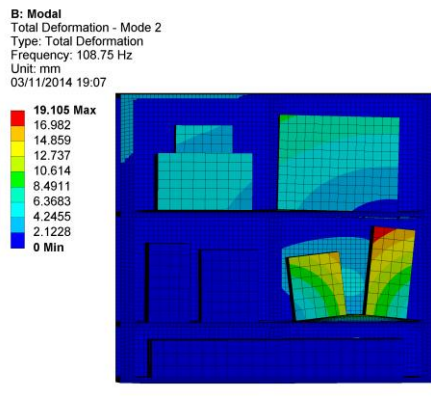


Figure 10.18 – Mode 2 ZX View

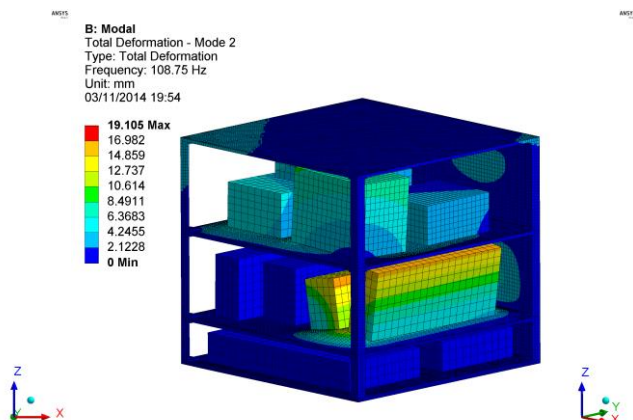


Figure 10.19 – Mode 2 3D View

10.2.1.3 Mode 3

The third mode is a pure lateral one in the Y axis. Note that the subsystems of Tray A are unaffected and that the lateral plates of the satellite are almost unaltered.

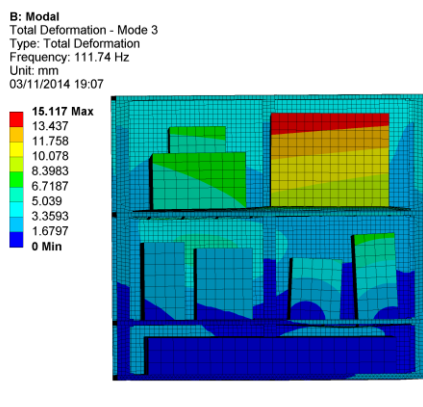


Figure 10.20 – Mode 3 ZX View

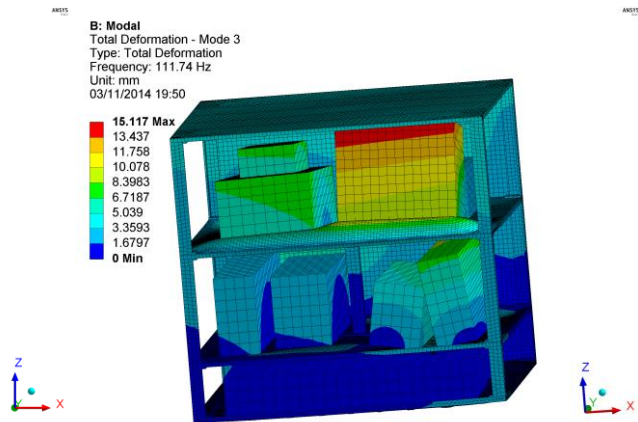


Figure 10.21 – Mode 3 3D View

As previously stated, the displacement 3D view of the mode is multiplied automatically by a factor greater than one, so in spite of the collision shown between two subsystems in Tray B, in reality there is no contact.

10.2.1.4 Mode 4

The fourth mode is pure longitudinal along the Z axis. It only affects the upper subsystems.

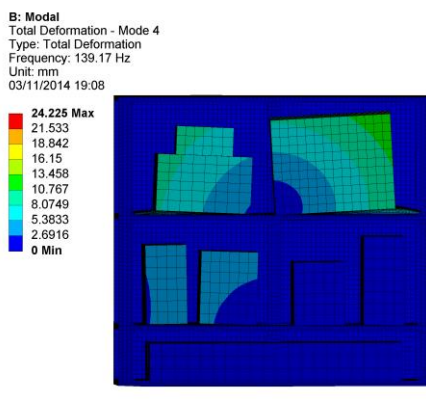


Figure 10.22 – Mode 4 ZX View

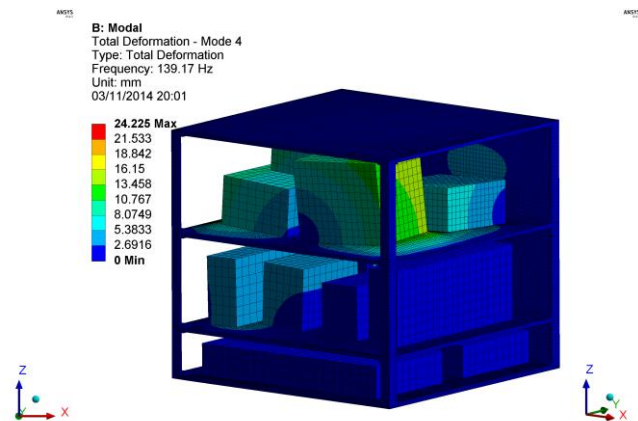


Figure 10.23 – Mode 4 3D View

The deformation of the lateral plates in this mode is relatively important, henceforth they have been highlighted. The criteria followed to decide if the plate's deformation should be shown or not is the magnitude of the deformation referenced with the rest of the satellite. To do that, the colours of the legend have been used as a guide using red as the trigger.

B: Modal
 Total Deformation - Mode 4
 Type: Total Deformation
 Frequency: 139.17 Hz
 Unit: mm
 03/11/2014 20:21

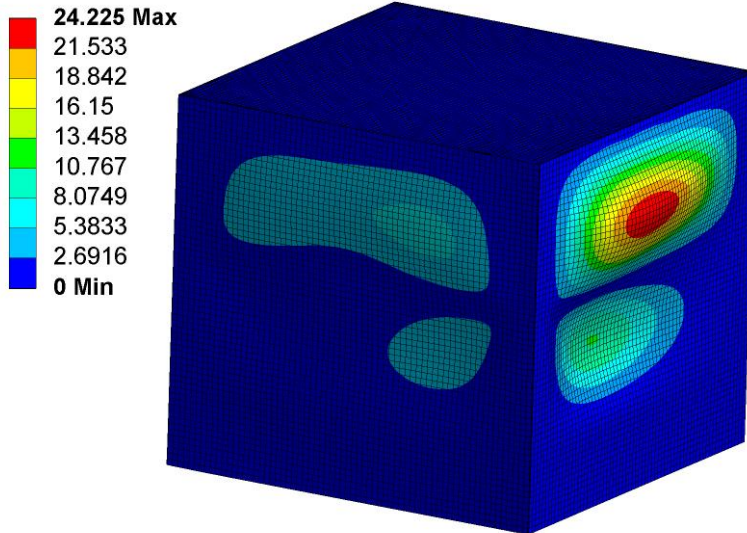


Figure 10.24 – Mode 4 Plates View Auto Scale

10.2.1.5 Mode 5

The fifth mode primarily warps the lateral plates. In addition to this, it affects the Payload 2, 3 and the ADCS.

B: Modal
 Total Deformation - Mode 5
 Type: Total Deformation
 Frequency: 152.07 Hz
 Unit: mm
 03/11/2014 20:17

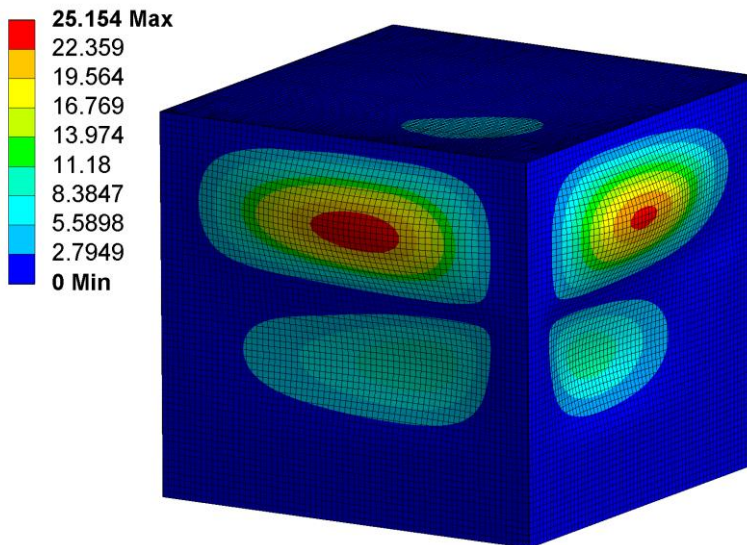


Figure 10.25 – Mode 5 Plates View

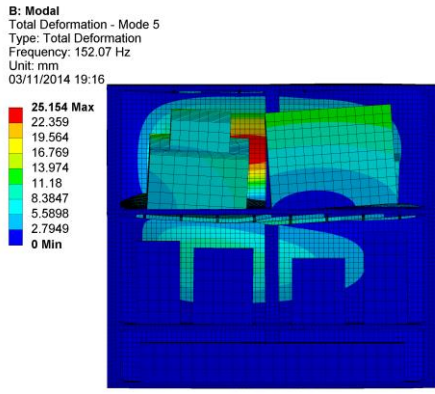


Figure 10.26 – Mode 5 ZX View

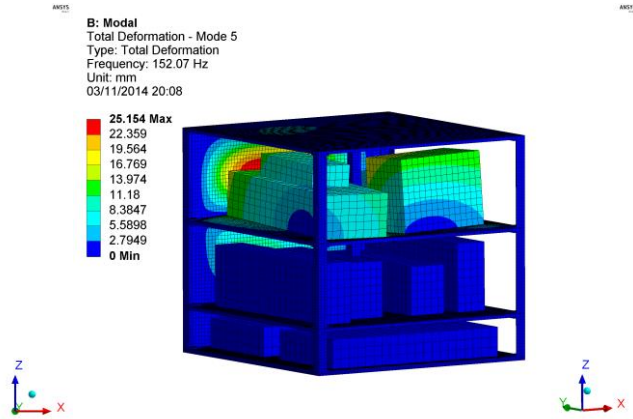


Figure 10.27 – Mode 5 3D View

10.2.1.6 Mode 6

The sixth mode is started mainly by the ADCS of the Tray B and the TTC. The subsystems of the upper tray (Tray C) are also involved, but they are less importantly implicated.

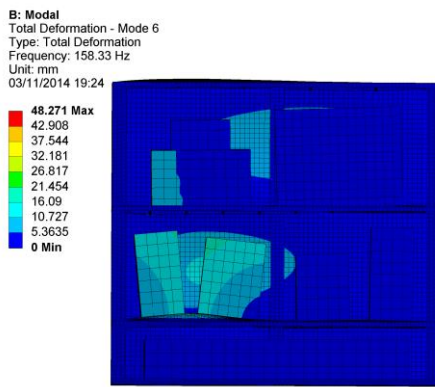


Figure 10.28 – Mode 6 ZX View

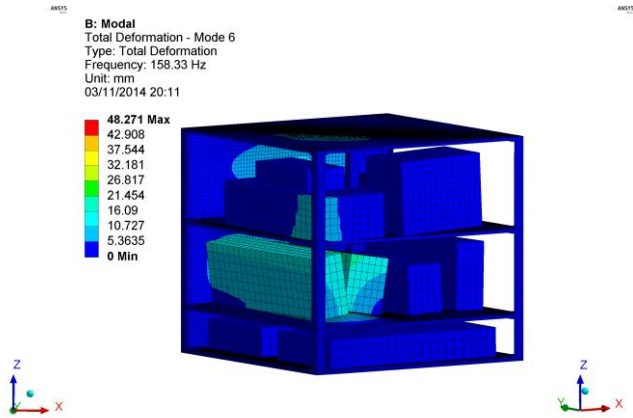


Figure 10.29 – Mode 6 3D View

In this mode the lateral plates are also affected, as is shown in Figure 10.30.

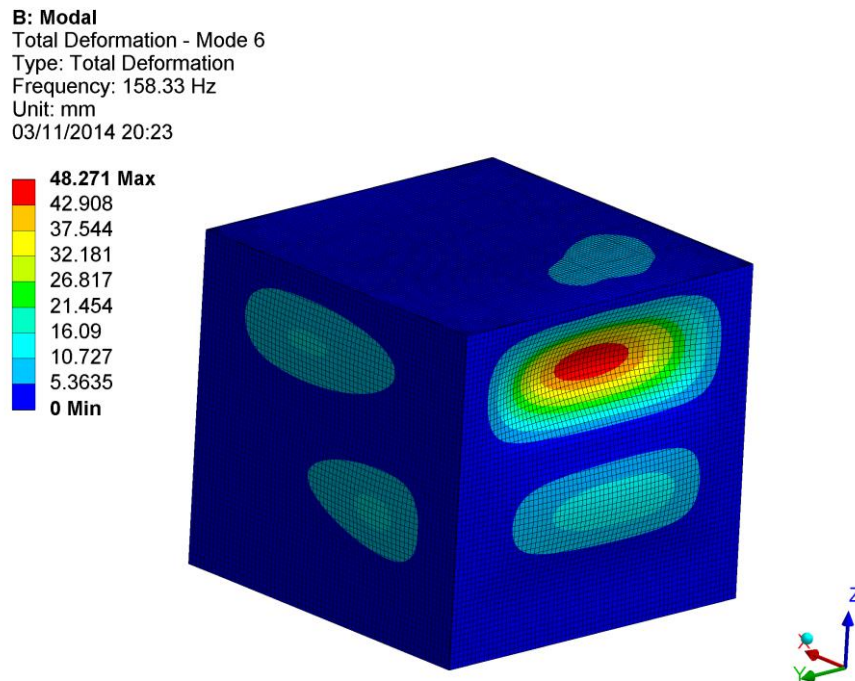


Figure 10.30 – Mode 6 Plates View

Needless to say that the modes shown are mainly caused by the weights and geometry of the subsystems. Therefore, the sizing of them has been crucial in correctly fulfilling the Final Project.

Another detail to be emphasized is the value of the deformations shown in the modal analysis. The nature of this chapter, as far as deformation is concerned, is completely qualitative, not quantitative, so the values of the displacements should not be taken seriously. What is relevant is the way its elements move (modal shapes), the values of the natural frequencies, and the type of each mode (lateral, longitudinal).

10.3 Harmonic Analysis

Sustained cyclic loads will produce sustained cyclic (or harmonic) responses in a structural system. Harmonic response analyses allow for the prediction of the sustained dynamic behaviour of any structure, thus enabling the verification of whether or not structural designs will successfully overcome resonance, fatigue, and other harmful effects caused by forced vibrations. A harmonic response analysis is a technique used to determine the steady-state response of a linear structure to loads that vary sinusoidally with time. This analysis technique can only calculate the steady-state forced vibrations of a structure. Transient vibrations, which occur at the beginning and ending of the excitation, are not taken into account by harmonic response analyses.

The general idea of a harmonic response analysis is to calculate the structure's response at several frequencies, and graph the response of various parameters (usually displacements and stresses) versus frequency. "Peak" responses are then identified on the graph and reviewed to ensure that the satellite fulfils the structural requirements requested by the LV

manufacturer. Peak harmonic responses occur when the forcing frequencies of the structure match its natural frequencies (resonance frequencies). Therefore, before performing harmonic analysis, the natural frequencies of the structure should be previously determined through a modal solution as it has been done in the last section.

It is specified in the manufacturer manual (“ASAP-5 User’s Manual” for piggyback payloads carried by Ariane 5 LV [21]) that during launch vehicle flight, the satellite-LV interface is affected by sinusoidal vibrations in the lateral and axial directions. The frequency band to be analysed in the lateral directions range from 2 to 100 Hz, while in the longitudinal direction it ranges from 4 to 100 Hz. This is shown in the following table of qualification requirements (Table 33):

	Frequency range (Hz)	Qualification levels (0 - peak)
Longitudinal	4 - 6	25 mm
	6 - 100	3.75 <i>G</i>
Lateral	2 - 6	20 mm
	6 - 100	2.5 <i>G</i>

Table 33 - Set up Conditions

As shown in Table 33, the excitation set up varies for each frequency range and direction. In the longitudinal direction a 25 mm displacement excitation (0-peak) in the range of 4-6 Hz is required while a range of 6-100 Hz requires an acceleration excitation (0-peak) of 3.75 *G*. On the other hand, in the lateral direction the harmonic analysis must include a 20 mm displacement excitation (0-peak) in the range of 2-6 Hz and a 2.5 *G* acceleration excitation (0-peak) in the range of 6-100 Hz. For the simulation, the satellite has been excited in all directions at the same time, this is, laterally (*X* and *Y* directions) and longitudinally (*Z* direction). The Harmonic Analysis requested is specified in the Regulation’s section 6.1.6.

In order to study and analyse the results, the calculations will be divided by the direction of their loads and then by ranges of their frequencies.

10.3.1 Longitudinal

Maximum values are displayed in the following graphs. The process carried out by ANSYS works as following: For each frequency, the whole structure is analysed looking for the maximum stresses and deformations. Once found, the data is saved and ANSYS moves on to the next frequency point and repeats the last step. Point by point a graph is built.

The longitudinal data will be given first and will show the deformations and loads manifested in the *Z* axis.

10.3.1.1 4-6 Hz

10.3.1.1.1 Deformation

Here is shown the directional deformation in the *Z* axis for the displacement. The graph starts in 25 mm because that is the displacement imposed for the analysis. No resonance peaks were found in these frequencies. Since a higher frequency implies bigger stresses and inertia, the curve is monotone increasing.

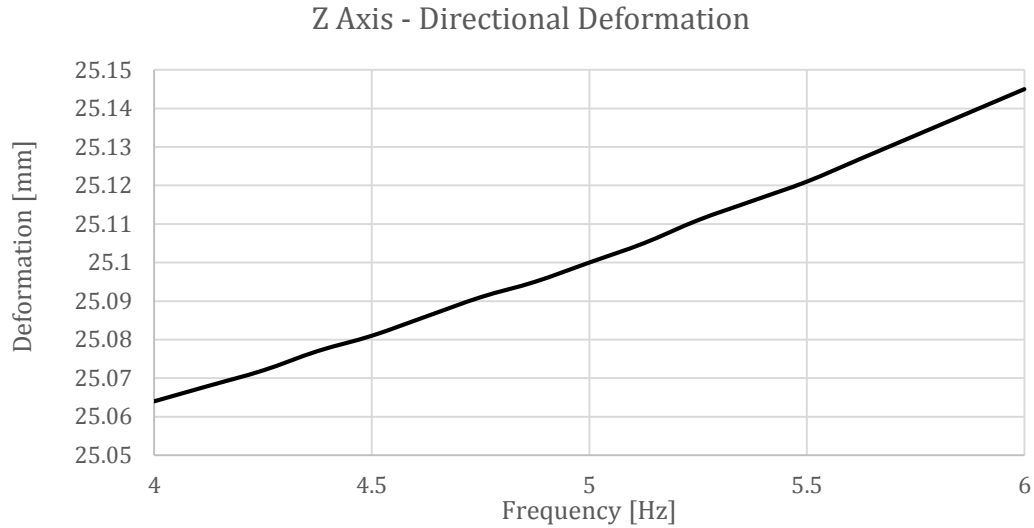


Figure 10.31 – Z Axis directional deformation / 4 – 6 Hz longitudinal

The peak deformation as it has been said before, occurs at 6 Hz and is only of 0.145 mm, so it is practically unappreciable. Figure 10.32 is a coloured true scale image of the directional deformation in the Z axis for the frequency and phase angle of the maximum Z axis deformation.

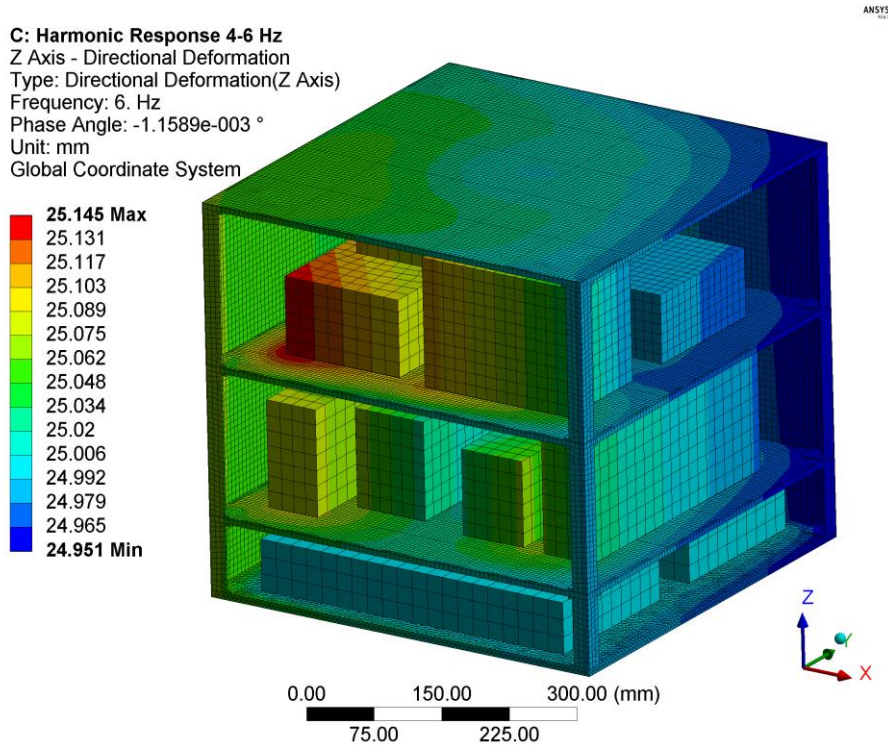


Figure 10.32 – Directional Deformation 6 Hz

10.3.1.1.2 Stress

This graph has the same behaviour as the previous one, because stresses are related with deformation. Nevertheless, it is necessary to note that the point of maximum stress could not be the same as the point of maximum deformation. Henceforth it was necessary to show both.

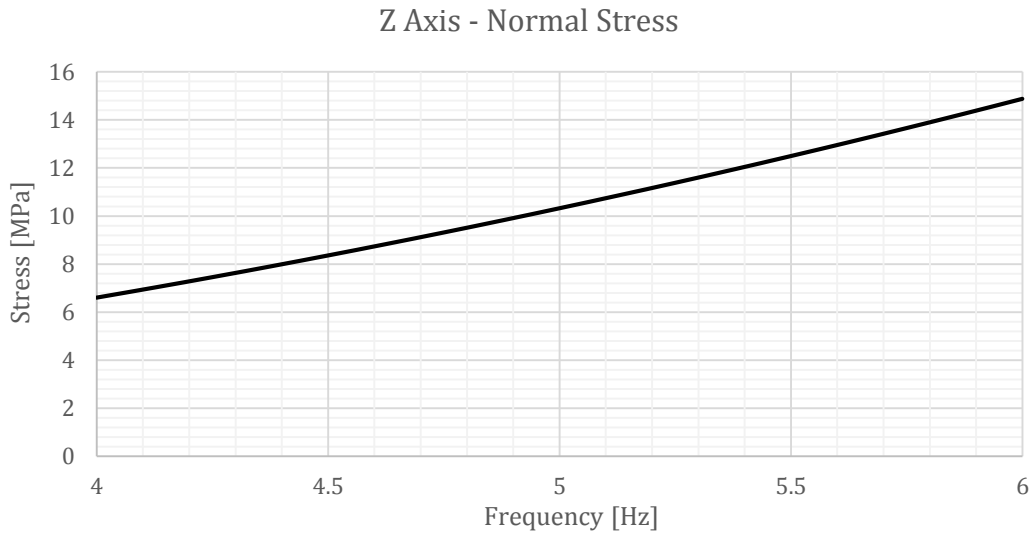


Figure 10.33 – Z Axis normal stress / 4–6 Hz longitudinal

As it can be seen in Figure 10.34, the maximum Z axis stress is located in Tray C near Payload 1. This point matches the area of maximum directional deformation seen in the previous section. In any case the maximum stress is only 14.878 MPa so taking into account the maximum yield strength of the 7075-T73 aluminium (over 400 MPa), this stress value is not a big deal for the structure.

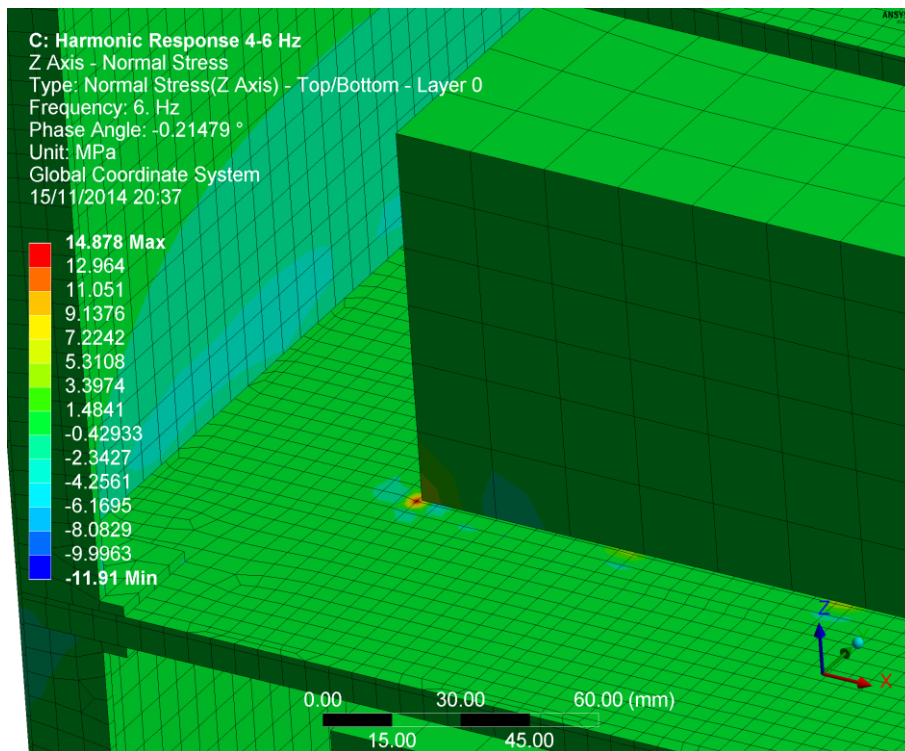


Figure 10.34 – Z Normal Stress 6 Hz longitudinal

10.3.1.2 6–100 Hz

10.3.1.2.1 Deformation

The graphs for the second range of frequencies are much more interesting. As previously stated, this curve corresponds with the points of the structure for every frequency in which

there is a maximum deformation. A detail to take into account and evaluate is the peak of the deformation near 94–95 Hz. This peak corresponds with the first pure lateral mode of the structure. Even though it is a lateral mode and this graph is about the longitudinal behaviour of the satellite, the structure is still affected longitudinally, in some way, by the lateral mode.

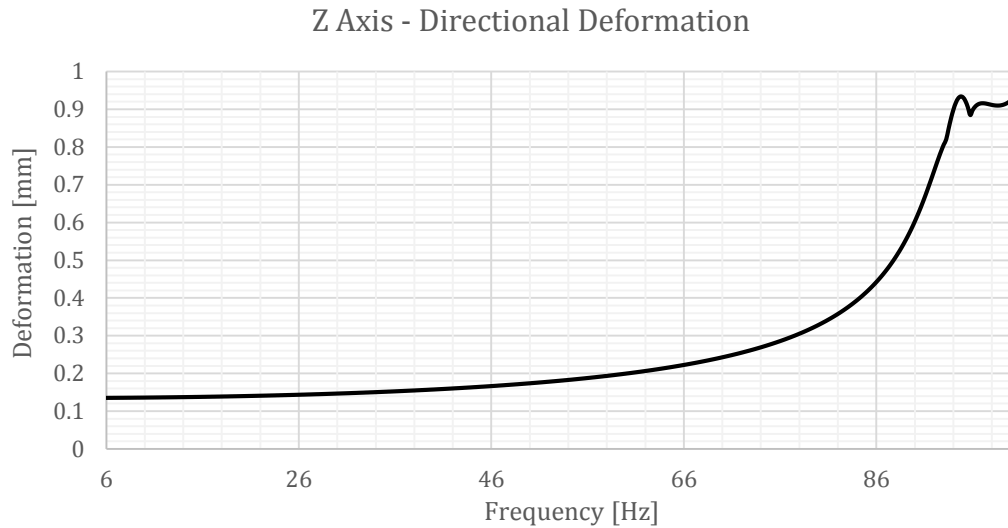


Figure 10.35 – Z Axis directional deformation / 6 – 100 Hz longitudinal

The deformation of the structure at the peak value of the frequency sweep is shown in Figure 10.36. It occurs at the first natural frequency (94.7989 Hz), but due to the lack of resolution in the results, 94.75 Hz has been considered, analysed, and studied as the resonance point. As done in the previous chapter (Modal properties), the deformations have been exaggerated. They have been multiplied by a factor bigger than one in order to more easily view the displacements.

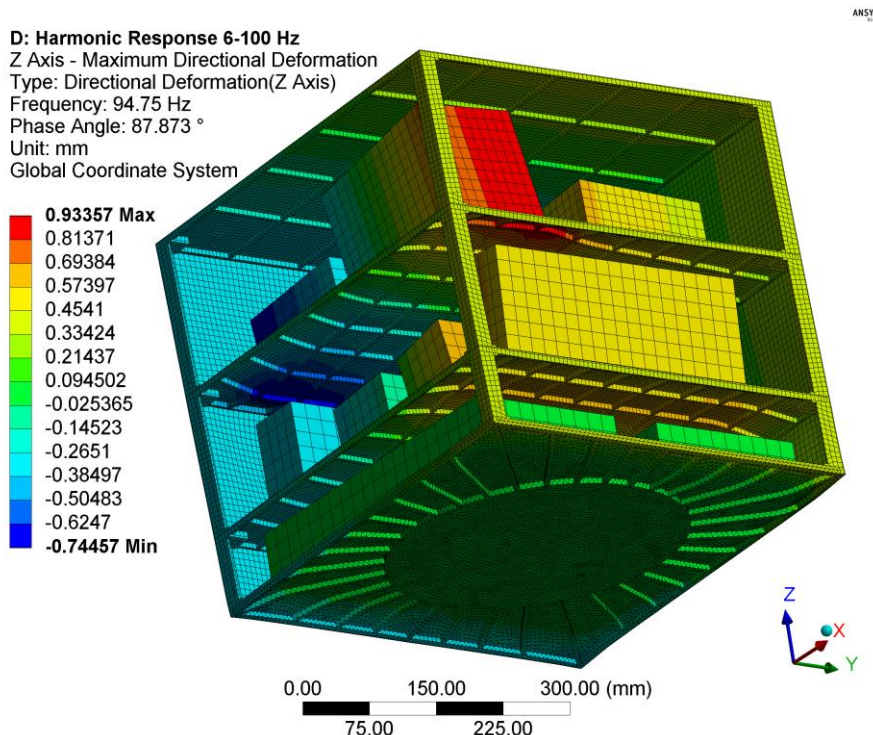


Figure 10.36 – Maximum Z Axis Directional Deformation 94.75 Hz 3D View

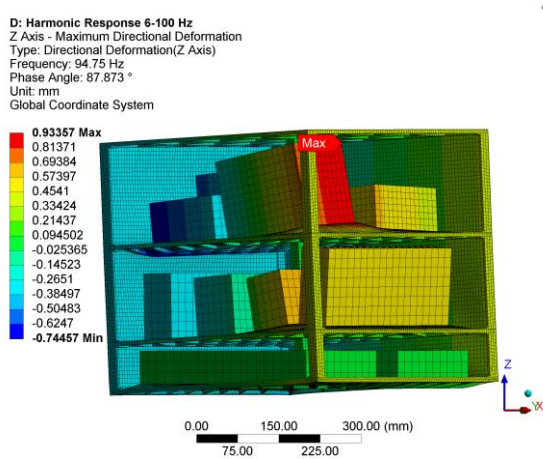


Figure 10.37 – Maximum Directional Deformation 94.75 Hz Auto Scale

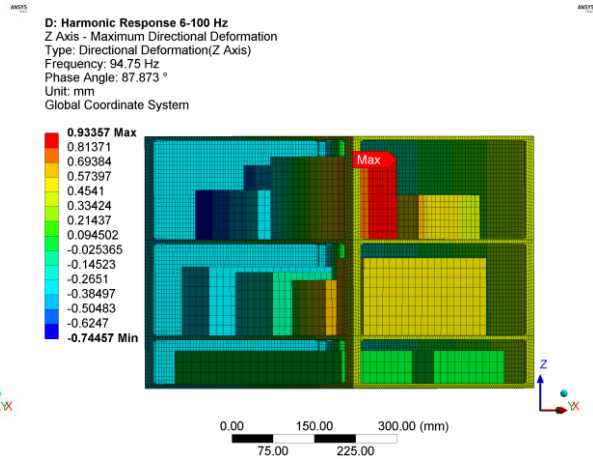


Figure 10.38 – Maximum Directional Deformation 94.75 Hz True Scale

In this result the maximum directional deformation occurs in the PL allocated on the Tray C of the satellite. It has a value of 0.93 mm approx., implying that it is not very significant.

10.3.1.2.2 Stress

The most important value to be analysed is the stress as it is the base for the structural design of the cube-shaped satellite. A maximum of the longitudinal stress and the frequency in which the resonance point occurs can be seen below. That does not necessarily mean that the point of the maximum longitudinal stress in the resonance is the same as the maximum deformation. In fact, it is not. This can be observed by making a comparison between Figure 10.37 and Figure 10.40. In these figures the maximum values of the structure are given in different parts of the satellite (Tray C near one subsystem in the 11.35 and in the top vertex of the same subsystem in 11.33).

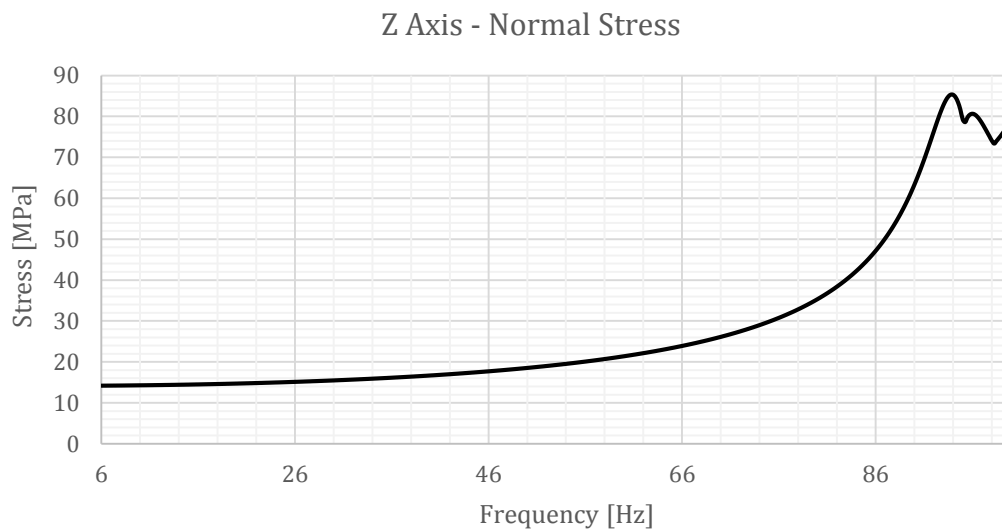


Figure 10.39 – Z Axis normal stress / 6 – 100 Hz longitudinal

The figure below (Figure 10.40) indicates where the maximum normal stress in the Z axis occurs. There are various important points to consider: the corners of the boxes and the ribs of the plates. Figure 10.40 shows one of these critical points. However, the maximum value obtained is about 85 MPa. This is not a big or risky value taking into account that the yield strength of the aluminium alloy used is over 400 MPa.

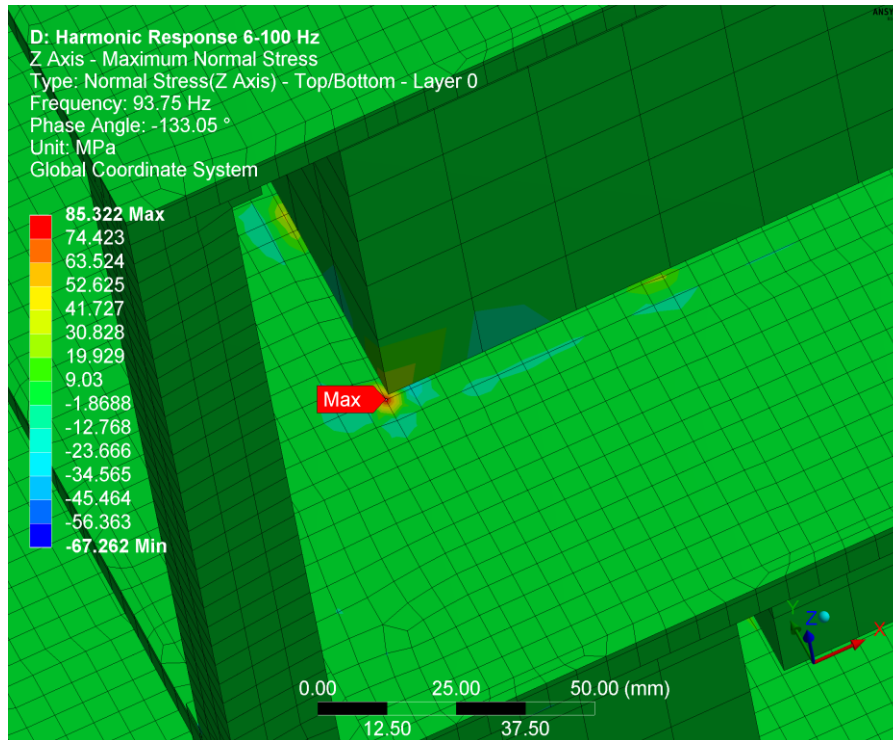


Figure 10.40 – Maximum Normal Stress Z Axis

10.3.2 Lateral

In the next chapter lateral behaviour of the satellites will be displayed and discussed. To do so, the lateral variables analysed were divided by its axes (X and Y).

10.3.2.1 2–6 Hz

10.3.2.1.1 Deformation

Firstly, and as in the previous breakdowns, the maximum deformation is plotted. In this case the range of frequency has changed. It goes from 2 to 6 Hz, inasmuch as the frequency requirements of the launcher are different for these axes. Other than that, the shape of the graph is mostly the same as the previous ones for these numbers. They are monotone increasing for the same reasons as given before.

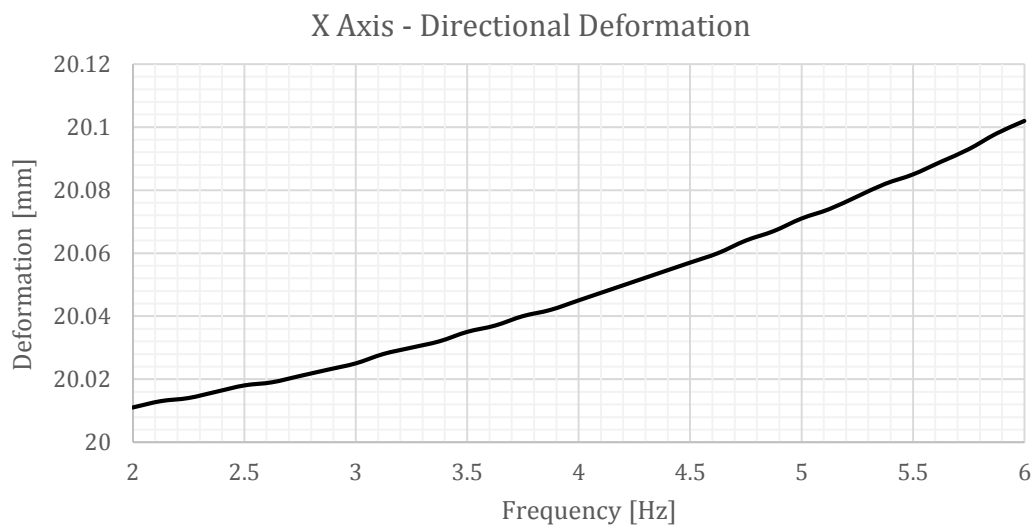


Figure 10.41 – X Axis directional deformation / 2 – 6 Hz lateral

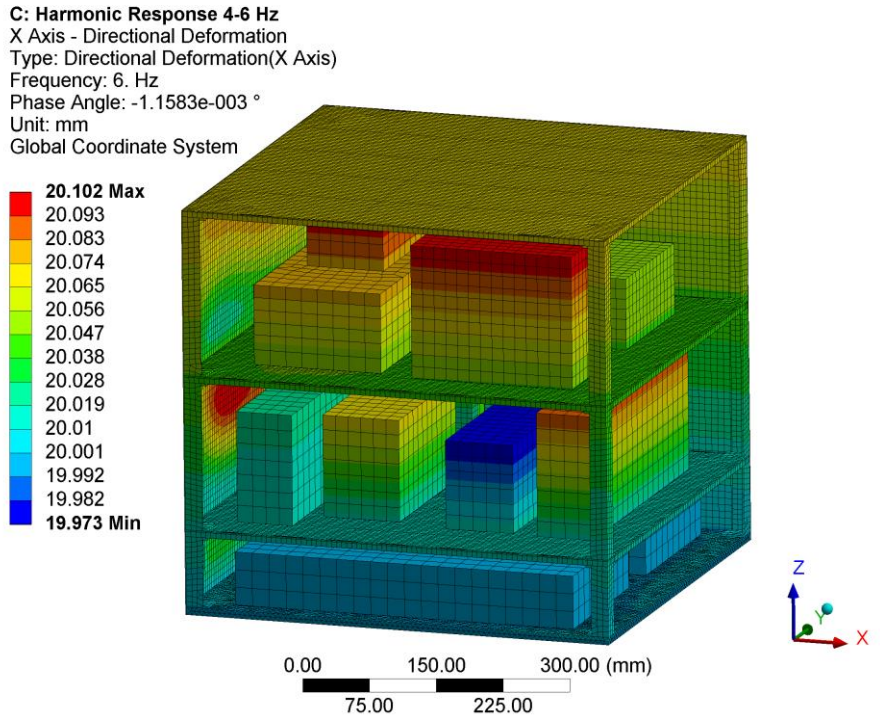


Figure 10.42 - Maximum Z Axis Directional Deformation 6 Hz 3D View

The following graph is the Maximum Deformation for the Y axis.

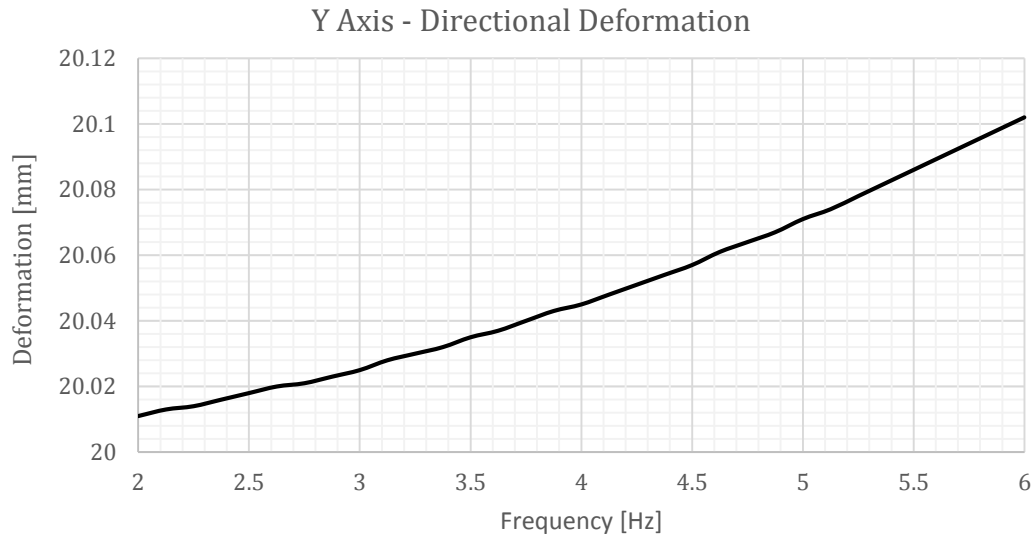
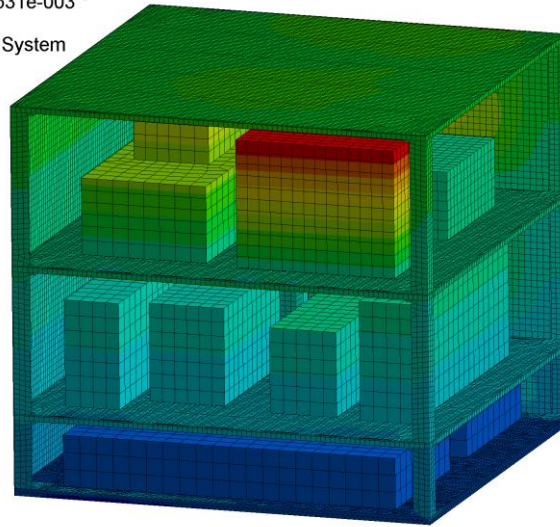


Figure 10.43 - Y Axis directional deformation / 2-6 Hz lateral

C: Harmonic Response 4-6 Hz
 Y Axis - Directional Deformation
 Type: Directional Deformation(Y Axis)
 Frequency: 6. Hz
 Phase Angle: -1.0531e-003 °
 Unit: mm
 Global Coordinate System

20.102 Max
 20.094
 20.085
 20.077
 20.069
 20.06
 20.052
 20.043
 20.035
 20.027
 20.018
 20.01
 20.001
 19.993
 19.984 Min



0.00 150.00 300.00 (mm)
 75.00 225.00

Figure 10.44 - Maximum Y Axis Directional Deformation 6 Hz 3D View

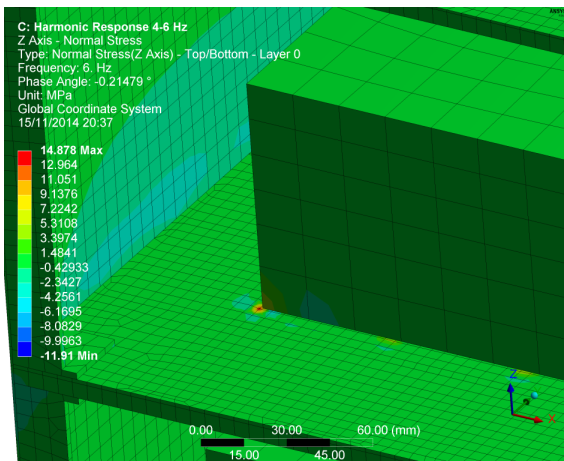


Figure 10.45 - Max Z Axis Normal Stress 6 Hz Detail 1

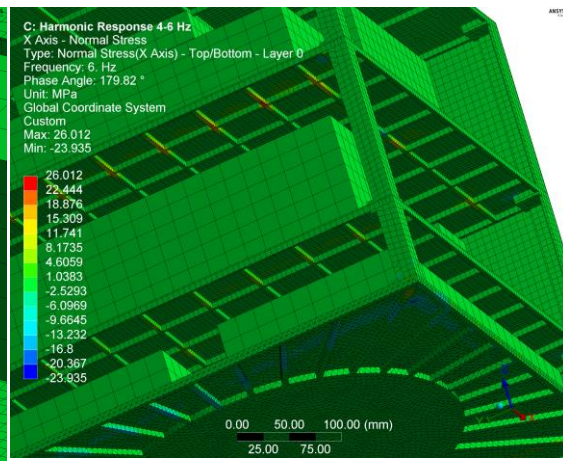


Figure 10.46 - Max X Axis Normal Stress 6 Hz Detail 1

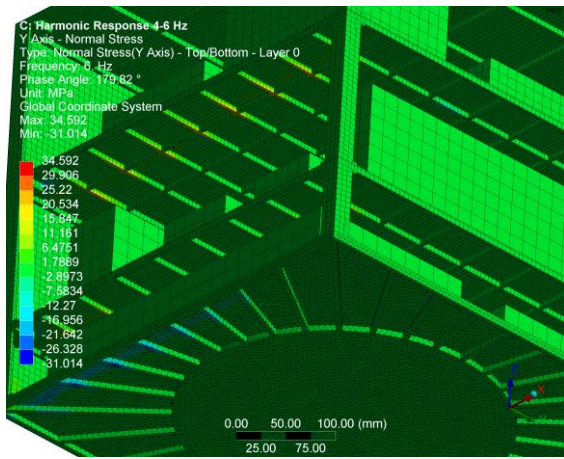


Figure 10.47 - Max Y Axis Normal Stress 6 Hz Detail 1

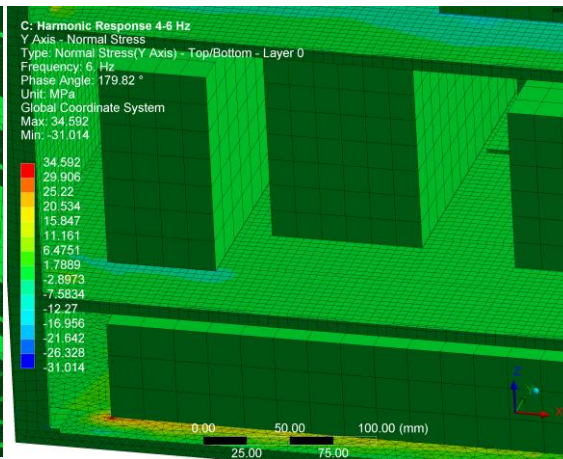


Figure 10.48 - Max Y Axis Normal Stress 6 Hz Detail 2

10.3.2.1.2 Stress

As well as the deformation graphs, the stresses also have a similar behaviour; having low values in all the range analysed. So this range was defined as not being dangerous.

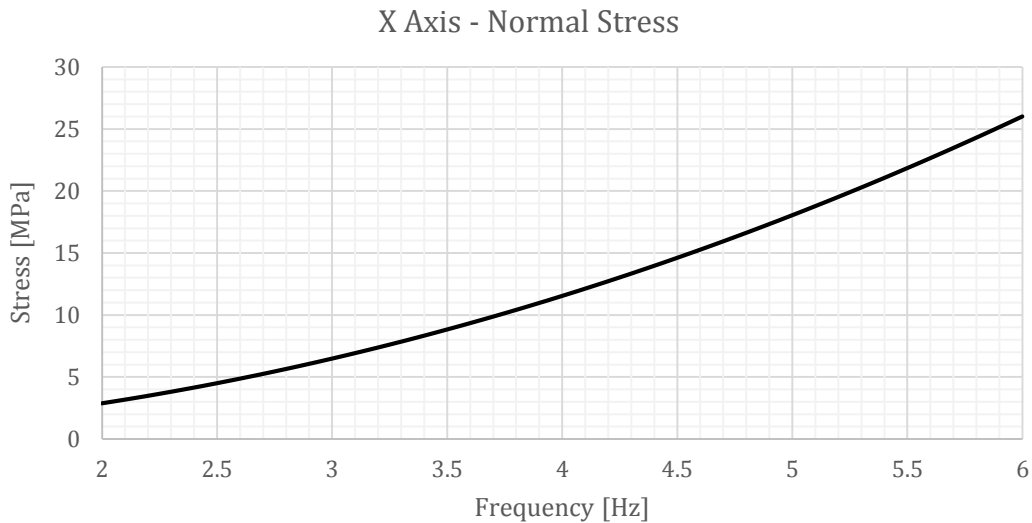


Figure 10.49 – X Axis normal stress / 2 – 6 Hz lateral

The following graphs are the variations of the maximum Y normal stresses as the frequency is changed.

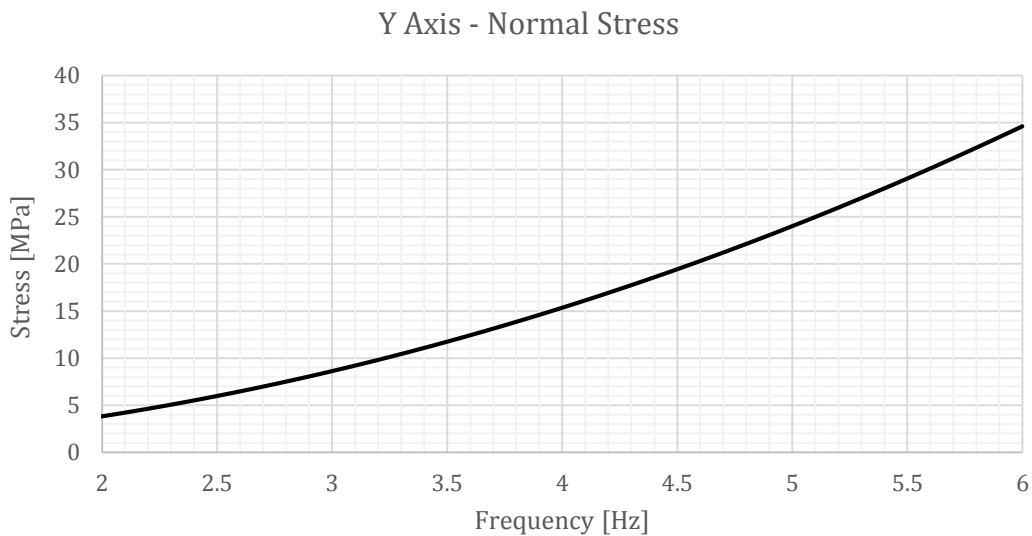


Figure 10.50 – Y Axis normal stress / 2 – 6 Hz lateral

Now that the 2 (or 4)–6 Hz range analysis has been done and discussed, it can be easily concluded that it is not a hazardous spectrum as all the stresses obtained are low and well below failure points.

10.3.2.2 6–100 Hz

10.3.2.2.1 Deformation

The 6–100 Hz range of frequencies is much more interesting because it is the most critical for the structure (it contains one natural frequency). The studies have been carried out in the X and Y axes separately.

In the first place, the X axis has been analysed. In the graph displayed below, where the X axis deformation vs frequency is represented, the resonance peak that corresponds to the first natural frequency (around 94–95 Hz) can be noticed. The peak is so clear because this first vibration mode is purely lateral in the X axis.

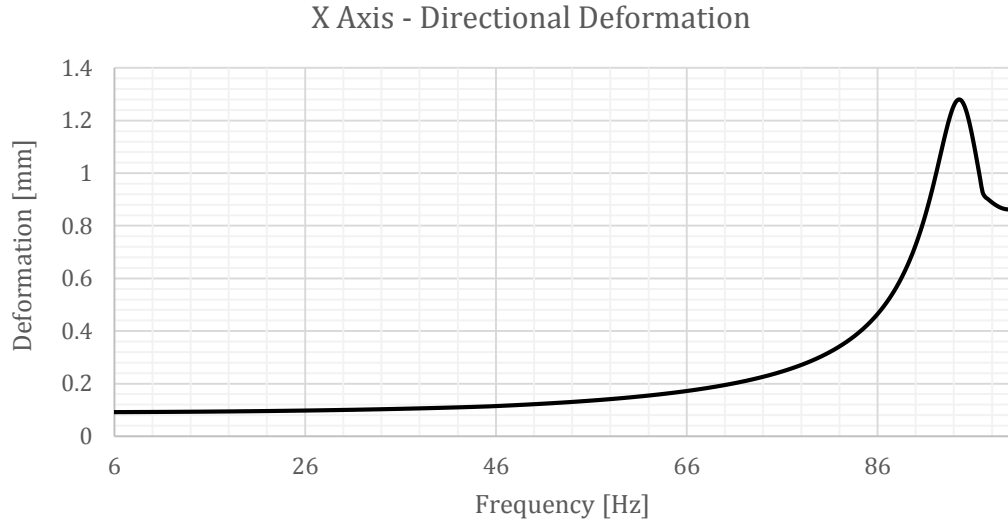


Figure 10.51 – X Axis directional deformation / 6 – 100 Hz lateral

The following images show the coloured deformation of the structure, both in real scale and multiplied by a factor for a better appreciation of the deformations. The figures correspond to the frequency and phase angle at which the X deformation of the satellite is maximum.

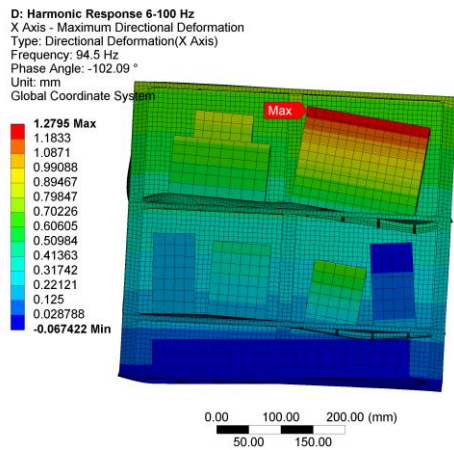


Figure 10.52 – Maximum Directional Deformation X Axis 94.5 Hz Auto Scale

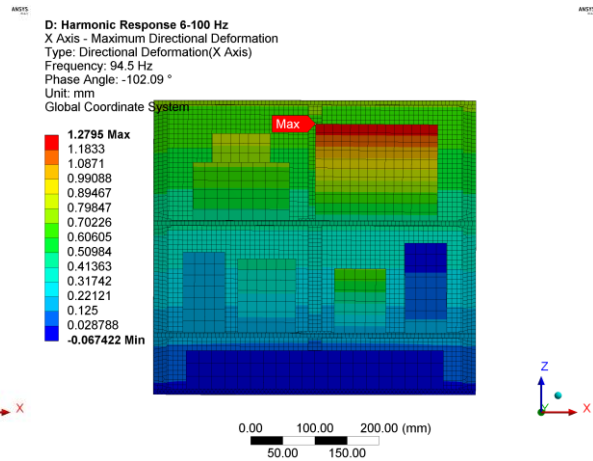


Figure 10.53 – Maximum Directional Deformation X Axis 94.5 Hz True Scale

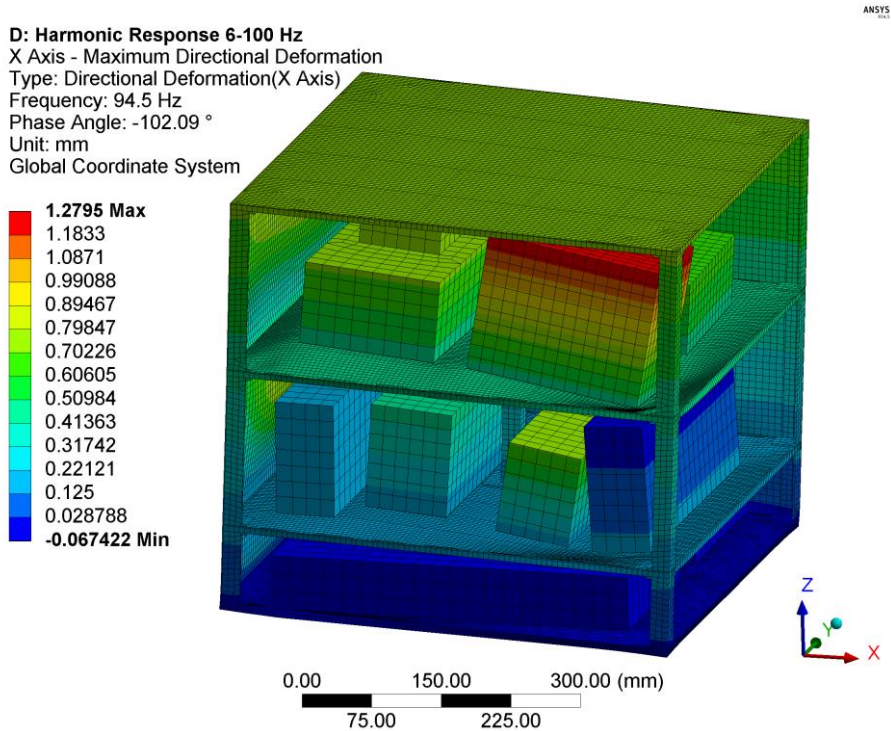


Figure 10.54 – Maximum Directional Deformation X Axis 94.75 Hz 3D View

In the case of the Y axis, the graph also shows a peak around the resonance frequency even without being a Y axis lateral mode. This can be explained because the phenomena of resonance affects the whole structure and the deformation of the components cannot be only in X axis because they are all connected and each one has its own deformation behaviour. In any case, the graph shows that after the peak it continues rising probably until a frequency around 111 Hz, which is the first Y lateral mode.

Y Axis - Directional Deformation

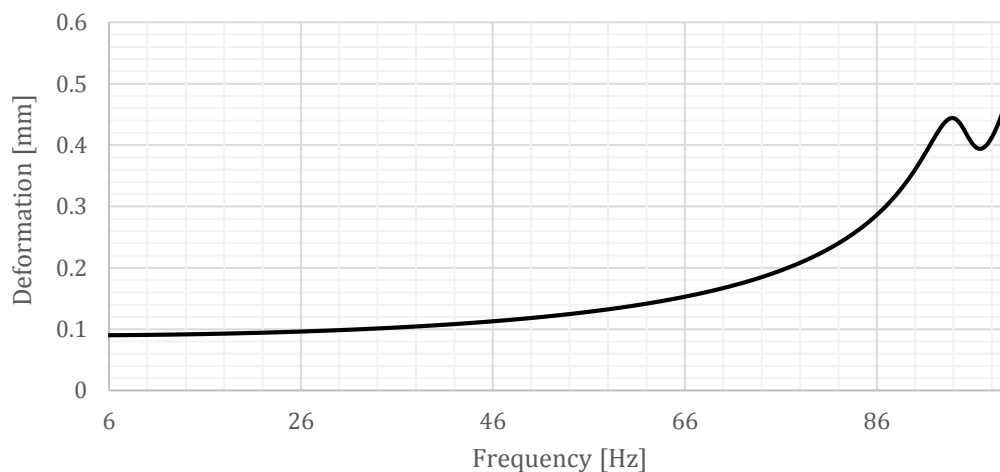


Figure 10.55 – Y Axis directional deformation / 6 – 100 Hz lateral

The following images show the coloured deformation of the structure in real scale and multiplied by a factor for a better understanding of the behaviour. The figures correspond to a frequency of 100 Hz and a phase angle of -154.75° where the Y deformation is maximum.

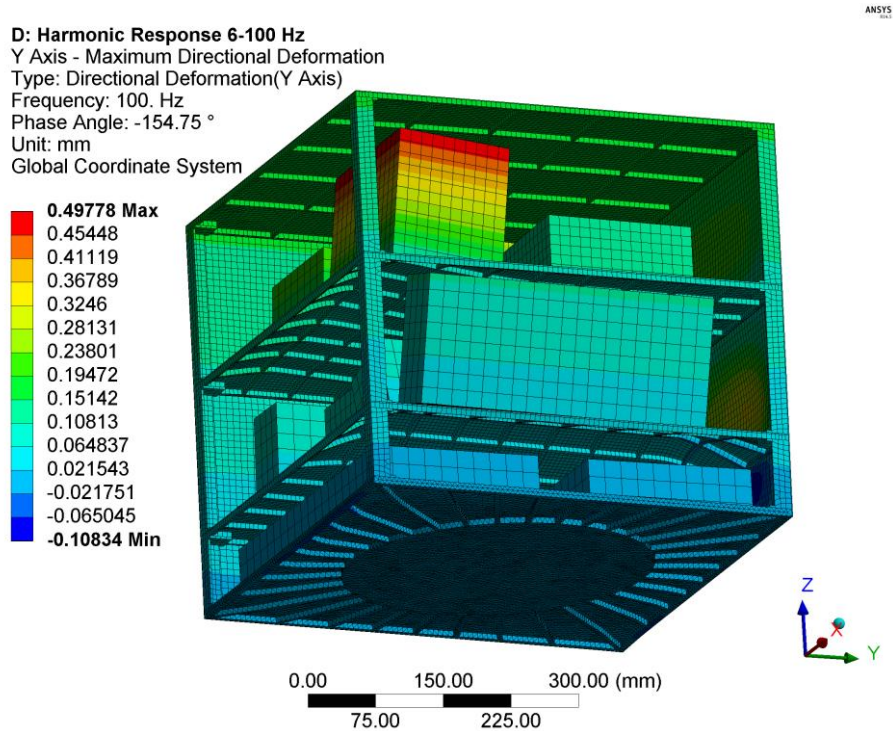


Figure 10.56 – Maximum Directional Deformation Y Axis 100 Hz 3D View

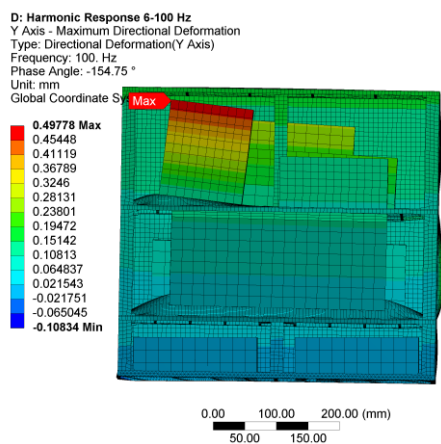


Figure 10.57 – Maximum Directional Deformation Y Axis 100 Hz Auto Scale

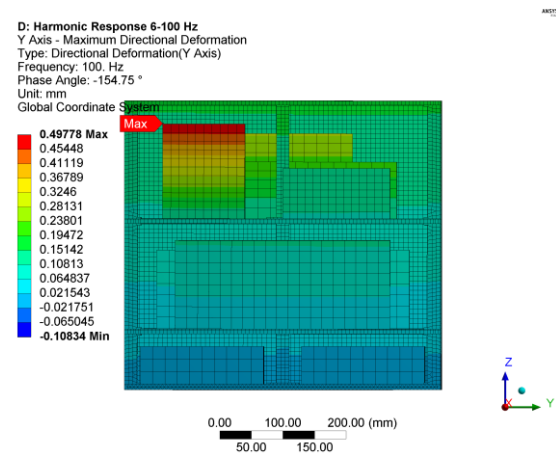


Figure 10.58 – Maximum Directional Deformation Y Axis 100 Hz True Scale

10.3.2.2.2 Stress

The stress value also have been analysed in the 6–100 Hz range for both axes, this parameter is the most important to assure the structural integrity of the satellite.

The stress has been studied in the X axis and it is represented in the graph shown below for each frequency. It is easy to see its rising tendency until the resonance point indicated by the maximum value around 200 MPa. In this case the point of the maximum X axis stress matches the point of maximum X axis deformation and it is important to remember that this resonance frequency is purely X axis lateral shaped.

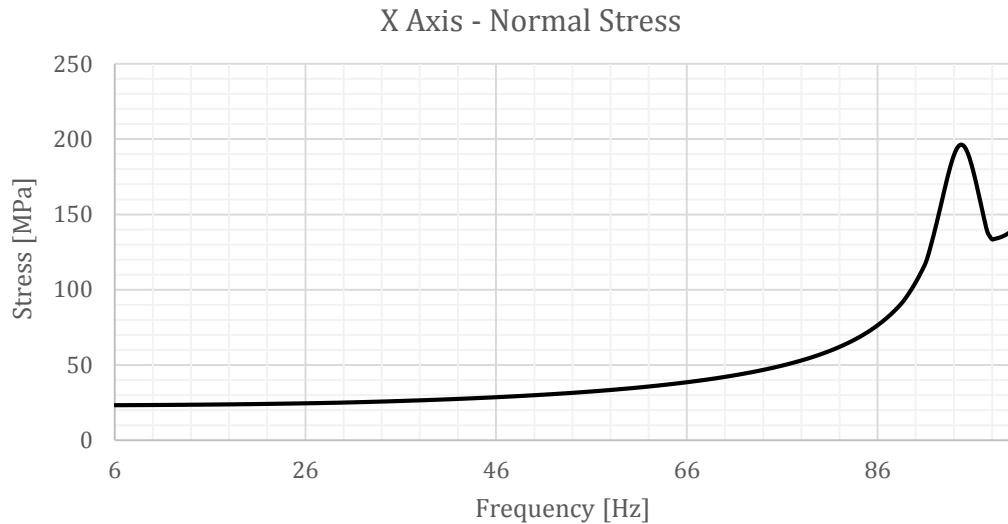


Figure 10.59 - X Axis normal stress / 6 - 100 Hz lateral

In the following figure, the point of maximum stress for the 6–100 Hz sweep is shown. It is situated in a rib under Tray C and its value is 196.33 MPa; therefore and taking into account the yield strength of the material (over 400 MPa) this load case is not a problem for the structural integrity.

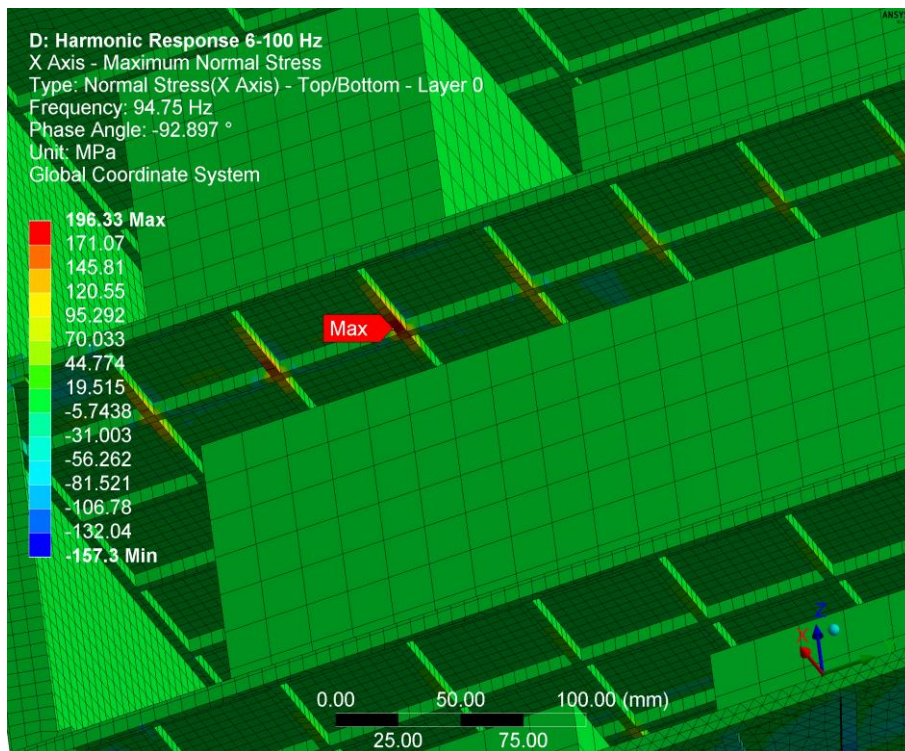


Figure 10.60 - Maximum Normal Stress X Axis 94.75 Hz Detail View

There is another graph showing the maximum stress values in the Y axis versus the frequency. It also has a rising tendency until the maximum value around 200 MPa. This is due to the influence of the X axis resonance mode on the whole structure. In this case the point of the maximum Y axis stress does not match the point of maximum Y axis deformation.

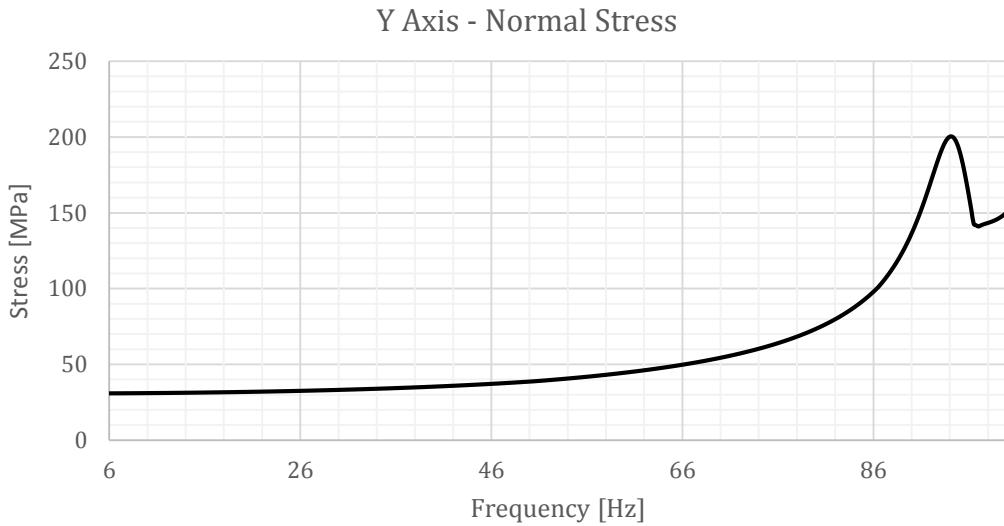


Figure 10.61 – Y normal stress / 6 – 100 Hz lateral

The following figure belongs to the frequency and phase angle of maximum Y axis stress. Its value is 200.15 MPa and occurs in Tray A near a subsystem. Once again it must be said that this value is not a danger for the satellite’s structure.

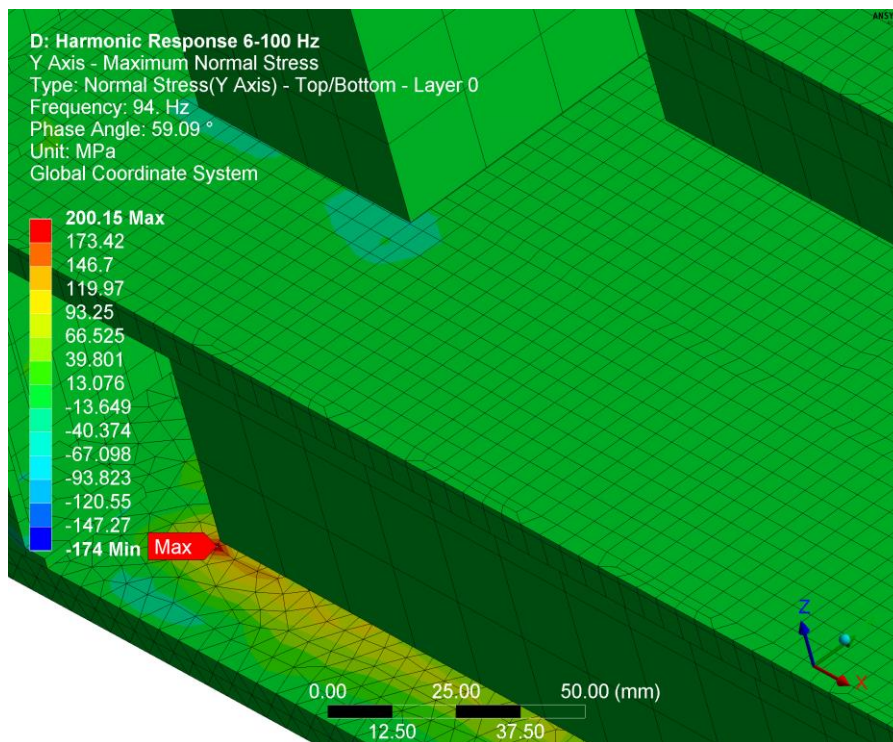


Figure 10.62 – Maximum Normal Stress Y Axis 94 Hz Detail View

10.3.3 Equivalent Loads

The next section will describe the von Mises stresses of the satellite as well of the total deformation (that is, the total longitude of the vector deformation, and not its projections in the axes, as has been shown before).

10.3.3.1 VM Stress

The von Mises stress is often used in determining whether an isotropic and ductile metal will yield when subjected to a complex loading condition. This is accomplished by calculating the von Mises stress and comparing it to the material's yield stress, which constitutes the von Mises Yield Criterion. von Mises Yield Criterion was the rule followed in section 10.1 to obtain the Safety Factor and will also be used in this section.

The VM Stress calculated corresponds to the resonance point of the structure. Despite the fact that only one VM stress distribution has been chosen, it is worth noting that for every frequency there is a VM distribution.

The maximum VM Stress reached in the resonance point is of 200.21 MPa. Knowing that the material Yield Strength is of 408 MPa, that gives a SF of 2.04, nearly the limit for acceptance required for Launcher User's Manual of Ariane 5 if qualification is not demonstrated by test [12]. In any case, the study is intended as an introduction for the complete design of the satellite structure, so as it has been written in section 12 one way of extending this study is to perform an experimental analysis of the previously designed structure. As this is the case, the SF used is of 1.25, comfortably exceeded by 2.04.

The criteria of Safety Factor written in [12] has been used because the documentation of [21] did not say anything about Safety Factors in Sine-Equivalent Dynamics.

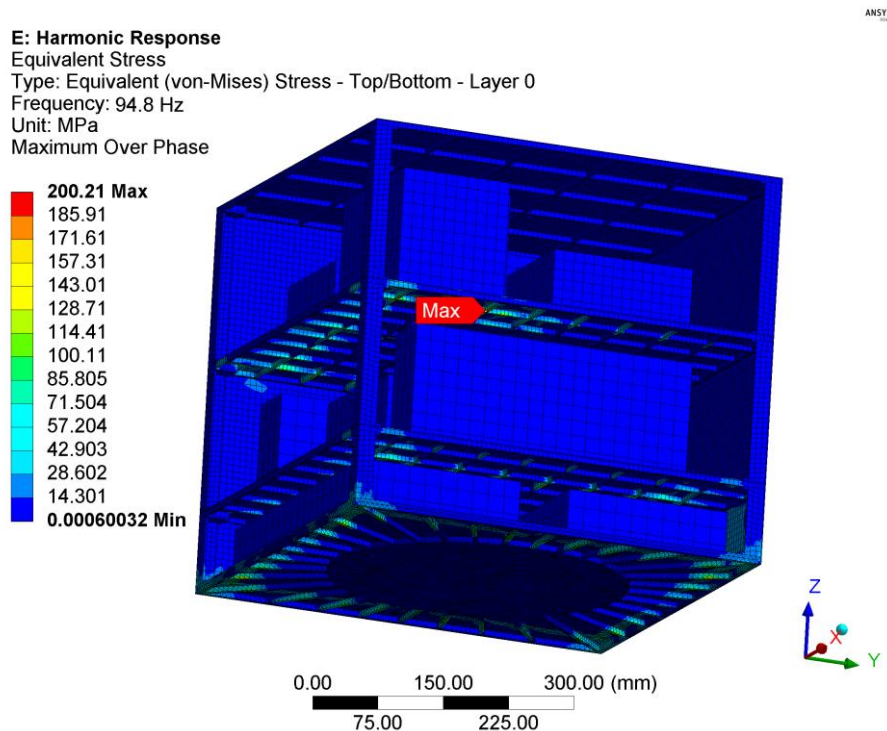


Figure 10.63 – VM Stresses distribution resonance point 3D view

The maximum stress is obtained, as usually expected, in the ribs of the trays (see Figure 10.64). This time, the biggest value is given in the third tray (Tray C).

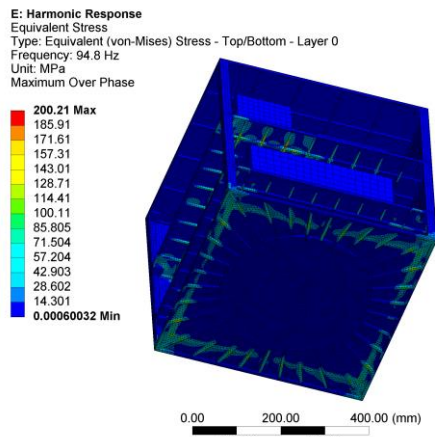


Figure 10.64 – VM Stresses distribution down-top view

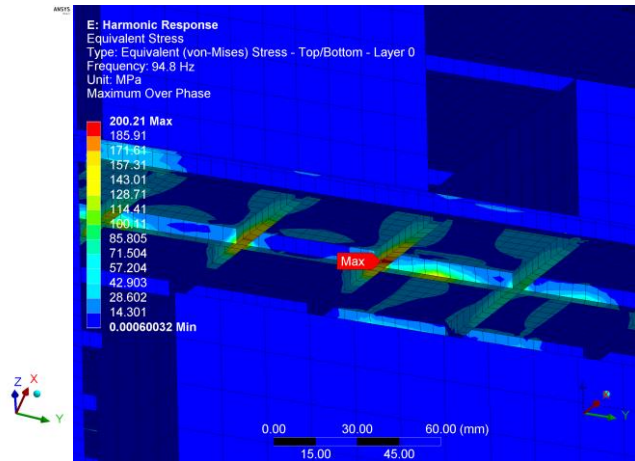


Figure 10.65 – VM Stresses distribution detail view

In order to show the stresses in the rib with the biggest loads more clearly, a detailed view is shown (Figure 10.65).

10.3.3.2 Total Deformation

Finally, the total deformation is exhibited. It is calculated for the frequency where the amplitude of the vibration is maximum (resonance point).

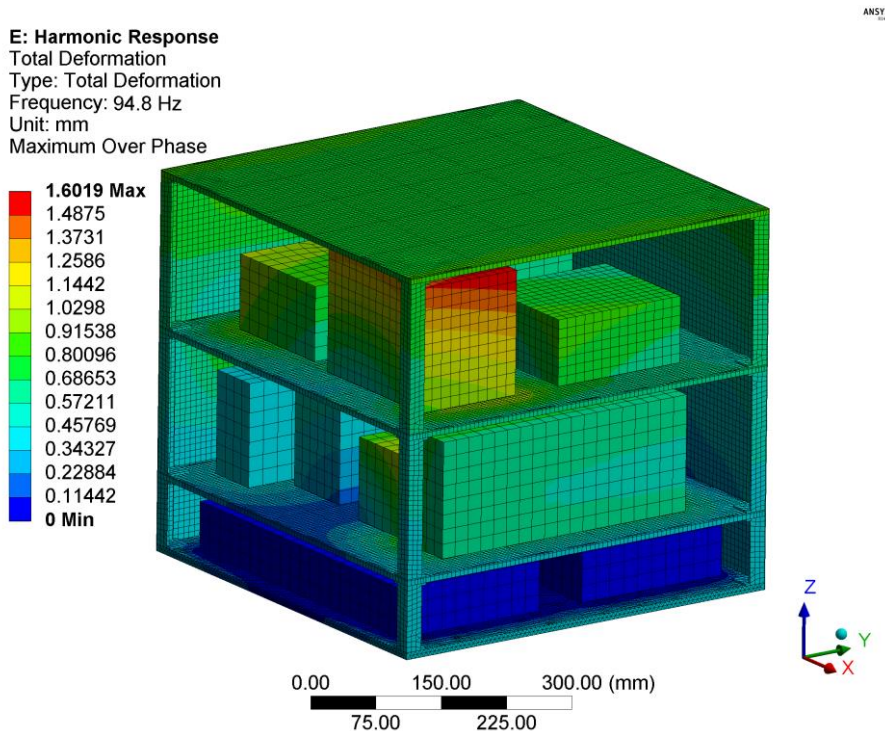


Figure 10.66 – Total Deformation in resonance point

As it can be seen, the vibration follows an almost lineal behaviour. The nearer to the SC/LV interface the part of the satellite is, the less it moves. Maximum deformation is obtained in one of Tray C's subsystems and has a value of 1.6019 mm. A meaningless displacement.

10.4 Compendium of Results

The design proposed for the satellite fulfils all requirements required by the Rocket User's Launch Manual, as it has been written throughout section 10. In any case, the results surpass safety factors and other requirements demanded by the launch manufacturer. So, as it was said in the scheme shown in section 8.1, the design proposed is valid.

11 Conclusions

The structure of a cube-shaped satellite appears to be a simple design when you see it for the first time, however once you have worked with it, it is easy to notice that what you thought was going to be “just another task”, becomes a real challenge. The structural design process ran through several unwanted iteration processes as can be appreciated in sections 8.2.1, 8.2.2 and 8.2.3. Once a final design was decided, the final calculation process began, obtaining the results shown in section 10.

These calculations (and the Final Project as a whole), were a very difficult task because of the lack of available documentation (online or in books) about the piggyback payload requirements. In fact, it has only been possible to find the official information for Ariane-5 auxiliary payload requirements and an unofficial requirement list for the Soyuz Launcher piggybacked payload.

Almost every requirement demanded by the rocket manufacturer has been fulfilled. To do so, the following analyses have been done: centre of gravity position; inertial moment measurements; static and dynamic load simulations and harmonic analyses. The only remaining analyses are the shock excitation and random vibration tests. These have not been studied because the Final Project was originally aimed at vibrations up to 100 Hz.

Another detail to be highlighted is the computational cost. These type of analyses usually require a large amount of memory and time, so the fact that the calculations were carried out in our personal computers has supposed a great handicap, slowing down the progress of the project. Due to all of this, it has been impossible to fulfil all the initial objectives of the project, such as a genetic algorithm analysis for a global optimization or sensitivity analyses to modify parameters.

The principal aim of the Final Project was the design of the structure itself, not the complete sizing of the satellite. That is why the subsystems have been chosen using similar satellite weights and distributions but they have not been designed in detail. That is a very important thing to consider because the rest of the subsystems influence and condition the structural design to a large degree. Therefore the subsystem modelling has been one of the most critical tasks of the project. The structure has been designed to serve a wide range of missions for clients who need a cheap way to put their payloads into orbit. Nevertheless, in the case of varying the subsystems and the need to accommodate different payloads, a customized structural analysis must be carried out.

In any case, all the results obtained in this project should be tested with experimental analyses for the certification. This could be considered for future developments.

12 Future Work

Spacecraft science it is a very complete and ambitious field that is evolving steadily. Regarding this Final Project, some improvements could be made.

Firstly, a real optimization of the satellite could be implemented. In this project the optimization has been made so that the design proposed could satisfy the launcher requirements. However, once this is done, a mass optimization could be performed. The parameters introduced in the model of the satellite could be amended in order to reduce the satellite mass fulfilling the manufacturer's demands. In fact, there is a tool in ANSYS that helps this types of tasks, but due to a lack of time it could not be used in these analyses. Also, it would largely surpass the project scope.

The design was only possible to do with the ASAP (S or 5) interface because of the inability of the authors to successfully find the requirement documents for piggyback payloads belonging to other launchers such as Rockot, Proton and DNEPR. So that is another possible way to extend the work already done.

In the conclusions section it has been said that experimental tests are obligatory for the satellite to be legally launched, so further expansion of the study would be by experimental analyses. It has also been written that the study lacks random vibrations and shock analyses. Hence, another road to be taken could be to widen the study by adding these simulations.

13 Glossary

AD&CS	Attitude Determination and Control Subsystem
ASAP	Ariane Structure for Auxiliary Payload
AVUM	Attitude and Vernier Upper Module
CAE	Computer Aided Engineering
CAD	Computer Assisted Design
C&DHS	Command And Data Handling Subsystem
EPS	Electric Power Subsystem
G	Gravity acceleration
LV	Launch Vehicle
LEO	Low Earth Orbit
OBDH	On Board Data Handling
PS	Propulsion Subsystem
SC	Spacecraft
SS	Structure Subsystem
SF	Safety Factor
SHM	Space Head Module
TT&CS	Telemetry, Tracking and Command Subsystem
TLC	Transport and Launch Canister
UPM	Universidad Politécnica de Madrid
UPV	Universitat Politècnica de València
VM	von Mises

14 References

- [1] P. Sanz-Aránguez, J. Llorente, J. Piñeiro and P. Etxaniz, Vehículos Espaciales II, Madrid: Universidad Politécnica de Madrid, 2005.
- [2] J. Mesenguer Ruiz and A. Sanz Andrés, El satélite UPM-Sat 1, Madrid: Informes a la Academia de Ingeniería, 1998.
- [3] UPM IDR, "UPM-Sat 1," [Online]. Available: http://www.idr.upm.es/tec_espacial/04_UPMSAT.html.
- [4] Anna University Chennai, "ANUSAT," [Online]. Available: <https://www.annauniv.edu/anusat/>.
- [5] cellular, "South Africa's First Satellite - SUNSAT," [Online]. Available: <http://www.cellular.co.za/sunsat.htm>.
- [6] Surrey Satellite Technology LTD, SSTL 100, 2014.
- [7] R. Mike, "RS-23 - Universitetsky-1 (TATIANA-1)," 02 10 2014. [Online]. Available: http://www.dk3wn.info/sat/afu/sat_tatiana1.shtml.
- [8] "Oculus-ASR nanosaellite," [Online]. Available: <http://www.aerospace.mtu.edu/projects/01%20Oculus-ASR/>.
- [9] "Gunter's Space Page," [Online]. Available: http://space.skyrocket.de/doc_sdat/oculus-asr.htm. [Accessed 25 9 2014].
- [10] University Of Colorado, "Dande Web Page," [Online]. Available: <http://dande.colorado.edu/>.
- [11] "eoPortal Directory," [Online]. Available: <https://directory.eoportal.org/web/eoportal/satellite-missions/r/rising-2>.
- [12] Arianespace, Ariane 5 User's Manual, Arianespace, 2011.
- [13] Arianespace, Ariane Structure for Auxiliary Payload 5 User's Manual, 2000.
- [14] Arianespace, Soyuz User's Manual, Arianespace, 2012.
- [15] J. Thiery, "ASAP and VESPA: The Access to Space for Small Satellites".
- [16] Arianespace, Vega User's Manual, Arianespace, 2014.
- [17] ISC Kosmotras, "DNEPR User's Guide," Moscow, 2001.
- [18] "Space Launch Report," 26 December 2012. [Online]. Available: <http://www.spacelaunchreport.com/log2012.html>.
- [19] K. Marjoniemi, L. Syvänen, M. Hoffrén and S. Langlois, "Modular Structure for Small Satellites," *ESTEC/ESA*.
- [20] M. Bille, T. Williams and T. Martin, ""Where do I start?" Rides to space for Scientific and Academic Payloads," p. 10.
- [21] SpaceWorks, "Nano/Microsatellite Market Assesment," 2014.
- [22] SpaceWorks, "Nano/Microsatellite Launch Demand Assessment 2011," 2011.

- [23] M. Calvo and R. Martínez, "Subsistemas del satélite.," *Comunicaciones por Satélite*, p. 65, 2008.
- [24] A. Ravanbakhsh and S. Franchini, "Rapid Sizing Tool for a Low Cost University Microsatellite Structure Subsystem," *IDR/UPM*, p. 5.
- [25] A. Ravanbakhsh and S. Franchini, "Preliminary Structural Sizing of a Modular Microsatellite Based on System Engineering Considerations," *IDR/UPM*, p. 8, 2010.
- [26] G. F. Abdelal, N. Abuelfoutouh and A. H. G. Gad, *Finite Element Analysis for Satellite Structures. Applications to Their Design, Manufacture and Testing*, El Cairo: Springer, 2013.
- [27] A. Pila Vigalondo, *Diseño y Ensayos en Tierra de Paneles Solares para un Satélite de Órbita Baja (LEO)*, Madrid: UPM, 2012.
- [28] J. Wijker, *Spacecraft Structures*, Leiden: Springer, 2008.
- [29] C. L. Stevens, *Design, Analysis, Fabrication, and Testing of a Nanosatellite*, Blacksburg: Virginia Polytechnic Institute, 2002.
- [30] B. Sheela Rani, T. Mahesh babu and M. Srinivasan, "Comparative Study of Different Structures of," Chennai.
- [31] ANSYS, *ANSYS Meshing User's Guide*, Canonsburg, 2013.
- [32] C. W. de Silva, *Vibration and Shock Handbook*, Bocarratón, Florida, EEUU: CRC Press, 2005, p. 1872.
- [33] T. Sharton, *NASA Force Limited Vibration Testing Monograph*, 1997.
- [34] NASA, *Force Limited Vibration Testing*, Washington, DC, 2012.
- [35] A. Calvi, "Spacecraft Loads Analysis: An Overview," Liege, 2011.
- [36] ANSYS Inc, "Module 2: Modal Analysis," *Ansyp Training Manual*, 2004.
- [37] Eurockot, *Rockot User's Guide*, EUROCKOT Launch Services GmbH, 2011.
- [38] J. Wijker, *Random Vibrations in Spacecraft Structure Design, Theory and Applications*, vol. 165, G. Gladwell, Ed., Leiden: Springer, 2009.
- [39] Cal Poly SLO, *CubeSat Design Specification*, San Luis Obispo: Cal Poly SLO, 2005.
- [40] G. Maral and M. Bousquet, *Satellite Communications Systems*, Toulouse: Wiley, 2009.
- [41] A. Inglis and A. Luther, *Satellite Technology: An Introduction*, Oxford: Elsevier, 1997.
- [42] L. Abou Nassar, R. Bonifant, C. Diggs, E. Hess, R. Homb, M. Lauren, E. Moore, P. Obrist and M. Southward, *Spacecraft Structures and Launch Vehicles*, 2004.
- [43] NASA, *Systems Engineering Handbook*, Washington: NASA, 2007.
- [44] J. Hyuk Lim, "A correlation study of satellite finite element model for coupled load analysis using transmissibility with modified correlation measures," p. 10, 2014.
- [45] The Aerospace Corporation, "Space Systems Engineering Lessons Learned. Carefully Evaluate Satellite-Launcher Interface," p. 1.

- [46] A. Sanz-Andrés, J. Meseguer, J. Perales and J. Santiago-Prowald, "A Small Platform for Astrophysical Research Based on the UPM-Sat 1 Satellite of the Universidad Politécnica de Madrid," *IDR/UPM*, p. 6.
- [47] A. I. Hamid Khan, "Design, Modeling and Analysis of Low Earth Orbit Satellite," *Department of Aeronautics and Astronautics, Institute of Space Technology*, p. 8, 2011.
- [48] N. Wells, "Countdown to launch of the first microsattellites qualified for flight on Ariane-5 ASAP," *Space Department, Defence Evaluation & Research Agency*, p. 7, 2000.
- [49] R. Onetto, H. Paas and H. Perez, "Cube Satellite Design," Florida International University, Florida, 2010.
- [50] QB50, "CubeSat Design Overview Report".
- [51] J. R. Maly, P. S. Wilke, E. C. Fowler, C. S. A. Haskett, D. Sciulli and T. E. Meink, "ESPA: EELV Secondary Payload Adapter with Whole-Spacecraft Isolation for Primary and Secondary Payloads," Kirtland Air Force Base, Newport Beach, 2000.
- [52] D. R. Solomon, "Analysis and Design of the Mechanical Systems Onboard a Microsatellite in LEO: An Assesment Study," Montana State University, Bozeman, 2005.
- [53] M. Ryschkewitsch, A. Obenschain and R. Day, "General Environmental Verification Standards (GEVS)," NASA Goddard Space Flight Center, Greenbelt, 1996.
- [54] M. Pons and C. Talbot, "Existing Space Access for small satellitesFuture technical trends and possibilities," in *Space Economy in the Multipolar World SEMW2010*, Evry,, 2010.
- [55] T. Scharton, Force Limited Vibration Testing Monograph, NASA, 1997.
- [56] M. Sedighi and B. Mohammadi, On the Static and Dynamic Analysis of a Small Satellite (Mesbah), Tehran.
- [57] V. Cipolla and M. Berger, "20th Annual AIAA/USU Conference on Small Satellites: General Architecture of ECLAIRs Microsatellite".
- [58] A. Chiplunkar, R. Pai and A. Subramanyam, "ANALYSIS AND VALIDATON OF THE STRUCTURE OF PRATHAM, INDIAN INSTITUTE OF TECHNOLOGY BOMBAY'S FIRST STUDENT SATELLITE," *Mahindra Satyam*, p. 11.
- [59] M. Billie and R. Kane, "Practical Microsat Launch Systems: Economics and Technology," *AIAA*.
- [60] C. D. Johnson, "Protecting Satellites From the Dynamics of the Launch Environment," *CSA Engineering, Inc.*, p. 11.
- [61] M. Billie, T. Williams and T. Martin, ""Where Do I Start?" Rides to Space for Scientific and Academic Payloads," p. 10, 2006.
- [62] M. Farhan Shafique, "Satellite Subsystems".
- [63] A. Calvi, "Spacecraft Structural Dynamics & Loads: An Overview," Liege, 2010.
- [64] Space Research Electives Seminars, "Spacecraft Design, Structure and Operations," in *AU Space Primer*, Alabama, Maxwell Air Force Base, 2003.

- [65] J. A. Schoenster, "Measurements And Analysis of Solid-Propellant-Rocket Vibrations Obtained During a Captive Flight," NASA, Hampton, 1971.
- [66] M. A. Mojica, Structural Subsystem Design. Analysis, and Optimization for a Nanosatellite, San José: San José State University, 2012, p. 73.
- [67] A. Calvi, "Fundamental Aspects on Structural Dynamics of Spacecraft," Noordwijk, 2008.
- [68] P. Tortora and E. Troiani, "The microsatellite research program at Università di Bologna," *Acta Astronautica*, p. 9, 2004.
- [69] K. Thyagarajan, J. Gupta, P. Goel and K. Jayaraman, "University small satellite program - ANUSAT," *Acta Astronautica*, p. 9, 2005.
- [70] S. Grocott, "The Future of the Microsatellite Program in Canada," in *19th Annual AIAA/USU Conference on Small Satellites*, Mississauga.

BUDGET

Budget Index

1	Budget Overview	5
1.1	Objectives Definition and Documentation.....	5
1.2	CAD and FEM Modelling and Simulation.....	5
1.3	Researching Studies	6
1.4	Elaboration of the Report and Technical Documentation.....	6
1.5	General Costs	6
2	Budget Execution	7
2.1	Labour Cost.....	7
2.2	Material Cost.....	7
2.3	Total Cost.....	7

1 Budget Overview

The present Final Degree Project has been proposed as if it were a consultant's office job. That is, the authors of the project were tasked to design a structure of a cube-shaped satellite by some fictional company. That is why launching costs, as well as space related ones will be ignored. It only have been taken into account direct costs such as calculation time, work time or the licences price of the software used.

This document is composed by 5 sections in which the budget is estimated for each part of the work carried out:

- Objectives Definition and Documentation
- CAD and FEM Modelling and Simulation
- Researching Studies
- Elaboration of Report and Technical Documentation
- General Costs

To calculate the hourly costs a net salary for each engineer of €3,200/month has been estimated, so the gross salary taking into account a 30% of taxes is €4,571.43/month. Also the company has to pay to the state the 40% and the 25% of the gross salary to Social Insurances and Income Tax respectively, this is €2,971.43/month. Taking the previous calculations into account, the working price must be €55.00 per hour.

1.1 Objectives Definition and Documentation

Firstly, an extensive review of the existing bibliography and regulations has been made.

Code	Topic Area	Quantity	Unit	Price	Cost
1.01	Regulations Review	20	hour	55.00	1,100.00
1.02	"State in the Art" Research	80	hour	55.00	4,400.00
TOTAL					€5,500.00

Table 1 –Objectives definition and documentation budget estimation

1.2 CAD and FEM Modelling and Simulation

In this section, a detailed breakdown of the tasks related to CAD modelling and FEM simulation has been done. The software licenses costs have been considered in Section 1.5.

The price of the CPU time has been considered as the 40% of the gross salary per hour.

Code	Topic Area	Quantity	Unit	Price	Cost
2.01	CAD Modelling	30	hour	55.00	1,650.00
2.02	Material Selection	5	hour	55.00	275.00
2.03	FEM Meshing Setup	6	hour	55.00	330.00
2.04	FEM Meshing (CPU Time)	20	hour	22.00	440.00
2.05	FEM Simulation Setup	10	hour	55.00	550.00
2.06	FEM Simulation (CPU Time)	190	hour	22.00	4,180.00
TOTAL					€7,425.00

Table 2 – CAD and FEM costs estimation

1.3 Researching Studies

There have been also costs associated to the FEM results handling and data analysis. All of them are specified in Table 4

Code	Topic Area	Quantity	Unit	Price	Cost
3.01	FEM Data Analysis	20	hour	55.00	1,100.00
3.02	CoG and Inertia Studies	5	hour	55.00	275.00
3.03	Structural Parameters Research	18	hour	55.00	990.00
3.14	Results Handling	8	hour	55.00	440.00
TOTAL					€2,805.00

Table 3 – Researching costs estimation

1.4 Elaboration of the Report and Technical Documentation

In Table 5 is detailed the costs breakdown of the documentation tasks.

Code	Topic Area	Quantity	Unit	Price	Cost
4.01	Report Writing	80	hour	55.00	4,400.00
4.02	Report Revision	20	hour	55.00	1,100.00
4.03	Planes Elaboration	10	hour	55.00	550.00
TOTAL					€6,050.00

Table 4 – Report and technical documentation costs estimation

1.5 General Costs

Like in every project, there are general costs that depend on the renting of the office and the necessary software licenses, as well as the hardware costs and office supplies (gas, electricity, internet...). An estimation of this expenses is showed in the Table 5.

The total time spent in the project is 523 hours or 3.27 months.

Code	Topic Area	Quantity	Unit	Price	Cost
5.01	Office Renting	3.27	month	3,000.00	9,810.00
5.02	Hardware	0.25	—	6,200.00	1,550.00
5.03	Office Supplies	3.27	month	250.00	817.50
5.04	2 x CATIA Licenses	3.27	month	2,166.00	7,082.82
5.05	2 x ANSYS Licenses	3.27	month	6,166.00	20,162.82
5.06	2 x Other Software Licenses	3.27	month	50.00	163.50
5.07	Printing and Binding	1	—	100.00	100.00
5.08	Other General Costs	1	—	100.00	100.00
TOTAL					€39,786.64

Table 5 – General costs estimation

2 Budget Execution

In this section the budget is classified by the type of cost: labour cost and material cost.

2.1 Labour Cost

Labour costs describe the costs that are directly involved with the manufacturing of a product. For example: assembly workers who put the products together, quality control engineers who test the products to be sure they are operational, engineers who design the product and draw up the plans for manufacturing (the case of this project), and warehouse workers that package and ship the products are all direct labourers.

Code	Topic Area	Cost
Table 1	Objectives Definition and Documentation	5,500.00
Table 2	CAD and FEM Modelling and Simulation	7,425.00
Table 3	Researching Studies	2,805.00
Table 4	Elaboration of the Report and Technical Documentation	6,150.00
TOTAL		€21,780.00

Table 6 - Labour cost

2.2 Material Cost

This cost includes the costs of the resources needed to manufacture a product. In this case these costs match the Table 5.

2.3 Total Cost

The total cost is the sum of the labour cost with the material cost plus the VAT tax.

Code	Topic Area	Cost
Table 6	Labour Cost	21,780.00
Table 5	Material Cost	39,786.64
TOTAL BEFORE TAXES		€61,566.64
T.21	VAT (21%)	12,928.99
TOTAL AFTER TAXES		€74,495.63

Table 7 - Total cost

The total budget of the project is:

**#SEVENTY FOUR THOUSAND FOUR HUNDRED NINETY FIVE EUROS AND SIXTY
THREE CENTS#**

#74,495.63€#

Valencia, December 2nd, 2015

GEOMETRICAL MODEL

List of Planes

Plane 1 - Exterior isometric views.....	5
Plane 2 – Interior isometric views.....	6
Plane 3 – Interior views	7
Plane 4 – Interior detailed front view	8
Plane 5 – Interior detailed right view.....	9
Plane 6 – Section C-C view	10
Plane 7 – Tray A view.....	11
Plane 8 – Tray B/C/D views	12

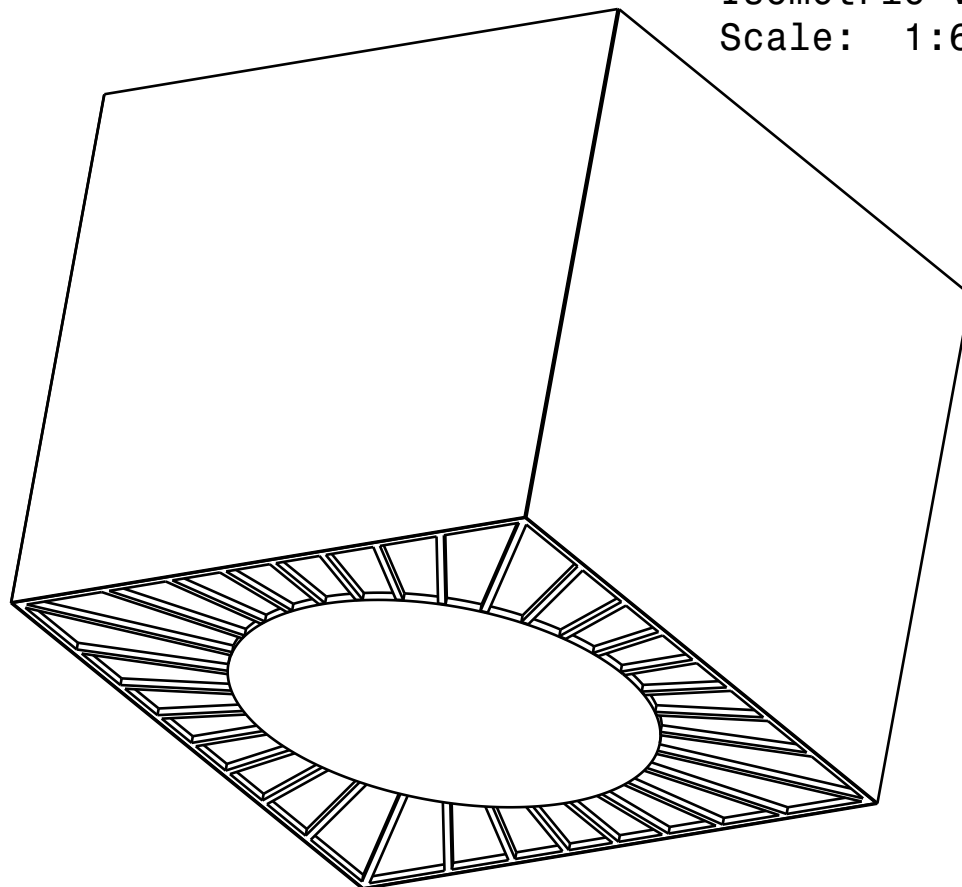
D

C

B

A

Isometric view
Scale: 1:6



4

3

2

1

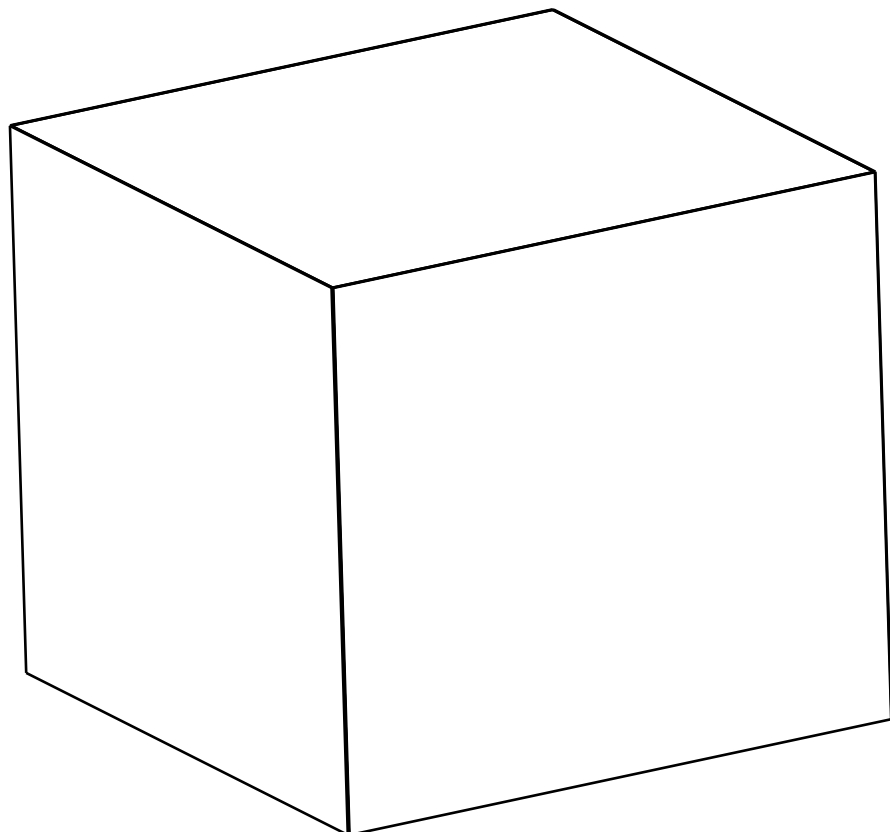
4

3

2

1

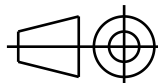
Isometric view
Scale: 1:6



DESIGNED BY:
Alejandro Pila
Sergio Fraile

CHECKED BY:
Andrés Rovira

SIZE
A4



SCALE
1:6

WEIGHT (kg)
50

DATE:
22/11/2014

Microsatellite

Universitat Politècnica de València

DRAWING NUMBER
001-0001

SHEET
1/8

I	-
H	-
G	-
F	-
E	-
D	-
C	-
B	-
A	-

This drawing is our property; it can't be reproduced or communicated without our written agreement.

D

A

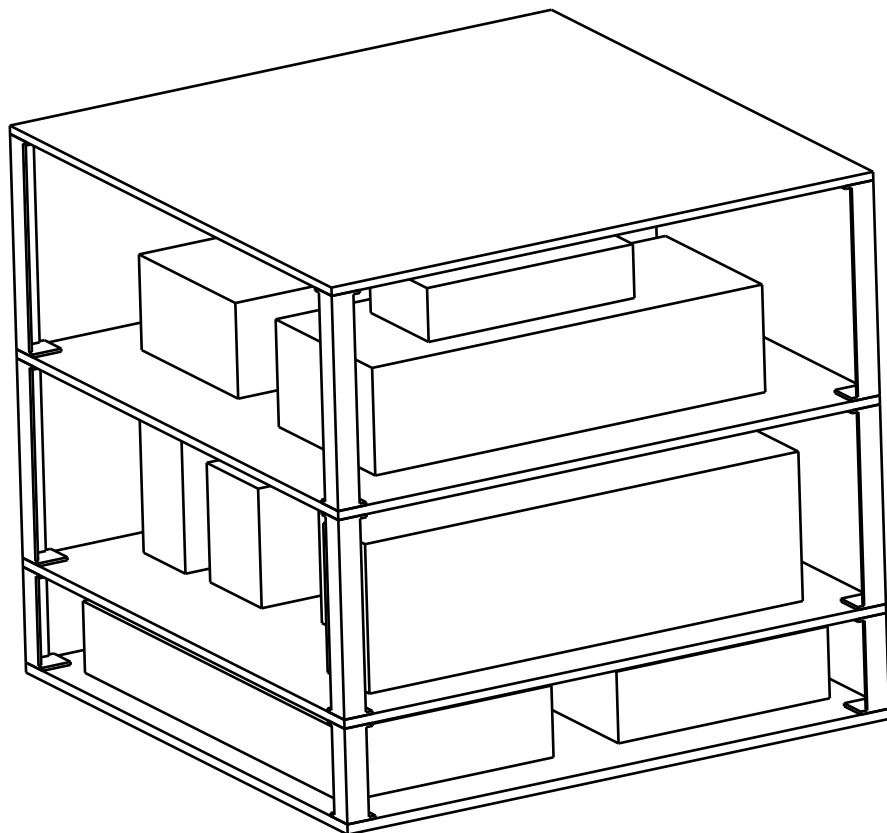
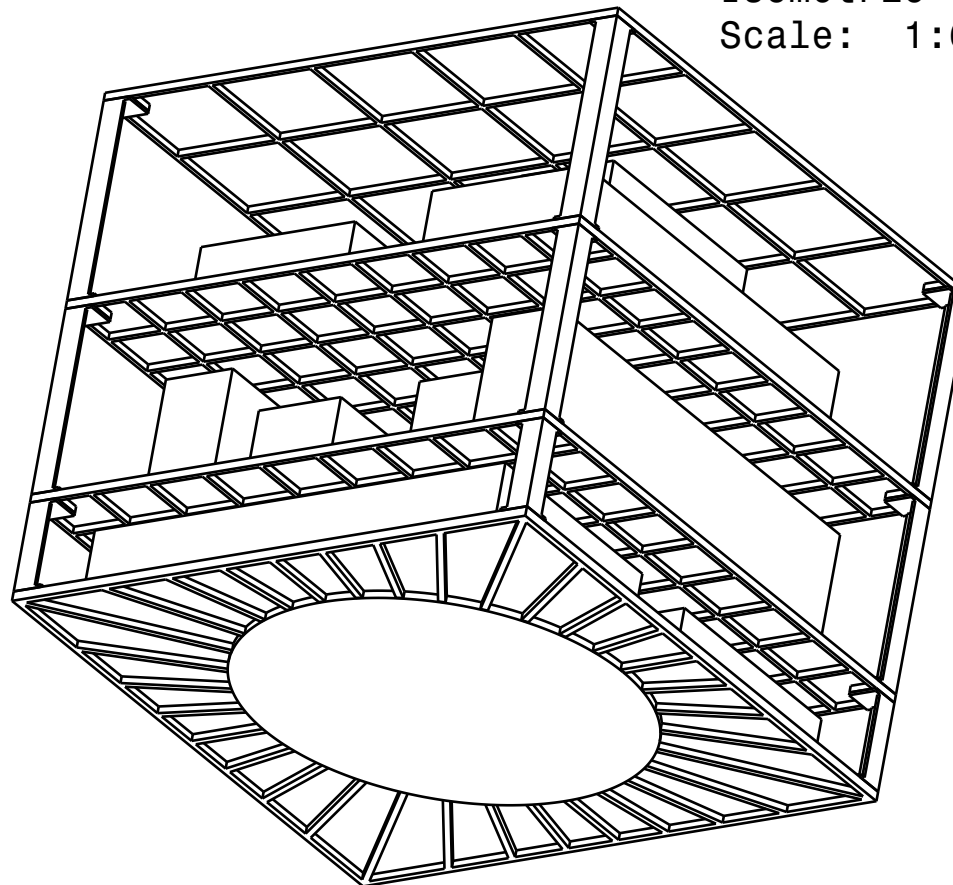
D

C

B

A

Isometric view
Scale: 1:6



Isometric view
Scale: 1:6

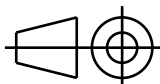
DESIGNED BY:
**Alejandro Pila
Sergio Fraile**

CHECKED BY:
Andrés Rovira

DATE:
22/11/2014

Microsatellite

SIZE
A4



Universitat Politècnica de València

SCALE
1:6

WEIGHT (kg)
50

DRAWING NUMBER
001-0002

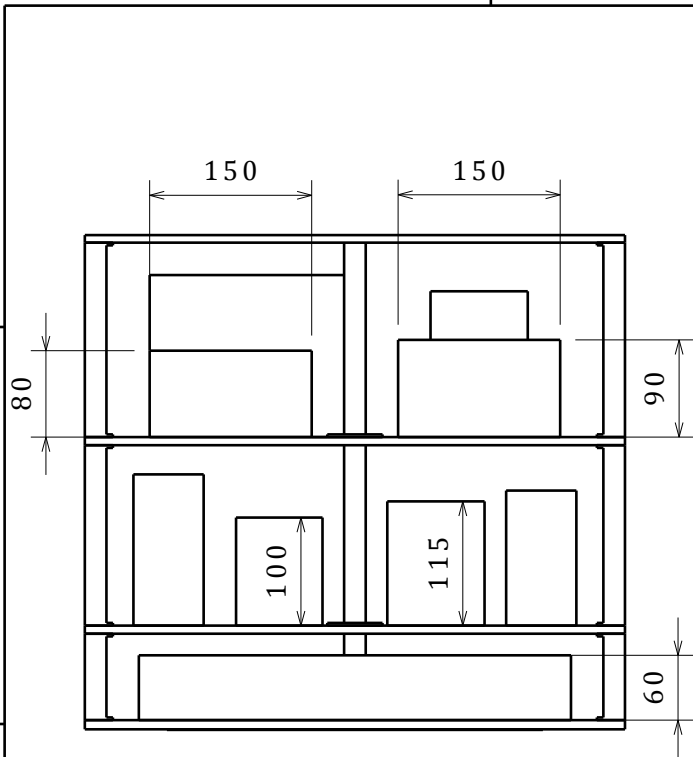
SHEET
2/8

I	-
H	-
G	-
F	-
E	-
D	-
C	-
B	-
A	-

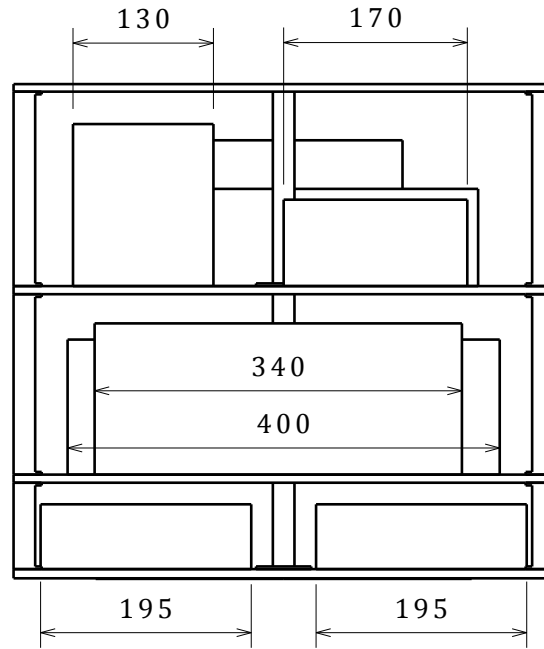
This drawing is our property; it can't be reproduced or communicated without our written agreement.

D

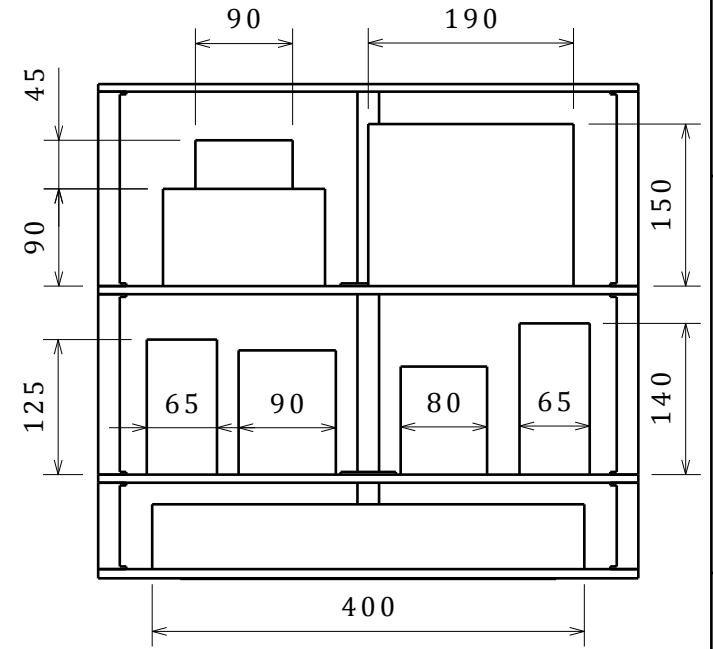
A



Right view
Scale: 1:7



Front view
Scale: 1:7



Left view
Scale: 1:7

DESIGNED BY: Alejandro Pila Sergio Fraile		<h1>Microsatellite</h1>		I	-	
CHECKED BY: Andrés Rovira				DATE: 22/11/2014	H	-
SIZE A4		Universitat Politècnica de València		G	-	
SCALE 1:7	WEIGHT (kg) 50			DRAWING NUMBER 001-0003	F	-
			SHEET 3/8	E	-	
This drawing is our property; it can't be reproduced or communicated without our written agreement.					D	-
					C	-
					B	-
					A	-

D

A

D

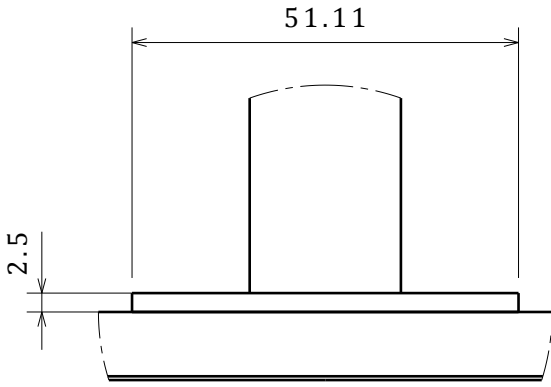
C

B

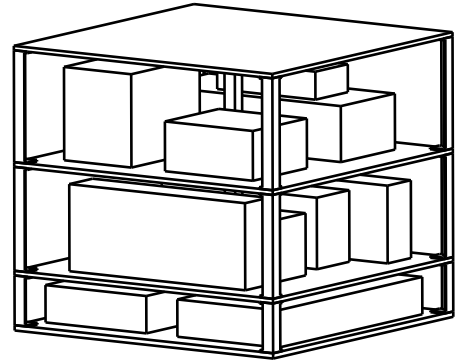
A

4

4



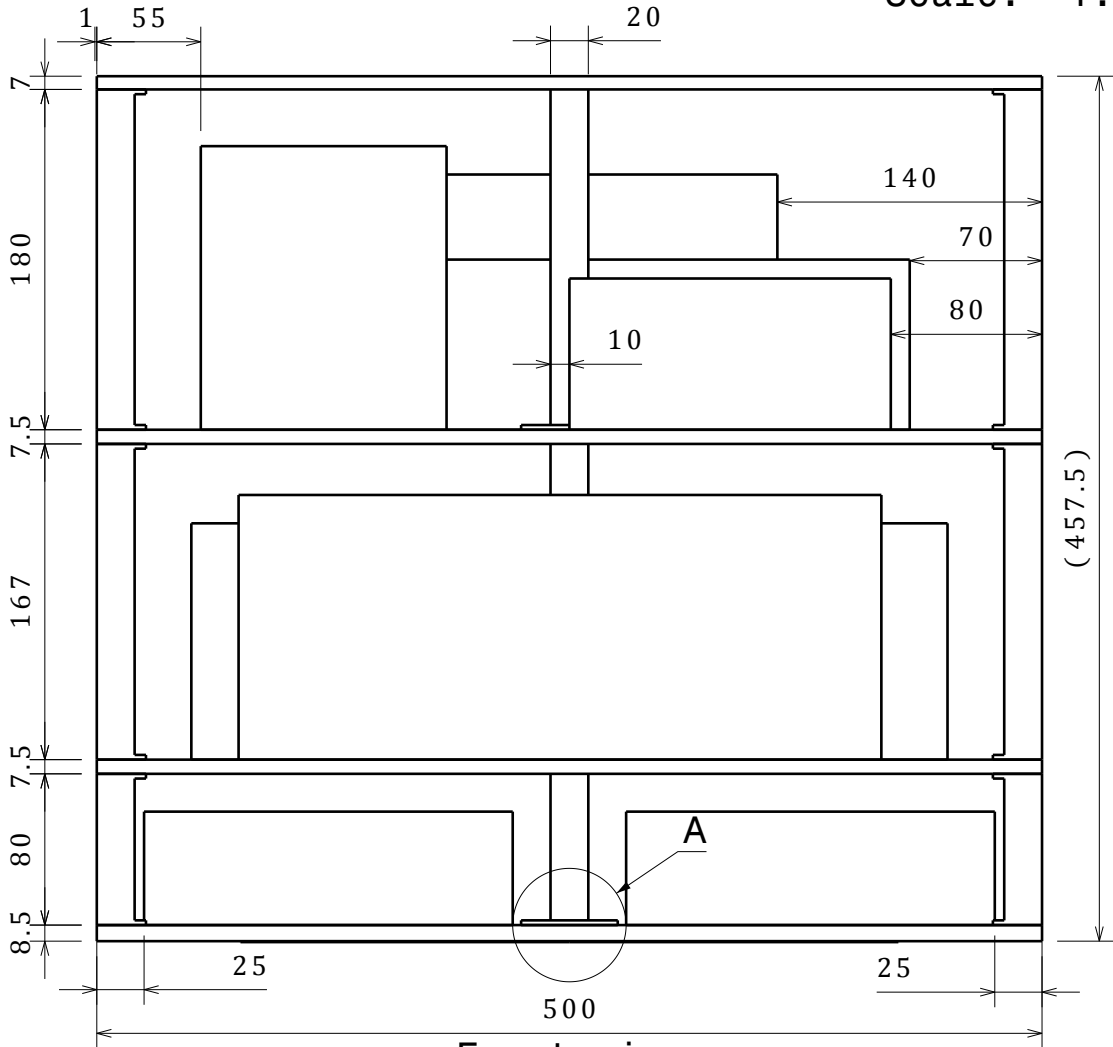
Detail A
Scale: 1:1



Isometric view
Scale: 1:12

3

3



Front view
Scale: 1:4

2

2

1

1

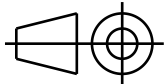
DESIGNED BY:
Alejandro Pila
Sergio Fraile

CHECKED BY:
Andrés Rovira

DATE:
22/11/2014

Microsatellite

SIZE
A4



Universitat Politècnica de València

SCALE
1:6

WEIGHT (kg)
50

DRAWING NUMBER
001-0004

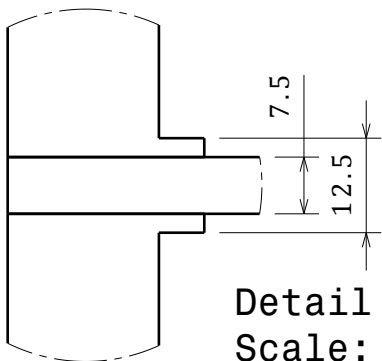
SHEET
4/8

I	-
H	-
G	-
F	-
E	-
D	-
C	-
B	-
A	-

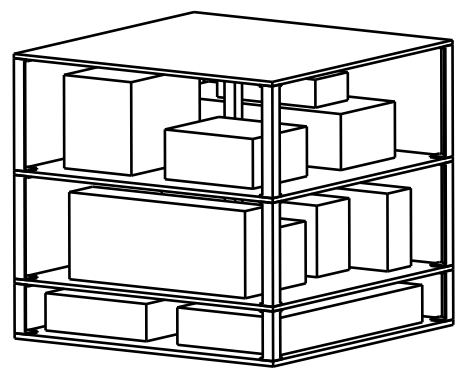
This drawing is our property; it can't be reproduced or communicated without our written agreement.

D

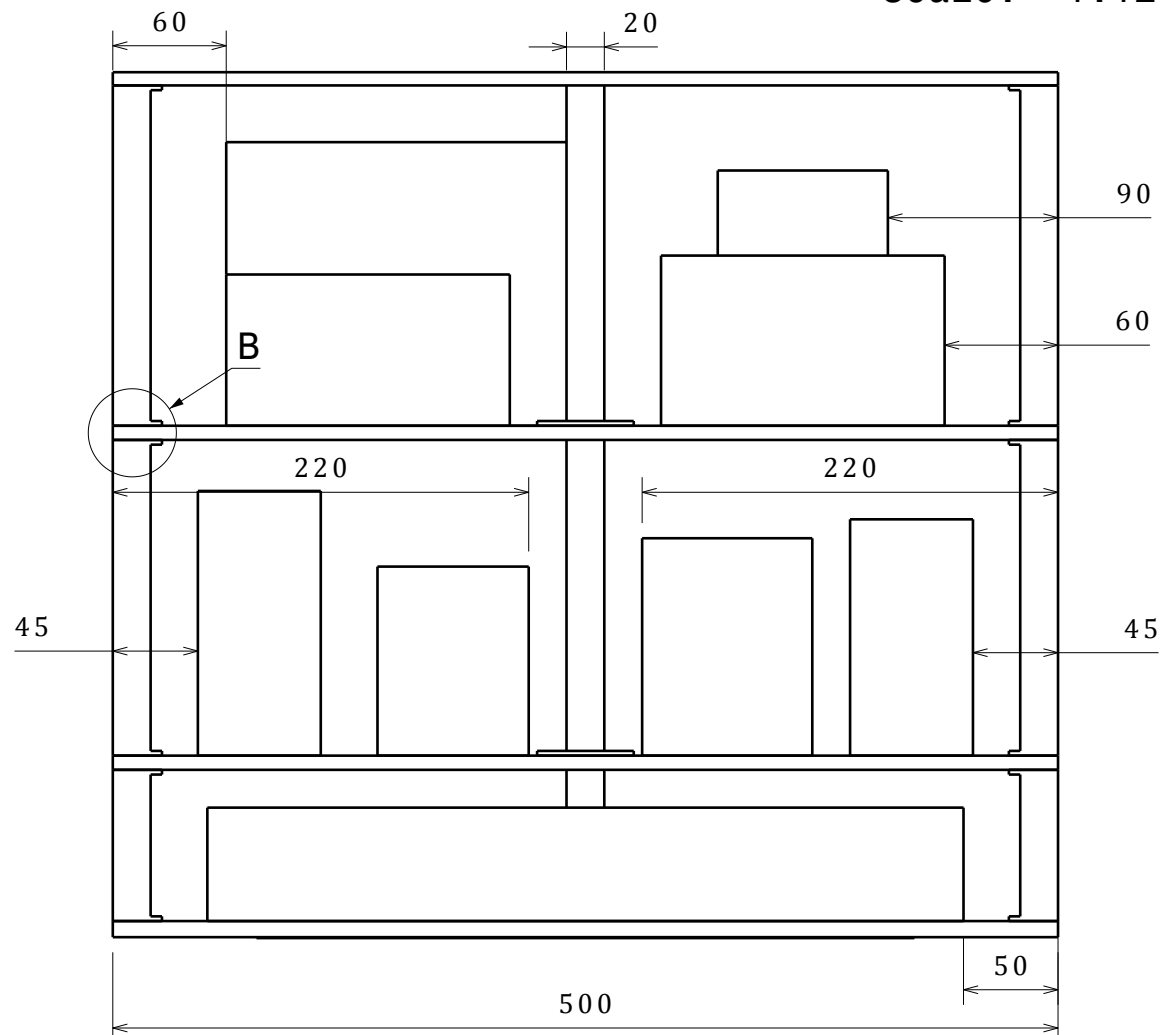
A



Detail B
Scale: 1:1



Isometric view
Scale: 1:12



Right view
Scale: 1:4

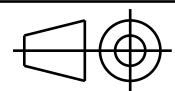
DESIGNED BY:
Alejandro Pila
Sergio Fraile

CHECKED BY:
Andrés Rovira

DATE:
22/11/2014

Microsatellite

SIZE
A4



Universitat Politècnica de València

SCALE
1:6

WEIGHT (kg)
50

DRAWING NUMBER
001-0005

SHEET
5/8

I	-
H	-
G	-
F	-
E	-
D	-
C	-
B	-
A	-

This drawing is our property; it can't be reproduced or communicated without our written agreement.

D

A

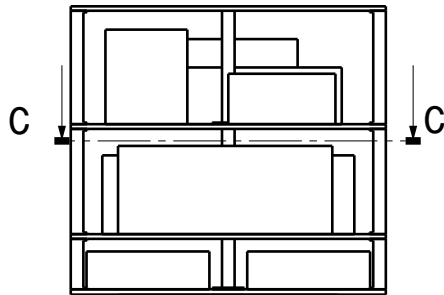
D

C

B

A

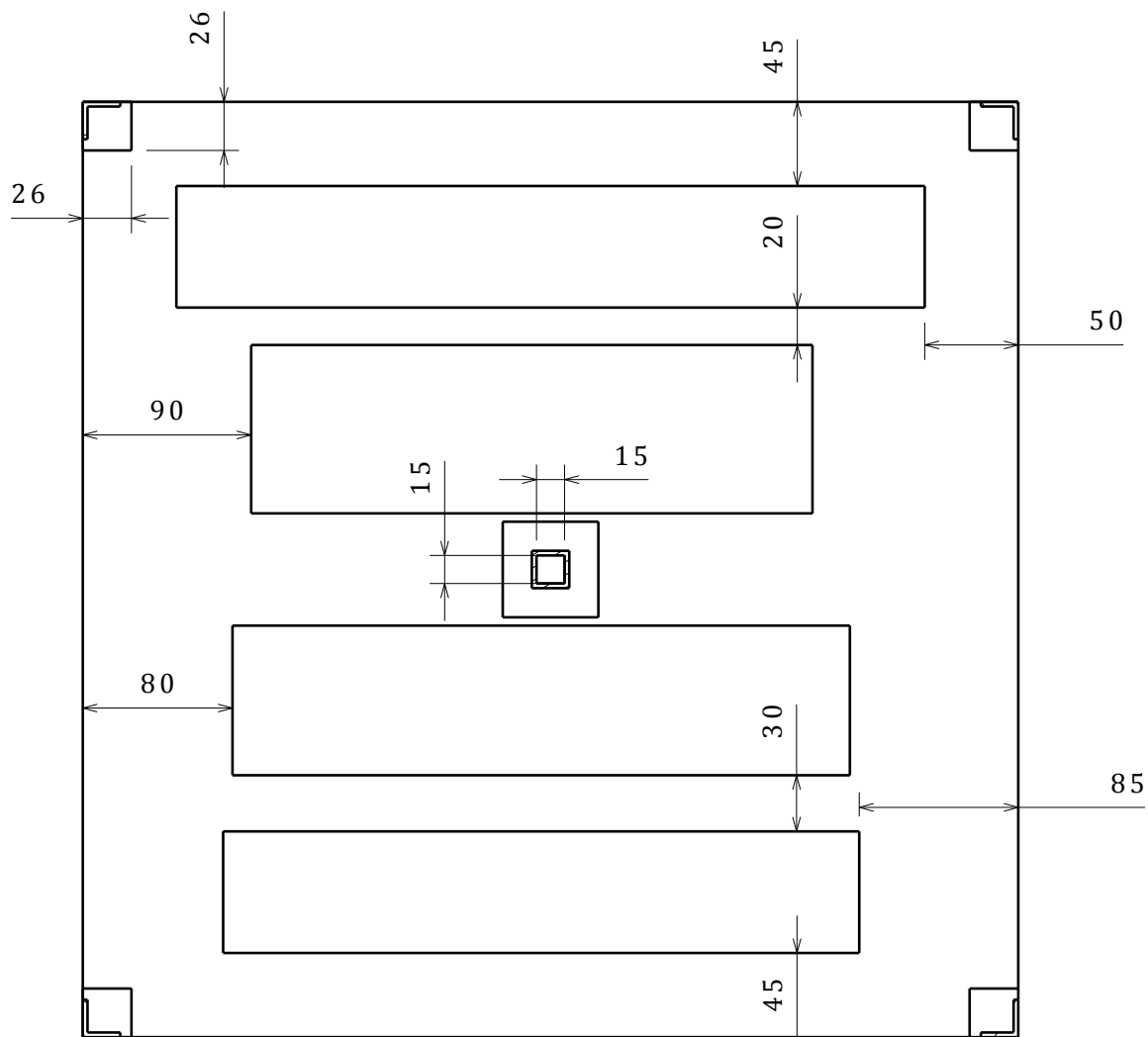
4



Front view
Scale: 1:12

4

3



Section view C-C
Scale: 1:4

3

2

2

DESIGNED BY:

Alejandro Pila
Sergio Fraile

CHECKED BY:

Andrés Rovira

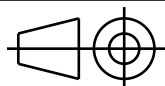
DATE:

22/11/2014

Microsatellite

SIZE

A4



Universitat Politècnica de València

SCALE

1:6

WEIGHT (kg)

50

DRAWING NUMBER

001-0006

SHEET

6/8

I	-
H	-
G	-
F	-
E	-
D	-
C	-
B	-
A	-

1

This drawing is our property; it can't be reproduced or communicated without our written agreement.

D

A

D

C

B

A

4

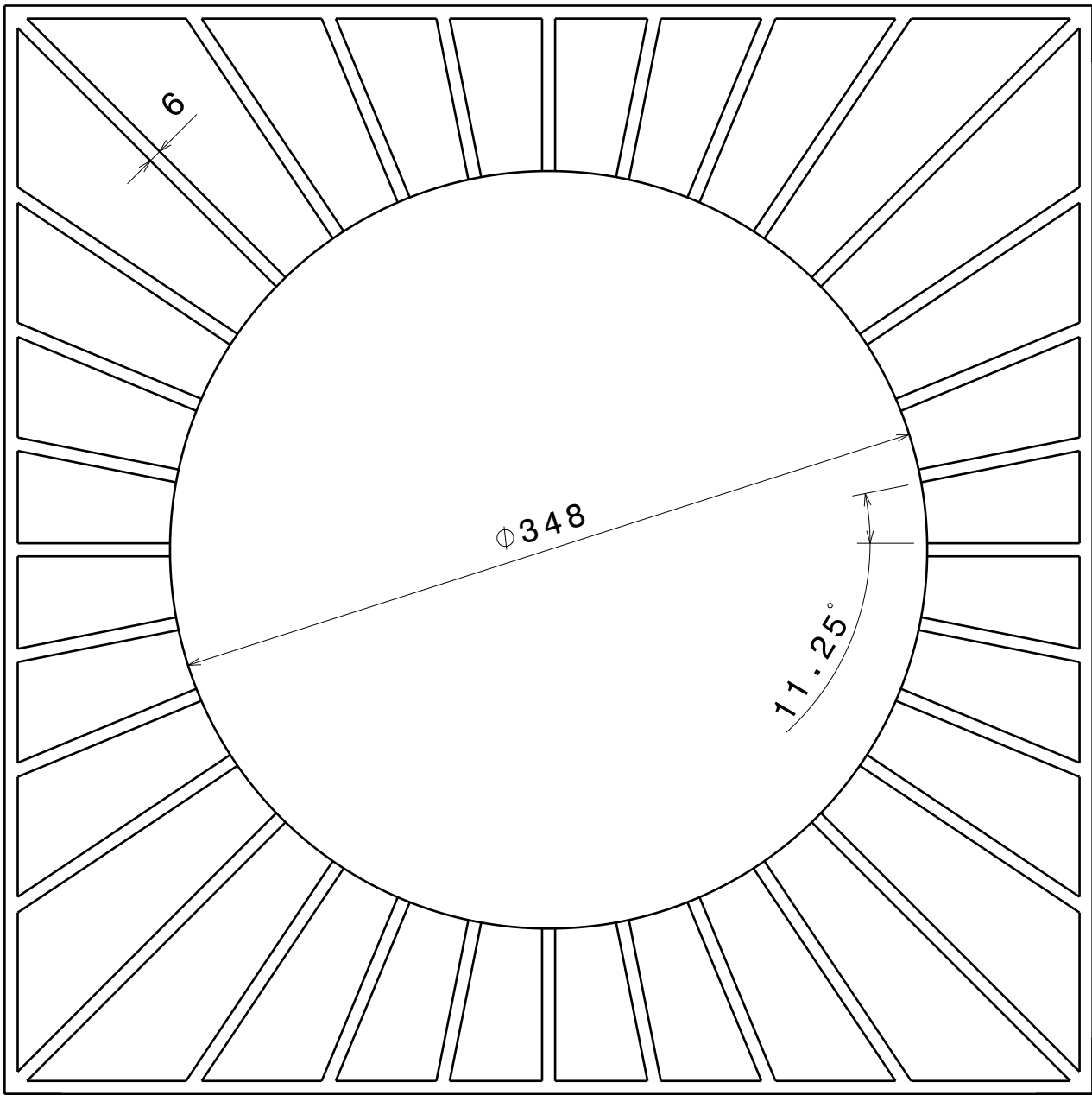
4

3

3

2

2



Front view
Scale: 1:3

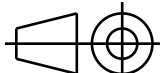
DESIGNED BY:
Alejandro Pila
Sergio Fraile

CHECKED BY:
Andrés Rovira

DATE:
22/11/2014

Tray A

SIZE
A4



Universitat Politècnica de València

SCALE
1:6

WEIGHT (kg)
4

DRAWING NUMBER
001-0007

SHEET
7/8

I	-
H	-
G	-
F	-
E	-
D	-
C	-
B	-
A	-

This drawing is our property; it can't be reproduced or communicated without our written agreement.

D

A

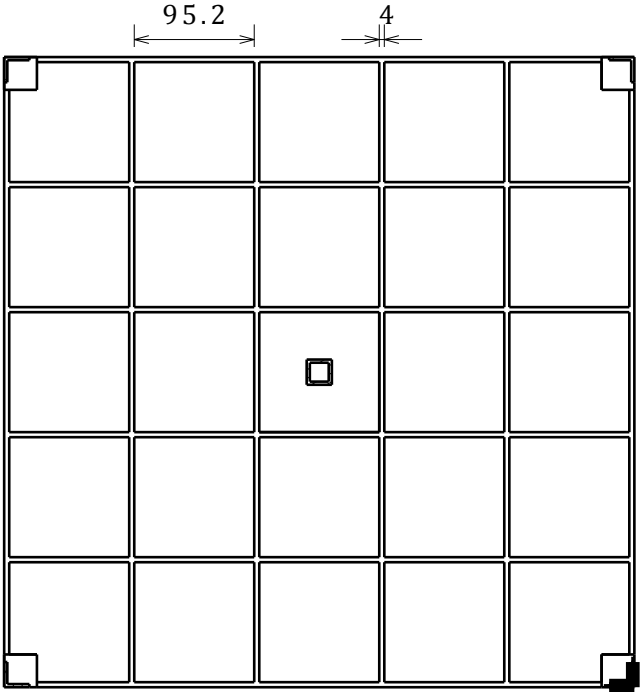
1

D

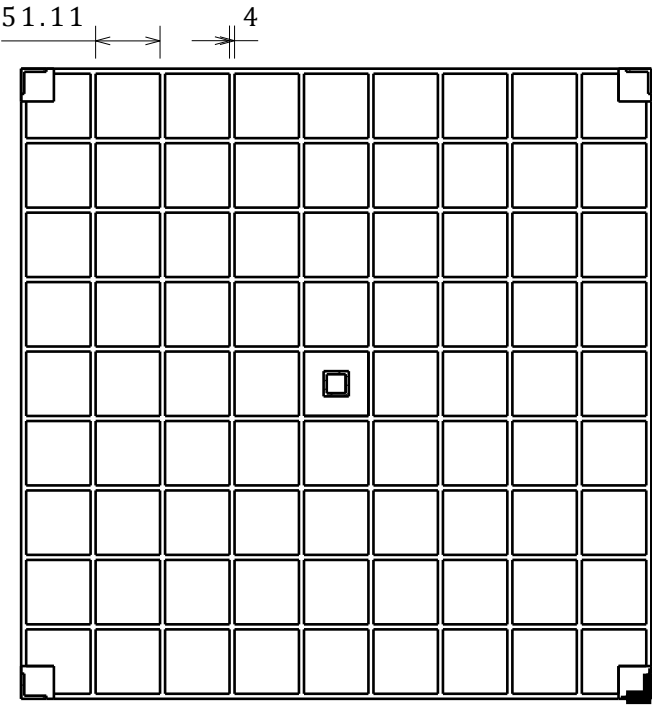
C

B

A

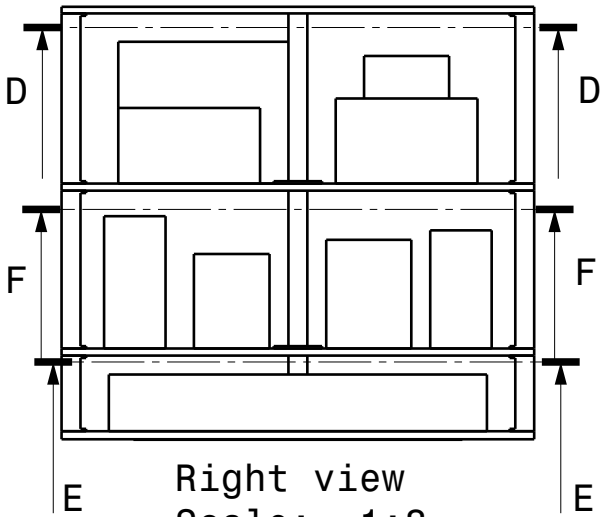


Section view D-D
Scale: 1:6

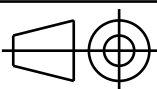


Section view E-E
Scale: 1:6

Sections F-F and E-E are equal
 Ribs Thickness: 6 mm
 Tray A Cylinder heigh: 6.5 mm
 Tray Thickness: 2.5 mm (A), 1.5 mm (B,C) and 1 mm (D)



Right view
Scale: 1:8

DESIGNED BY: Alejandro Pila Sergio Fraile		<h1>Tray B/C/D</h1>		I	-
CHECKED BY: Andrés Rovira				DATE: 22/11/2014	H
SIZE A4		Universitat Politècnica de València		G	-
SCALE 1:6	WEIGHT (kg) 1.7	DRAWING NUMBER 001-0008	SHEET 8/8	F	-
This drawing is our property; it can't be reproduced or communicated without our written agreement.				E	-
				A	-

D

A

4

4

3

3

2

2

1

1